



Norwegian University of
Science and Technology

Distributed propulsion for ships

Vilde Nylund

Marine Technology

Submission date: June 2017

Supervisor: Sverre Steen, IMT

Norwegian University of Science and Technology
Department of Marine Technology



MASTER THESIS IN MARINE TECHNOLOGY

SPRING 2017

FOR

FOR

Vilde Nylund

Distributed propulsion for ships

An efficient ship requires an efficient propulsion system. Today, most cargo ships use either one or two large propellers for propulsion. An idea for the future of ship propulsion is to use many small propellers instead. This is a concept known as distributed propulsion, and is already suggested for electric airplanes. By using many small propellers, rather than a few large ones, a much larger propeller area can in theory be used, without violating spatial constraints. In addition, each propeller can be optimized to its local flow field, so as to better take advantage of the ship wake. The idea is that this could significantly increase the total propeller efficiency. This concept would most likely require the propellers to be driven by many small electric motors, which would get electricity from either batteries or generators.

From the project thesis it is clear that placement of the propellers to utilize the wake is important, as well as optimizing the propellers for their actual operation taking cavitation into account. Furthermore, the aft body design should probably be different for a ship to be propelled by many small propellers than a ship propelled by a single large propeller.

On this background, the objective of the master thesis is to investigate whether (and how much) propulsive efficiency can be improved by use of many small propellers, if the propeller design, placement and aft body shape is optimized.

In the thesis the candidate shall present his personal contribution to the resolution of problem within the scope of the thesis work.

Theories and conclusions shall be based on mathematical derivations and/or logic reasoning identifying the various steps in the deduction.

The thesis work shall be based on the current state of knowledge in the field of study. The current state of knowledge shall be established through a thorough literature study, the results of this study shall be written into the thesis. The candidate should utilize the existing possibilities for obtaining relevant literature.

The thesis shall be organized in a rational manner to give a clear exposition of results, assessments, and conclusions. The text should be brief and to the point, with a clear language. Telegraphic language should be avoided.



The thesis shall contain the following elements: A text defining the scope, preface, list of contents, summary, main body of thesis, conclusions with recommendations for further work, list of symbols and acronyms, reference and (optional) appendices. All figures, tables and equations shall be numerated.

The supervisor may require that the candidate, in an early stage of the work, present a written plan for the completion of the work. The plan shall include a budget for the use of laboratory or other resources that will be charged to the department. Overruns shall be reported to the supervisor.

The original contribution of the candidate and material taken from other sources shall be clearly defined. Work from other sources shall be properly referenced using an acknowledged referencing system.

The thesis shall be submitted electronically (pdf) in DAIM:

- Signed by the candidate
- The text defining the scope (this text) (signed by the supervisor) included
- Computer code, input files, videos and other electronic appendages can be uploaded in a zip-file in DAIM. Any electronic appendages shall be listed in the main thesis.

The candidate will receive a printed copy of the thesis.

Supervisor : Professor Sverre Steen

Co-supervisor : Jarle A. Kramer

Start : 12.01.2017

Deadline : 11.06.2017

Trondheim, 12.01.2017

Sverre Steen
Supervisor

Preface

This is my master thesis which is part of the study program Marine Technology at the Norwegian University of Science and Technology (NTNU). It has been carried out during the spring semester of 2017.

The idea of using distributed electric propulsion on ships was suggested by PhD candidate Jarle A. Kramer, inspired by NASA's research on using it on small airplanes. The reason why I chose this topic for my thesis is because I have always been fascinated by propellers, and eager to learn more about propeller design. In addition, I like that the topic is innovative and has room for creativity.

I would like to thank Jarle for his support and guidance throughout this work. I appreciate his helpful assistance and encouragement. I would also like to thank Professor Sverre Steen for useful consultations and good advices.

It is preferred that the reader of this work is familiar with basic concepts of propeller modelling and marine hydrodynamics.

Trondheim, 2017-06-02



Vilde Nylund

Summary

It is anticipated that using distributed electric propulsion (DEP) on conventional ships will increase the total propulsive efficiency. This is mainly due to two reasons; firstly, because the total propeller disk area can be increased. Secondly, because each propeller can be optimised for the local wake where it is operating. In this work, the benefits of using DEP has been investigated for a 14 000 TEU container ship.

Based on a literary study of the present state of propeller modelling methods, it was decided to use lifting line theory to determine the thrust and torque of propellers in DEP configurations. The blade section geometry of the Wageningen B-screw series was used.

Emphasis was placed on programming a lifting line code in MatLab that could estimate propeller performance with sufficient accuracy. It was validated against polynomials describing the open water characteristics of the Wageningen B-screw series. It was found to provide sufficient accuracy for three- and four-bladed propellers, while relatively large discrepancies was present for two- and five-bladed propellers.

A built-in optimisation function in MatLab called `fmincon` was used to find the optimal geometry of each propeller. Its objective was to minimise the effect delivered to the propellers, without cavitation and with the propellers providing the required thrust for the ship to maintain its operational speed. The latter was achieved by application of a quadratic penalty method to force the total thrust within 3% of the required thrust.

The rate of revolution was optimised for each propeller, while all propellers were optimised to have the same blade area relationship in each configuration. The pitch was adjusted for each propeller by iteration such that the effective angle of attack was sufficiently small to prevent cavitation.

Configurations of propellers placed in a grid were analysed. The width of the grid was equal

to B_{WL} and the height was as the diameter of the original propeller. Problems regarding cavitation occurred for configurations with two rows of propellers. Thus emphasis was placed on configurations with one row.

Based on potential theory, it was expected that five propellers would be most efficient as they had the greatest total propeller disk area, and hence lightest total thrust loading. However, it was the configurations with seven propellers that were most efficient for three- and four-bladed propellers. Influence of nominal wake and relatively small difference in thrust loading between five and seven propellers are anticipated to be the reason why seven propellers resulted in the highest efficiency.

Overall it was concluded that application of DEP to conventional ships can increase the total propulsive efficiency. Results suggests that a DEP configuration of seven four-bladed propellers in one row can increase the propulsive efficiency by 10.75%. However, more extensive analysis are recommended and practical challenges remains to be investigated.

Sammendrag

Det forventes at den totale virkningsgraden på konvensjonelle skip kan økes ved bruk av distribuert elektrisk fremdrift (DEP). Dette skyldes hovedsakelig to grunner; for det første fordi det totale propellarealet kan økes. For det andre, fordi hver propell kan optimaliseres i forhold til hvor den er plassert. I dette arbeidet har fordelene ved å bruke DEP blitt undersøkt for et 14 000 TEU containerskip.

Basert på en litteraturstudie av metoder for propellmodellering, ble det besluttet å bruke løftelinjeteori til å beregne fremdrift og dreiemoment fra propeller i DEP-konfigurasjoner. Bladgeometrien til Wageningen B serien ble brukt.

Det ble lagt vekt på å programmere en løftelinjekode i MatLab som kunne estimere propellens ytelse med tilstrekkelig nøyaktighet. Den ble validert mot polynomer som beskriver friprøvediagrammer for Wageningen B-skrueserien. Resultat fra løftelinjekoden viste tilstrekkelig nøyaktighet for propeller med tre og fire blad, mens relativt store avvik oppstod for propeller med to og fem blad.

En innebygd optimaliseringsfunksjon i MatLab kalt `fmincon` ble brukt til å finne den optimale geometrien til hver propell. Målet for optimaliseringen var å minimere effekten som ble levert til propellene, uten kavitasjon og med nok fremdrift til å opprettholde marsjfart. Sistnevnte ble oppnådd ved anvendelse av en kvadratisk straffemetode for å tvinge fremdriften innenfor 3% av nødvendig fremdrift.

Turtallet ble optimalisert for hver propell, mens alle propeller ble optimalisert for samme bladarealsforhold i hver konfigurasjon. Stigningen på propellene ble justert for hver propell ved iterasjon slik at den effektive angrepsvinkelen var tilstrekkelig liten til å forhindre kavitasjon.

Konfigurasjoner med propeller plassert i et gitter ble analysert. Gitteret hadde bredde lik B_{WL} og høyde som diameteren av den opprinnelige propellen. Når to rader av propeller ble

brukt, oppstod problemer med kavitasjon. Dermed ble det lagt vekt på konfigurasjoner med en rad av propeller.

Basert på potensialteori var det forventet at fem propeller ville resultere i høyest virkningsgrad da de hadde det største totale propellarealet, og dermed den letteste belastningen. Det var imidlertid konfigurasjonene med syv propeller som hadde høyest virkningsgrad for propeller med tre og fire blad. Påvirkning av skipets kjølevann og relativt liten forskjell i belastning mellom fem og syv propeller forventes å være årsaken til at syv propeller resulterte i høyest virkningsgrad.

Det ble konkludert med at bruk av DEP på konvensjonelle skip kan øke den totale virkningsgraden. Resultatene tyder på at en DEP-konfigurasjon av syv firebladede propellere på rekke kan øke den totale virkningsgraden med 10.75%. Imidlertid anbefales det mer omfattende analyse, og det er fortsatt praktiske utfordringer som må løses.

Contents

Preface	i
Summary	ii
Sammendrag	iv
List of Figures	x
List of Tables	xiv
Nomenclature	xvii
1 Introduction	1
1.1 Background	1
1.1.1 Research by NASA	2
1.1.2 Concept	3
1.1.3 Calculation example: airplane propeller versus ship propeller	4
1.1.4 Previous work	5
1.2 Scope of work	7
1.3 Structure of this report	8
2 Propeller modelling methods	9
2.1 Numerical propeller modelling methods	9
2.1.1 Momentum theory	10
2.1.2 Blade element momentum theory	11
2.1.3 Lifting line theory	12

2.1.4	Lifting surface theory	13
2.1.5	Reynolds averaged Navier Stokes	15
2.1.6	Hybrid models	16
2.2	State-of-the-Art in propeller modelling	17
2.2.1	Potential flow solvers	17
2.2.2	Viscous solvers	18
2.3	Concluding remarks	19
3	Theoretical background for optimisation of propeller design	23
3.1	Interior-point optimisation	24
3.2	Particle swarm optimisation	25
3.3	Discussion of Literary Example	25
3.4	Quadratic Penalty Method	26
4	Background theory of propeller modelling	27
4.1	Propeller blade geometry	27
4.2	Xfoil	29
4.3	Propeller performance characteristics	32
4.4	Wageningen B-screw series	34
5	Analysis Procedure	41
5.1	Assumptions	41
5.2	Vessel	42
5.3	Lifting line implementation	42
5.4	Validation of lifting line	49
5.5	Wake implementation	54
5.6	Cavitation check	59
5.7	Optimisation procedure	62
5.8	Uncertainties	65
5.9	Code structure	66
6	Results	69

6.1	Potential theory	70
6.2	Grid configurations with three- to five-bladed propellers	72
6.3	Further analysis of four-bladed propellers	74
6.4	Most efficient configuration	78
7	Discussion of results	83
7.1	Potential theory	83
7.2	Grid configurations with three- to five-bladed propellers	83
7.3	Further analysis of four-bladed propellers	85
7.4	Most efficient configuration	87
8	Conclusions and recommendations for further work	89
8.1	Summary and conclusions	89
8.2	Recommendations for further work	91
	References	92
	Appendix A Induction Factors	I
	Appendix B Validation Plots	III
B.1	Z=2	III
B.2	Z=3	IV
B.3	Z=4	V
B.4	Z=5	VII
	Appendix C MatLab Codes	IX

List of Figures

1.1	LEAPTech configuration of propellers on a small aircraft (Stoll 2015)	2
1.2	Grid configuration	5
1.3	T-configuration	6
4.1	Induced drag on a foil section (Steen 2014)	28
4.2	Force and velocity components of propeller blade section	29
4.3	Command window in Xfoil	30
4.4	Polar exported from Xfoil	30
4.5	Foil section in Xfoil	31
4.6	Inviscid analysis in Xfoil for $\alpha = 0^\circ$	31
4.7	Open water diagram for pitch to diameter ratio of 0.6 and 1.2 for a Wageningen B4-80 propeller	33
4.8	Geometric sectional parameters of the Wageningen B-screw series (Oosterveld & van Oossanen 1975)	35
4.9	Values for the constant V_1 of the blade sections in the Wageningen B-screw series (Oosterveld & van Oossanen 1975)	37
4.10	Values for the constant V_2 of the blade sections in the Wageningen B-screw series (Oosterveld & van Oossanen 1975)	37
4.11	Pitch distribution of the Wageningen B-screw series, applied to all propellers in this work (Steen 2014)	38
5.1	Lifting line of propeller blade	43
5.2	Convergence plot for number of foil sections required in lifting line. N is the number of foil sections	48

5.3	Validation plot for Wageningen B4-55 single screw propeller with $(P/D)_{0.7} = 0.6$. . .	51
5.4	Validation plot for Wageningen B4-55 single screw propeller with $(P/D)_{0.7} = 1.2$. . .	51
5.5	Difference between open water efficiencies for $A_E/A_0 = 0.5$	53
5.6	Difference between open water efficiencies for $A_E/A_0 = 0.9$	53
5.7	Unscaled wake	54
5.8	Diameter calculation of six propellers where col=3 and row=2	55
5.9	Convergence plot for number of angular positions required for lifting line calculations. n_θ is the number of angular positions	58
5.10	Cavitation plots before and after reducing α_e of the outermost blade section 12 o'clock, for a single screw four-bladed propeller	61
5.11	Cavitating part of cavitation plot for a single screw four-bladed propeller, when α_e has been reduced	61
5.12	Outline of three propellers placed in the ship wake	64
5.13	optimisation procedure for seven four-bladed propellers in one row	64
5.14	Code structure	68
6.1	Thrust loading versus total propeller disk area	70
6.2	Thrust loading versus number of propellers	71
6.3	Ideal efficiency versus number of propellers	71
6.4	Propulsive efficiency versus number of propellers for $Z=3-5$	72
6.5	Hull efficiency versus number of propellers	73
6.6	Propulsive efficiency versus total propeller disk area for four blades	74
6.7	Grid configuration of four propellers over two rows	75
6.8	Grid configuration of six propellers over two rows	75
6.9	T-configuration including propeller geometry	76
6.10	Configuration of five propellers including propeller geometry	77
6.11	Configuration of five propellers with compressed domain including propeller geometry	77
6.12	Configuration of seven propellers including propeller geometry	78
6.13	Lift coefficients for propeller number 4 and 5	79

6.14 Lift coefficients for propeller number 6 and 7	79
6.15 Cavitation plot from first and last iteration of α_e for propeller number 4	80
6.16 Cavitation plot from first and last iteration of α_e for propeller number 5	80
6.17 Cavitation plot from first and last iteration of α_e for propeller number 6	80
6.18 Cavitation plot for propeller number 7, no iteration was necessary for α_e	81

List of Tables

1.1	Comparison of ideal properties for a ship propeller and an airplane propeller . . .	4
1.2	Data for original propeller of test vessel	5
2.1	Summary of numerical modelling methods based on potential theory and their ability to be used in a DEP analysis	20
2.2	Summary of numerical modelling methods including viscosity and their ability to be used in a DEP analysis	21
4.1	Dimensions of Wageningen B-screw propellers with two or four to seven blades (Oosterveld & van Oossanen 1975)	34
4.2	Dimensions of Wageningen B-screw propellers with three blades (Oosterveld & van Oossanen 1975)	35
4.3	Coefficients for K_T polynomial of the Wageningen B-screw series, valid for $R_e = 2 \cdot 10^6$ (Oosterveld & van Oossanen 1975)	39
4.4	Coefficients for K_Q polynomial of the Wageningen B-screw series, valid for $R_e = 2 \cdot 10^6$ (Oosterveld & van Oossanen 1975)	40
5.1	Test vessel data	42
5.2	Propellers from the Wageningen B-screw series that has been used for validation of lifting line code (Carlton 2011)	50
6.1	Grid configurations analysed for propellers with three to five blades	69
6.2	Resulting efficiencies of grid configurations	73
6.3	Additional configurations analysed for four-bladed propellers	74
6.4	Properties of grid configuration with five propellers	77

6.5 Geometry of propellers in grid configuration with seven propellers horizontally . . 79

Nomenclature

Abbreviations

BEMT Blade Element Momentum Theory

BET Blade Element Theory

CFD Computational Fluid Dynamics

DEP Distributed Electric Propulsion

DES Detached Eddy Simulation

IP Interior-point

LEAPTech Leading Edge Asynchronous Propellers Technology

LES Large Eddy Simulation

MOPSO Multi-Objective Particle Swarm optimisation

NACA National Advisory Committee for Aeronautics

NASA National Aeronautics and Space Administration

PSO Particle Swarm optimisation

RANS Reynolds Averaged Navier Stokes

RPM Revolutions per minute

TEU Twenty-foot equivalent unit

Greek

α	Angle of attack	[rad]
α_e	Effective angle of attack	[rad]
α_i	Induced angle of attack	[rad]
β	Hydrodynamic pitch angle	[rad]
β_i	Induced hydrodynamic pitch angle	[rad]
$\Delta\eta_0$	Deviation in open water efficiency	[-]
η	Efficiency	[-]
η_0	Open water efficiency	[-]
η_D	Propulsive efficiency	[-]
η_H	Hull efficiency	[-]
η_i	Ideal efficiency	[-]
η_R	Relative rotative efficiency	[-]
Γ	Total circulation around propeller blade	[m ² /s]
γ_F	Strength of free vortex	[m ² /s]
Γ_i	Circulation around foil section number i	[m ² /s]
μ	Dynamic viscosity	[Pa · s]
μ_T	Quadratic penalty for thrust	[-]
ν	Kinematic viscosity	[m ² /s]
ϕ	Pitch angle	[rad]
ρ	Seawater density	[kg/m ³]

σ	Cavitation number	[–]
σ_S	Safety factor	[–]
θ	Angular position of lifting line	[<i>rad</i>]
φ	Velocity potential	[–]

Lowercase

a	Distance between leading edge and generator line	[<i>m</i>]
b	Distance between leading edge and location of maximum thickness	[<i>m</i>]
c	chord length of blade section	[<i>m</i>]
dD	Drag force from foil section	[<i>N</i>]
dT	Thrust from foil section	[<i>N</i>]
h	Submergence	[<i>m</i>]
n	Rate of revolution	[1/ <i>s</i>]
n_p	Number of propellers	[–]
obj	Objective	[–]
p	Pressure	[<i>Pa</i>]
p_a	Atmospheric pressure	[<i>Pa</i>]
p_v	Vapor pressure	[<i>Pa</i>]
r_0	Fixed radial blade position	[<i>m</i>]
r_h	Radial position of hub	[<i>m</i>]
t	Thrust deduction fraction	[–]
t_m	Maximum thickness	[<i>m</i>]

$t_{l.e.}$	Leading edge thickness	[m]
$t_{t.e.}$	Trailing edge thickness	[m]
v	Horizontal velocity component	[m/s]
w	Vertical velocity component	[m/s]
w	Wake fraction	[-]
y	Fraction of radial position, r/r_0	[-]
y	Horizontal Cartesian coordinate	[m]
y_n	Horizontal coordinate of lifting line	[m]
y_{back}	Coordinate for foil section	[m]
y_{centre}	Horizontal centre coordinate of propeller	[m]
y_{face}	Coordinate for foil section	[m]
y_{lim}	Horizontal dimension of grid	[m]
z	Vertical Cartesian coordinate	[m]
z_n	Vertical coordinate of lifting line	[m]
z_{centre}	Vertical centre coordinate of propeller	[m]
z_{lim}	Vertical dimension of grid	[m]
z_{max}	Maximum vertical Cartesian coordinate of grid	[m]
g	Acceleration of gravity	[m ² /s]
r	Radial position	[m]
r	Running radial blade position	[m]
t	Time	[s]

u Horizontal velocity component [m/s]

Uppercase

$(P/D)_{0.7}$ Pitch to diameter ratio at 0.7R [-]

$(P/D)_{1.0}$ Pitch to diameter ratio at 1.0R [-]

F_{AD}^{\rightarrow} Body forces on vector form [N]

\vec{V} Velocity vector [m/s]

A_E/A_0 Expanded blade area ratio [-]

A_P Total projected propeller disk area [m²]

B_{WL} Breadth in waterline [m]

C_B Block coefficient [-]

C_L Lift coefficient [-]

C_T Thrust loading coefficient [-]

C_F Frictional coefficient [-]

C_{Lc} Lift coefficient at zero angle of attack [-]

$C_{p,min}$ Minimum pressure coefficient [-]

C_{WA} Waterplane area coefficient [-]

D Propeller diameter in full-scale [m]

D_i Induced drag force [N]

D_M Propeller diameter in model scale [m]

D_y Propeller diameter limited by horizontal grid dimension [m]

D_z Propeller diameter limited by vertical grid dimension [m]

I_A	Axial induction factor	[–]
I_T	Tangential induction factors	[–]
J	Advance number	[–]
J_0	Open water advance number	[–]
K_Q	Torque coefficient	[–]
K_T	Thrust coefficient	[–]
L	Lift force	[N]
L_{PP}	Length between perpendiculars	[m]
N	Number of sections represented by a lifting line	[–]
P	Total effect delivered to propeller(s)	[W]
Q	Torque	[Nm]
Re	Reynolds number	[–]
T	Draught	[m]
T	Thrust	[N]
T	Total thrust of propeller(s)	[N]
T_{req}	Required thrust of propeller(s)	[N]
U_A	Axial induced velocity	[m/s]
U_T	Tangential induced velocity	[m/s]
V	Horizontal velocity	[m/s]
V_∞	Resulting inflow velocity	[m/s]
V_A	Advance velocity	[m/s]

V_S	Ship velocity	$[m/s]$
Z	Blade number	$[-]$
R	Propeller radius	$[m]$
Z	Number of propeller blades	$[-]$

[This page is intentionally left blank]

Chapter 1

Introduction

This first chapter is an introduction to the concept of distributed electric propulsion (DEP) and the work that has been done investigating the potential benefits of using it on conventional ships. First, a detailed background description is provided. Then the scope of the work is defined. Lastly is given the structure of this report.

1.1 Background

When designing a modern cargo ship, a propulsion system with single or double screw propeller is usually preferred. This is mainly due to practical reasons as it is not efficient to have several small combustion engines. However, with electrical propulsion comes new possibilities of using configurations of several small engines in strategical locations as they don't have the same scaling problems as combustion engines. Another benefit of electrical propulsion is that it is likely to save maintenance cost as electrical engines have less moving parts than combustion engines.

The concept of distributed electrical propulsion is currently of broad interest in the aviation industry. National Aeronautics and Space Administration (NASA) has recently published some of their work regarding DEP. It is therefore convenient to present a short summary of their concept in the next subsection. A conceptual description for ships will then follow, as well as a summary of a pre-study that I conducted in the autumn of 2016. Some paragraphs in this section originates from the pre-study.

1.1.1 Research by NASA

NASA is currently investigating the use of DEP on small aircrafts with lightly loaded propellers. The configuration they have used is called Leading Edge Asynchronous Propellers Technology (LEAPTech) and includes eighteen electric motors mounted in nacelles in the span-wise direction on small aircraft wings (Stoll et al. 2014). This is illustrated in Figure 1.1. During take-off and landing, the motors power one propeller each (Stoll 2015). The benefit of this is that the dynamic pressure over the wings is increased, which results in increased lift. This allows use of a smaller wing to obtain a given stall speed. A smaller wing is not only beneficial in terms of resistance reduction, it also improves ride quality as it is less sensitive to gust (Stoll et al. 2014). Results indicate that a LEAPTech configuration gives an increased efficiency and significantly reduced noise.

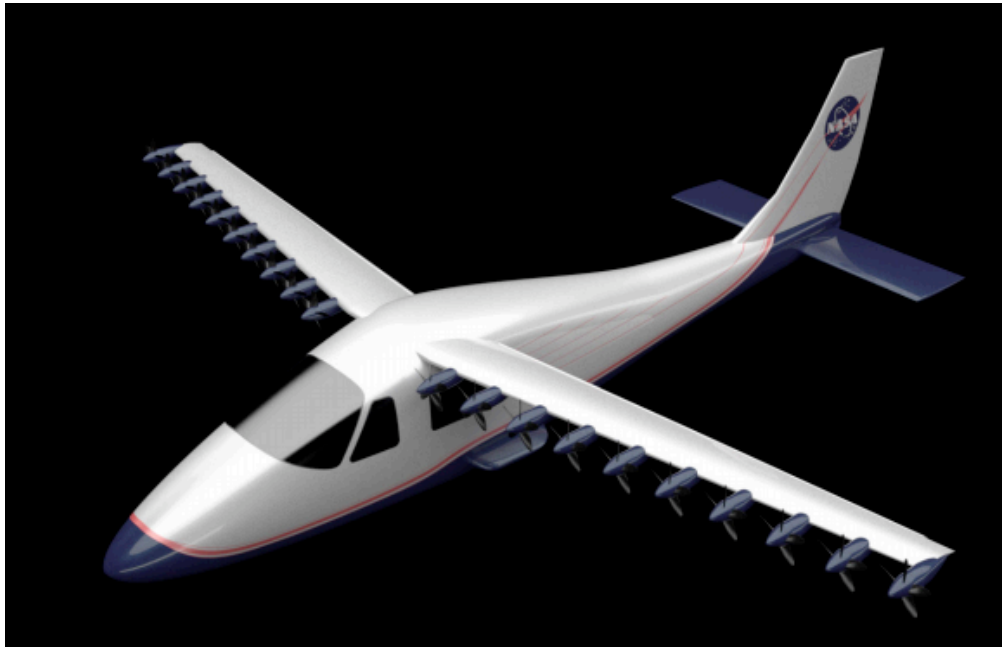


Figure 1.1: LEAPTech configuration of propellers on a small aircraft (Stoll 2015)

1.1.2 Concept

Inspired by the research done by NASA it is anticipated that DEP can be applied to ships to increase the propulsive efficiency. During the last 20 years it has been a rapid development of electrical propulsion on certain ship types, such as offshore ships (Pestana 2014). Due to increased environmental awareness that leads to stricter regulations, it is reason to believe that electrical propulsion will be implemented on cargo ships in the future. Therefore a concept like DEP is most likely feasible. However, it remains to be investigated if it is beneficial, and there are some obvious practical challenges that must be overcome.

There are mainly two reasons to believe that a DEP configuration can be beneficial. Firstly, using several small propellers versus one or two large ones will result in a larger total propeller area, as the diameter of a ship propeller is limited by the presence of the hull itself. Thus, for a given thrust, the propellers will be lighter loaded, resulting in a higher ideal efficiency and generally less risk of cavitation.

Secondly, it gives the opportunity to optimise each propeller for operation in a specific part of the ship wake. Generally, it is desired that a ship propeller should work in a homogenous wake field. This is favourable with respect to propeller blade design. If there are large wake variations, the blade design becomes a compromise between the optimal geometry for high and low wake fractions.

Due to the form of the hull it is impossible to achieve a completely homogenous wake for a single or double screw conventional propeller. With DEP the location of the propellers are more flexible. They can be designed to operate in a more homogenous wake field. In theory, this will lead to an increased total propeller efficiency. It can also be considered to alter the design of the stern in order to optimise the operating conditions of the propellers.

As previously mentioned there are practical challenges, for example regarding the arrangement of the propulsion system. It is undesirable to have a shaft from each propeller into the hull. Therefore it is anticipated that the electrical motors must be mounted in nacelles in front of the propellers. The nacelles will lead to additional appendage resistance and must therefore be designed as streamlined as possible to minimise drag. However, solving such challenges are outside the scope of this work.

1.1.3 Calculation example: airplane propeller versus ship propeller

A calculation example has been conducted in order to compare airplane propellers and ship propellers. In general, airplane propellers are known to have higher propulsive efficiency than ship propellers. A calculation example based on simple momentum theory is provided to investigate this. The airplane used in the example is a Cessna 172 Skyhawk. It has a maximum cruise speed of 66.4 m/s and is powered by a 119 kW piston engine (Palt 2017). At cruise speed it uses 75% engine power (CessnaAircraftCompany 2004). Thus its cruise power is 89.25 kW. It has a propeller diameter of 1.9304m, which results in a propeller disk area of 2.9267m^2 . Typically, airplane propellers have a propulsive efficiency of 0.85 (Spakovszky 2009). The Cessna is assumed to have a propulsive efficiency of 0.85 and a mechanical efficiency of 0.98. Multiplying cruise power by the efficiencies and dividing by cruise speed, the resulting thrust is 1142.5 N.

The principles of simple momentum theory will be presented in Chapter 2 about propeller modelling methods. The application of it implies that the ideal efficiency, η_i , can be calculated by Equation 2.1, where the thrust loading coefficient, C_T , is given by Equation 2.2. In the calculations for the Cessna, air density of $0.9633\text{kg}/\text{m}^3$ was used. The thrust loading coefficient and ideal efficiency of a single screw container ship was calculated in the pre-study, prior to this work. Its propeller data are provided in Table 1.2.

Resulting thrust loading coefficients and ideal efficiencies are presented in Table 1.1. It should be noted that this is ideal properties, as effects of propeller geometry are not included.

Table 1.1: Comparison of ideal properties for a ship propeller and an airplane propeller

	Cessna	Container ship
C_T	0.1838	0.2749
η_i	0.9578	0.9394

From the results it is seen that the ship propeller are heavier loaded than the airplane propeller, even though its diameter is much larger than the airplane propeller. Consequently, the ideal efficiency of the airplane propeller is higher than for the ship propeller. Thus the reason why airplane propellers in reality have higher propulsive efficiency than ships can be explained by the ship propellers being heavier loaded and limited by cavitation.

1.1.4 Previous work

The autumn of 2016 I conducted a pre-study aiming to indicate the potential benefits of using DEP on conventional ships. This work will be further referred to as the project thesis. A summary of the project thesis will now be given.

A test vessel called Duisburg Test Case was used as reference vessel. Its hull design is of a typical 14 000 TEU container ship (el Moctar et al. 2012), powered by the use of a single screw propeller. Specifications of the original propeller is provided in Table 1.2. This vessel was also used as reference vessel in the analysis of this work, which will be described in Chapter 5.

Table 1.2: Data for original propeller of test vessel

$Z[-]$	5
$(P/D)_{0.7}[-]$	0.959
$A_E/A_0[-]$	0.8
$D_M/D[m]$	0.150/8.911

In the project thesis simplified calculations were conducted to indicate if application of DEP could be beneficial in terms of increasing the propulsive efficiency. The calculations were based on Wageningen B-series propellers. As simplified formulas were applied, the blade geometry was not accounted for in the analysis. To account for the nominal wake, the average wake fractions within the propeller disks were used. Thus, the results can only be treated as indications.

Two types of configurations were tested for various number of propellers. One configuration type were a grid configuration with propellers of equal diameter placed in a rectangular grid. This configuration is illustrated in Figure 1.2.

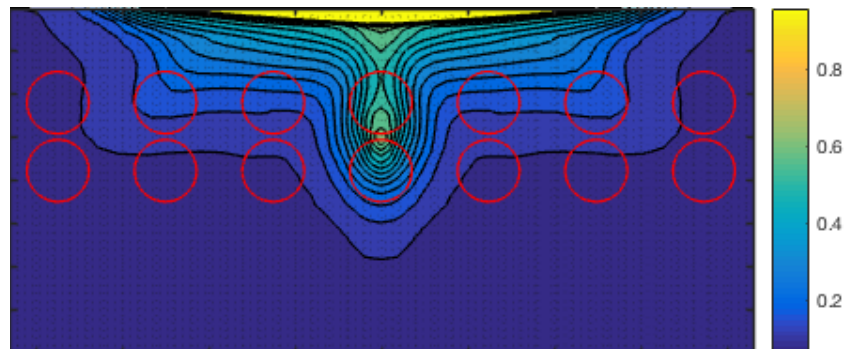


Figure 1.2: Grid configuration

Results showed that the magnitude of the wake fraction had great influence on the propulsive efficiency. Thus the aim of the second configuration was to exploit the wake better than in the grid configuration. This was done by placing one large propeller at the location of the original propeller, where the wake fractions were large, and use a small rectangular grid of propellers above. This type of configuration will be further referred to as a T-configuration. It is illustrated in Figure 1.3.

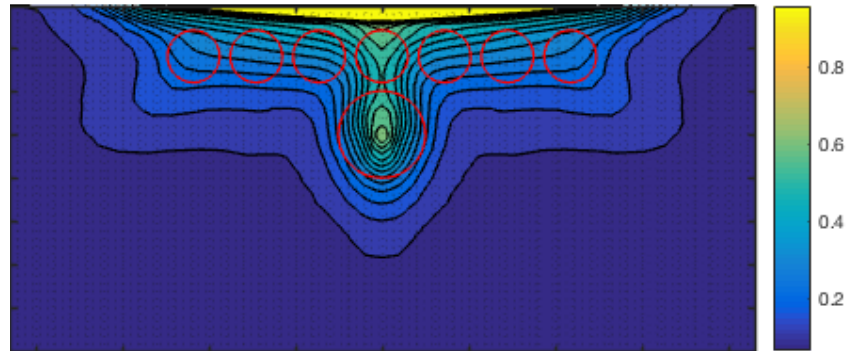


Figure 1.3: T-configuration

A brute force approach were used to find the combination of advance number, pitch and blade area relationship resulting in highest propulsive efficiency for two- to five-bladed propellers. It was anticipated that cavitation would be of great significance. However, the effects of it was included in a highly simplified manner using a curve fit of a Burrill diagram.

Results indicated that it can be possible to achieve higher propeller efficiency with DEP than with a conventional propulsion system. However, it should be emphasised that only a rough analysis was conducted, and that more detailed calculations are required to draw conclusions. The utilisation of the ship wake and thereby the design of the aft ship, as well as cavitation was shown to be of great significance. It was therefore concluded that a more extensive analysis that includes these effects to a larger extent are necessary in this work in order to quantify the benefits with higher accuracy.

1.2 Scope of work

The scope of the work is defined in this section to make the reader familiar with objective, methods, simplifications and limitations that has been applied.

The main objective of this work was to investigate the use of DEP with sufficient accuracy to conclude whether it can be beneficial or not for conventional cargo ships.

It was concluded in the project thesis that it was necessary to include the effects of wake field and cavitation with higher accuracy. Hence a more extensive approach for the analysis had to be used in this work. In order to choose a sufficient method, a thorough literature study regarding the present state of propeller modelling was conducted. Based on the literary study it was concluded that within the time frame of this work, application of lifting line theory for performance calculations would be most appropriate.

An analysis approach of lifting line theory was coded in MatLab. It calculates the propeller performance in terms of thrust, torque and propulsive efficiency based on that the propeller blades are straight lines. Wake data from CFD analysis was provided by co-supervisor. In such a lifting line code, the propeller geometry is required as input. Thus an optimisation algorithm had to be implemented. The blade section geometry of the Wageningen B-screw series was applied to limit the number of variables in the optimisation. However, lifting line theory allows for use of other geometry if desired.

A built-in optimisation function in MatLab called `fmincon` was used to find the optimal propeller design in terms of blade area relationship and rate of revolutions. The default interior-point algorithm was used. All propellers in one configuration were given the same blade area relationship, while the rate of revolution was optimised for each propeller. A particle swarm algorithm was applied to polynomials representing the open water characteristics of the Wageningen B-series in order to find the initial values required by the interior-point algorithm. To ensure that the propellers supplied the desired amount of thrust, a quadratic penalty method was used.

Cavitation was accounted for by running an open source program called Xfoil via MatLab to determine minimum pressure coefficients. Since a propeller blade is most prone to cavitation when located in its top position (12 o'clock), the minimum pressure coefficients of the foil sec-

tions was found for this position. They were then compared with the dimensionless cavitation number, σ . The pitch of each propeller was adjusted such that the effective angle of attack of the outermost foil section in top position was close to zero. This was necessary in order to prevent cavitation.

The limitations that were set in order to complete the work within the time frame of the master thesis are listed below.

- The foil section geometry of the Wageningen B-series is applicable
- Interaction effects between the propellers are negligible
- Built-in optimization algorithms in MatLab are applicable
- Skew and rake are not included

1.3 Structure of this report

This report is organised as follows. In Chapter 2, is included a literature study of propeller modelling methods. Subsections concerns theoretical descriptions, a state-of-the-art study and concluding remarks. Theoretical background for the optimisation methods used are provided in Chapter 3, together with an example of application from recent literature. Then in Chapter 4 is included some background theory for the approach of the analysis. This concerns propeller blade geometry, Xfoil, propeller performance characteristics and the Wageningen B propeller series.

The approach of the analysis is provided in Chapter 5. In this chapter assumptions are stated and the test vessel is presented. Thereafter a through review of the lifting line procedure with associated equations is provided. It is explained with equations and text how effects such as cavitation and wake were included in the analysis. The optimisation procedure is also explained in this chapter, which is ended with a list of uncertainties and an overview of the code work. In Chapter 6 the results of the analysis are presented. They are further discussed in Chapter 7. In Chapter 8, conclusions and recommendations are provided.

Chapter 2

Propeller modelling methods

A state-of-the-art literature study of propeller modelling methods was conducted in the project thesis. This chapter originates from the project thesis, but alterations have been made. It contains an overview of different propeller modelling methods that were considered to be used to analyse the performance of DEP configurations. Concluding remarks, that justifies the choice of propeller modelling method, are provided in the end of the chapter.

2.1 Numerical propeller modelling methods

The performance of a propeller can be assessed by empirical methods, experiments or numerical analysis. Empirical methods, like the Wageningen B-screw series, are not applicable for design or analysis of propellers (Steen 2014). They are only useful to determine diameter, pitch and blade area at early stages of the design process. Much of the knowledge about propeller performance has, until recent years, been gained through experiments (Kerwin & Hadler 2010). However, the use of numerical modelling, such as CFD, for marine applications has recently increased due to the availability of software and more efficient computers. An overview of common methods for numerical propeller modelling follows. This concerns momentum theory, blade element momentum theory, lifting line theory, lifting surface theory, Reynolds averaged Navier Stokes and hybrid methods.

2.1.1 Momentum theory

A propeller can be described as a device that gives a vessel a forward momentum by giving the fluid a backward momentum. This is directly linked to Newton's 3rd law. An idealisation of the propeller can therefore be studied by means of momentum theory, where axial momentum theory is the simplest form (Carlton 2011). It is based on the following three assumptions

- The propeller works in an ideal fluid, and consequently does not experience energy losses due to frictional drag
- The propeller can be replaced by an actuator disk
- The propeller can produce thrust without causing rotation in the slipstream

As the name implies, this method is derived from the principles of conservation of fluid momentum. The propeller is modelled as an actuator disk, which is equivalent to a propeller with an infinite number of blades and zero chord length (Kerwin & Hadler 2010). When ideal fluid passes through the actuator disk, it introduces a pressure jump to the fluid. The pressure jump results in a uniform acceleration of the fluid through the disk, which gives a thrust in the opposite direction through the conservation of fluid momentum.

Applying the simplest form of momentum theory implies that the actuator disk does not absorb any torque because no tangential velocity components are induced. The efficiency of an actuator disk can be derived as the relationship between the useful work done by the disk and the total energy supplied to it. Since no torque is absorbed, the efficiency calculated based on simple momentum theory is the theoretical maximum efficiency of a propeller. It can be expressed by means of a thrust coefficient, which implies that the ideal efficiency varies with the loading of the propeller.

Expressions for thrust coefficient and ideal efficiency derived from momentum theory are given in Equation 2.2 and 2.1, respectively. As seen in Equation 2.1, the thrust coefficient and ideal efficiency are inversely proportional. It is further referred to (Steen 2014) for numerical derivations.

$$\eta_i = \frac{2}{1 + \sqrt{1 + C_T}} \quad (2.1)$$

$$C_T = \frac{T}{\frac{\rho}{2} A_P V^2} \quad (2.2)$$

The rotational motion of an actuator disk can be accounted for by introducing a rotating annular stream tube and satisfying the conservation of angular momentum (Kulunk 2011). Then the third assumption in the above list is invalid. This results in a more realistic description of the propeller action, and adds a new level of complexity with respect to the simple momentum theory. It is further referred to (Kulunk 2011) for numerical derivations.

Momentum theory is not able to account for the effects of propeller geometry, and it is therefore not applicable for use in propeller design or analysis. Thus it is considered insufficient for analysis of DEP. However, it is a useful method to calculate the ideal efficiency and estimate the average velocity induced by the propeller (Steen 2014). A major advantage is that it is relatively easy to use, and clearly depicts the ideal effects of adjusting the propeller diameter. An illustrative example comparing a ship propeller and an airplane propeller by means of simple momentum theory is included in Chapter 1.

2.1.2 Blade element momentum theory

Blade element momentum theory (BEMT) is a combination of momentum theory and blade element theory (BET). The propeller performance is determined by dividing the blade in two-dimensional foil sections, typically between ten and twenty, and analyse each section separately (Kulunk 2011). The following additional assumptions applies in combination with those defined for momentum theory in the previous section.

- No hydrodynamic interaction between blade elements
- The forces on the blade elements are determined by the lift and drag coefficients

The effect of the blade geometry is accounted for in BET. The resulting incident velocity on each foil section consists of an axial and a rotational component, varying linearly up the blade (Carlton 2011). Thus, the effective angle of attack and hence the lift varies for each foil section. The effective angle of attack, and consequently thrust and torque, are obtained by considering the two-dimensional lift and drag coefficients of each foil section combined with the changes in

fluid momentum from momentum theory (Amini 2011). At the same time, a balance of angular momentum with the force on the blade within each strip is applied. This results in a set of non-linear equations that can be solved by iteration to obtain the thrust and torque of each strip. Then the total thrust and torque can be calculated by integration along the blade, and sum over the number of propeller blades.

BEMT is efficient and simple to use as it treats a three-dimensional problem by discretising one dimension and allows use of two-dimensional considerations. An advantage over more advanced potential flow methods is that it allows the lift and drag properties of the foil sections to include viscous effects such as stall and laminar separation at low Reynolds numbers by using empirically based lift and drag curves for the blade sections.

One important effect that is not included in BEMT is the interaction on one blade section from the remaining blade sections. Because of this, the accuracy of BEMT is considered to be too low for it to be used in an analysis of DEP in this work.

2.1.3 Lifting line theory

The radial distribution of lift from a foil section is proportional to the radial distribution of circulation. In lifting line theory the radial distribution of circulation is considered. It can be used to solve a design problem if the circulation distribution is known, or it can be used to solve an analysis problem if the propeller geometry is known. The application of lifting line theory to a propeller implies the following assumptions

- The propeller works in an ideal fluid
- Radial variation of circulation, inflow and propeller blade geometric parameters
- Lightly loaded propeller, which means no contraction of the slip stream

When applying lifting line theory, the propeller blade is modelled as a straight line and discretised into a number of N foil sections. With each foil section comes a set of one bound and two free vortex sheets with strength of a certain magnitude. This results in a radial distribution of bound and free vortex sheets (Kerwin & Hadler 2010). The circulation around each section is described by a bound vortex of strength $\Gamma(r)$, located one quarter from the leading edge. It is directly linked to the sectional lift force through Kutta Joukowski's theorem, which is given in

Equation 2.3. Thus the thrust and torque from each section can be calculated by application of Kutta Joukowski's theorem. Total thrust and torque are determined by integration over the propeller blade.

$$L = \rho V_{\infty} \Gamma \quad (2.3)$$

Drag contributes to additional torque and reduced thrust. When applying lifting line theory it can be separated into induced and frictional drag. The induced drag can be directly implemented into Kutta Joukowski's theorem in terms of tangentially and axially induced velocities. The induced velocities are calculated using Biot Savart's law together with a correction method to account for the effect of finite blade number on the induced velocities. Viscous drag is commonly included by means of a drag coefficient, which can be determined using a friction line.

Lifting line theory is computationally simple. Thus, it does not require a lot of computational time to gain a satisfying accuracy. Unlike in BEMT, the interaction effect between the foil sections are accounted for. Consequently, it can describe radial pressure variations across the blade.

It is most suitable for lightly to moderately loaded propellers with thin blades as the blades are described by straight lines. In a DEP configuration, the propellers are anticipated to be lightly loaded. Lifting line theory are therefore considered applicable. It is an advantage that it is computationally simple and extensively used for marine propeller applications. Another benefit is that it allows for relatively accurate predictions of cavitation as cavitation number can be calculated and compared with minimum pressure coefficient for each blade section.

2.1.4 Lifting surface theory

Lifting surface theory takes the lifting line theory one step further by including the chord-wise circulation around the propeller blades (Kerwin & Lee 1978). This is done by placing a distribution of vortices on the camber surface of each blade, together with a distribution of vortices shed into the wake. Thus, the real blade geometry is included to a larger extent in lifting surface theory than in lifting line theory, since the blade is represented by a surface instead of a line. Lifting surface theory is based on the following two assumptions

- The propeller works in an ideal fluid, and consequently does not experience energy losses due to frictional drag.
- The propeller blades can be represented by infinitely thin surfaces

Vortex lattice methods are a subclass of lifting surface theory (Carlton 2011). Then a finite set of straight line elements of constant strength are placed with end points on the blade camber surface. This results in a lattice of line segments, with control points on the mean camber surface. Thus the lifting surface is modelled as infinitely thin. A consequence of neglecting the thickness of foil sections is that the pressure distributions on the leading and trailing edges are poorly described (Breslin & Andersen 1993).

Another subclass of lifting surface theory is panel methods. Then the distribution of vortices are placed on the actual camber surface, instead of the mean camber surface. This means that the effect of thickness is also included. However, the inclusion of thickness in panel codes comes with a cost in terms of computational time with respect to vortex lattice codes.

In lifting surface theory the fundamental equation of potential flow, called the Laplace equation, is solved to find the local pressure and velocity components within boundaries defining a confined fluid domain. The Laplace equation is given in Equation 2.4 where φ is the velocity potential.

$$\nabla^2\varphi = 0 \tag{2.4}$$

According to (Breslin & Andersen 1993), all lifting line and lifting surface theorists recognised that including the effects of local trajectories of the trailing vortices were crucial when estimating flow and forces induced on propeller blades. In a lifting surface analysis not only the propeller blades are discretised, but also the wake. This leads to a better representation of the trailing vortices, and the forces on the blades can be calculated with higher accuracy. However, accuracy usually comes with a cost in terms of computational time and this is no exception.

One great advantage with panel codes is that it is possible to include bodies such as hub, pods and rudder in the analysis (Steen 2014). According to (Carlton 2011), results from panel methods has shown to be in good agreement with theoretical and experimental results for blade pressure distributions and open water characteristics. However, lifting surface methods in gen-

eral are discarded for further analysis of DEP as it is computationally demanding. In addition, it is relatively limited access of material needed to generate such a code within the time frame of this work.

2.1.5 Reynolds averaged Navier Stokes

The Navier Stokes equations gives a complete description of a continuous Newtonian viscous flow in both space and time. Water can be assumed to be of constant density and viscosity, the equations can then be written on the compact form shown in Equation 2.6. They can be solved analytically for highly simplified cases, but must be solved numerically to describe the flow around a propeller. In a viscous CFD analysis the local velocity components and pressure are calculated by solving the Navier Stokes equations and the Continuity equation in a grid within a defined fluid domain. The Continuity equation is given in Equation 2.5. For high Reynolds number flow, a turbulence model must be applied.

$$\frac{\partial \rho}{\partial t} + \nabla \cdot (\rho \vec{V}) = 0 \quad (2.5)$$

$$\rho \cdot \frac{D\vec{V}}{Dt} + \nabla p - \mu \nabla^2 \vec{V} = \rho \vec{g} \quad \text{where} \quad \vec{V} = [u, v, w] \quad (2.6)$$

The most common CFD approaches for analysis of flow around propellers are the Reynolds Averaged Navier Stokes (RANS) method, Large Eddy Simulation (LES) techniques and Detached Eddy Simulations (DES) (Carlton 2011). Due to its computational efficiency, RANS codes are usually preferred for analysis of marine propellers.

The grid generation is the most time consuming and crucial part of the application of RANS, as the whole fluid domain must be discretised. This requires highly qualified users to gain sufficient accuracy of the analysis. The grid should be refined and smooth around areas where it is crucial to capture fluid phenomenas. This implies high grid resolution in boundary layer regions, in the wake and at the blade tips in order to capture tip vortices. According to (Carlton 2011), unstructured grids are favoured since they can easily handle complex geometries and good clustering of grid cells in regions of the flow where large pressure gradients occur.

Using a coupling between a RANS code and a potential solver is considered as applicable for

DEP analysis. This is called a hybrid model and will be explained in detail in the next section.

2.1.6 Hybrid models

When a potential flow solver is coupled to a viscous solver, it results in a hybrid model. The main motivation for using a hybrid solver for performance analysis of marine propellers is that it saves computational time as the action of the propeller is simplified with a potential approach.

This leads to an iterative procedure that starts with importing the nominal wake from the viscous solver to the potential solver. The action of the propeller is calculated in terms of thrust and torque in the potential flow solver, and imported back into the viscous solver. The forces are then distributed over the volume of the propeller disk. These forces enter the Navier Stokes equations as body forces (Sánchez-Caja et al. 2014). This is illustrated in Equation 2.7, where $F_{AD}^{\vec{}}$ is the body forces.

$$\rho \cdot \frac{D\vec{V}}{Dt} + \nabla p - \mu \nabla^2 \vec{V} = \rho \vec{g} + F_{AD}^{\vec{}} \quad (2.7)$$

The viscous solver calculates the velocity components from the Navier Stokes equations, which is then the effective wake. However, since the input to the potential solver is the wake without the presence of the propeller, the effective wake must be corrected with propeller induced velocities before it is sent back to the potential solver for the next iteration. Thus, the induced velocities calculated in the potential solver must be subtracted from the effective wake. Then the effective wake is used as input to the next iteration where new body forces are calculated, and the same procedure as described for the first iteration are repeated. In this way, the interaction between the nominal wake and induced wake are accounted for. The iterations are conducted until satisfying convergence is achieved.

A hybrid model is considered to be applicable for the analysis of DEP. However, even though a lot of computational time is saved with respect to using RANS only, the time frame of this work is considered too short for the implementation of such a method.

2.2 State-of-the-Art in propeller modelling

The state-of-the art in numerical propeller modelling is dominated by CFD applications. During the last two decades there has been significant progress on the subject, and a review of its state will be given in this section. It is then convenient to distinguish between potential flow solvers and viscous solvers in this chapter.

2.2.1 Potential flow solvers

Potential flow methods have long been a widely used tool for propeller modelling (Dejhalla & Prpic-Orsic 2006). In general they are relatively affordable and more extensively validated compared to viscous methods. However, they are gradually losing their importance as large progress has been made on the development of CFD in recent years (Szantyr 2008).

Potential flow solvers are mainly based on lifting surface theory, and mostly concerns panel codes. Panel codes, which is mainly boundary element codes (BEM), are preferred for performance analysis due to their good accuracy within a reasonable computational time (Dejhalla & Prpic-Orsic 2006).

In the early 20th Century the foundation for potential flow solvers was discovered when Lanchester suggested that the idea of circulation was related to lift (Carlton 2011). Independently of his work Kutta and Joukowski came to the same conclusion, and Joukowski quantified it by the well-known Kutta-Joukowski's theorem. This work was extended by Prandtl, who developed the classical lifting line theory. Around fifty years later, when computers were available, lifting line theory was further developed. Lerbs, Goldstein and Betz can be mentioned to have contributed extensively.

In the early 1960, the computational capability had significantly increased, allowing for the development of lifting surface theory. Even though theoretical foundations for lifting surface theory was already laid, Pien has been credited as the first to produce the lifting surface theory subsequent to 1960. Since then, his work has been followed up and further developed by others. One of them is Kerwin, whom introduced vortex lattice methods. Others are (Hess & Valarezo 1985) who developed the first 3D BEM for marine propellers in steady flow. Since then, BEM has been further extended to include both unsteady performance and cavitation predictions.

(Politis 2004) developed a BEM model of a propeller in unsteady flow using a time stepping approach with vortex filaments. Applications of this method on both steady and unsteady cases has resulted in good predictions of forces and pressure distributions. According to (Dejhalla & Prpic-Orsic 2006) the recent improvements in panel method codes shows good agreement with experimental results.

The free software OpenProp is an open source tool based on vortex lattice lifting line theory. It can be used for both design and analysis purposes of marine propellers. (Epps et al. 2009) shows the numerical derivations, as well as some design cases.

In recent literature there are several examples of the application of potential flow solvers coupled to viscous solvers for design and analysis purposes of marine propellers. An example is (Sánchez-Caja et al. 2014), who used a coupling between a lifting line code in off-design mode and a RANS solver to demonstrate a suggested correction procedure for induced velocities calculated by a potential flow solver used in a hybrid model.

2.2.2 Viscous solvers

Today, the majority of propeller flow computations are performed using CFD methods (Szantyr 2008). In most cases, RANS codes are favourable due to their efficiency.

The development of CFD has increased in line with available computational power. Around 1980 computers were powerful enough to solve the Navier Stokes equations. However, initially the free surface was not included in the codes, as it was made for other applications than naval purposes. It therefore took some time before the free surface was included and the codes were validated to be used for propeller flow.

Since 1980 there has been arranged workshops around every 5th year to assess the state-of-the-art in numerical prediction of viscous flow for naval purposes (Larsson et al. 2014). It was not before 1990 and onwards that RANS started to dominate the workshops, and on the fourth workshop in 2000, self-propulsion was included in the test regime.

During the last few years, there has been a significant development in RANS codes for marine propeller applications (Dejhalla & Prpic-Orsic 2006). It has become a well established method for analysis of interaction between hull, propeller and rudder. It can be used to accurately predict the propeller open water characteristics under design conditions, and shows satisfying

agreement in off-design conditions.

In literature, there are numerous examples of CFD being applied to propellers in order to gain insight in flow phenomenas and fluid behaviour. (Huuva & Törnros 2016) has applied RANS to an open propeller and an azimuth thruster in an attempt to capture pressure pulses of higher order with respect to cavitation. Potential flow methods are generally not able to capture such pulses, and it is therefore desired to use CFD. Results showed that the method was able to capture tip vortex cavitation, bubble cavitation, sheet cavitation and root cavitation. However, tip vortex cavitation was somewhat underestimated. Nevertheless, all the mentioned cavitation phenomenas are important with respect to noise and vibrations and can not be picked up using potential flow methods.

At present, there are several programs available for CFD analysis of marine propellers. Examples are Star CCM+, Fluent and OpenFoam. All programs require skilled users in order to gain sufficient accuracy of the analysis. In addition the CFD tools are known to be expensive. However, an exception is OpenFoam which is an open source code.

2.3 Concluding remarks

It has now been presented a thorough literature study regarding numerical propeller modelling. Based on this, Table 2.1 and 2.2 has been made to summarise the main points with respect to the analysis of DEP. It is concluded that within the time frame of this work, lifting line theory is well suited to be used in the analysis.

Table 2.1: Summary of numerical modelling methods based on potential theory and their ability to be used in a DEP analysis

Method	Pros	Cons	Conclusion
Momentum theory	Very simple to implement	Fails to represent blade geometry	Too simple to provide accurate results, but useful to calculate ideal efficiency
BEMT	Simple to implement	Does not account for the interaction effect on one foil section from the other sections	Too low accuracy
Lifting line theory	Fairly simple to implement, includes interaction effects between foil sections	Propeller blade is represented by line segment so best accuracy for thin, lightly loaded propellers	Applicable within the scope of this work
Lifting surface theory	Includes blade geometry to a larger extent than lifting line theory	Not extensively developed codes to use as examples	Considered inapplicable for the time frame of this work as it requires comprehensive code work

Table 2.2: Summary of numerical modelling methods including viscosity and their ability to be used in a DEP analysis

Method	Pros	Cons	Conclusion
RANS	Includes viscous effects, superior accuracy wrt. potential solvers	Requires a lot of CPU and computational time, as well as highly skilled users	Inapplicable within the time frame of this work
Hybrid solvers	Includes viscous effects, high accuracy	Computationally demanding and requires skilled users to handle RANS	Inapplicable within the time frame of this work

Chapter 3

Theoretical background for optimisation of propeller design

The analysis procedure of DEP implies that the geometry of the propeller blades is optimised. This becomes a nonlinear, multi-variable, multi-objective optimisation problem where the objective function should minimise the effect delivered to the propeller(s) and prevent cavitation.

In this work, a built-in algorithm from the optimisation toolbox in MatLab was used. Due to several bounded constraints of the problem, the function called `fmincon` was found appropriate. An internal-point (IP) algorithm is default and was used. It worked well when combined with the quadratic penalty method, which was considered important.

This chapter contains fundamental background theory of optimisation algorithms. Firstly is presented theory regarding IP algorithms, where emphasis has been placed on calculation of step length. In addition, sections regarding particle swarm algorithms and quadratic penalty methods are included since they were used in this work. A discussion of an example from literature where propeller geometry is optimised is also provided in this chapter.

3.1 Interior-point optimisation

IP algorithms were developed for convex nonlinear optimisation problems in the 1960's, but were not widely used (Nocedal & Wright 2006). Success of IP algorithms for linear optimisation resulted in renewed interest for nonlinear optimisation in the late 1990's. IP algorithms have proven to be a successful tool for nonlinear optimisation, and are currently one of the most powerful algorithms for optimisation of large scale problems with many free variables.

Generally speaking, optimisation algorithms are used to find an improved solution of an objective function, based on initial values of its variables. Exceptions are genetic algorithms and particle swarm algorithms, as they usually don't require initial values. The objective is improved using an iterative procedure, where the method used to move from one iteration to the next is depending on the type of algorithm that is used. An IP algorithm for nonlinear optimisation can either be based on line search or trust region strategies. They are two fundamental approaches of optimisation, which both require differentiation of the objective function, and hence initial values.

When searching for an objective for their next iteration, both line search methods and trust-region methods generate steps. However, their treatment of the steps differs. In line search methods, the steps are used to compute a search direction and then a suitable step length in order to minimise the objective function. Trust-region methods define a region within the optimisation problem where it is trusted that the model is a satisfactory representation of the objective function. Then the step is chosen to be an approximate minimiser of the model within this trust region.

The IP algorithm applied in this work uses one of the approaches listed below to generate steps (MathWorks 2017). If the first approach fails, the second is applied.

- Using a Newton step, which involves solving a linear approximation of the problem.
- Using conjugate gradient method

If the reader is interested in a thorough description of IP algorithms, including mathematical expressions, it is further referred to (Nocedal & Wright 2006). A more detailed description regarding the algorithm used in this work is found in (MathWorks 2017).

3.2 Particle swarm optimisation

In this work, Particle swarm optimisation (PSO) was used to find initial values for the IP algorithm, using polynomial representations of the open water characteristics of the Wageningen B-screw series. It is a population based, stochastic optimisation technique that is based on group intelligence and individual intelligence of the members in a population (Hu 2010).

The particle swarm algorithm was firstly introduced by Dr. Eberhart and Dr. Kennedy in 1995. It was developed based on the social behaviour of birds flocking and fish schooling, in addition to some aspects of human behaviour to prevent collision of the particles (Kennedy & Eberhart 1995). One of the fundamental principles for the development of PSO was that social sharing among members in a group offers an evolutionary advantage.

When a population of particles is defined, the particles are programmed to search for the minimal solution of an objective function, within a confined space. They store their current best solution, which is usually referred to as *pbest*. The best global function value is called *gbest*. At each time step the particles are accelerated towards *pbest*. Then, in most cases, the swarm comes closer and closer to the global best function value, which is the desired function value of the optimisation. It can also be mentioned that in more complex versions of PSO, there is included a *lbest*. This is the best function value in the proximity of a particle.

One of the greatest advantages of PSO is that it is easy to solve complicated nonlinear optimisation problems as no differentiation is required. In addition, it is cheap and does not require a lot of computational power relative to more advanced methods.

3.3 Discussion of Literary Example

In (Mirjalili et al. 2015) the use of a multi-objective particle swarm optimisation (MOPSO) algorithm was used to find the optimal propeller design in terms of maximum blade thickness and chord length of foil sections. It was estimated ten NACA foil sections along the propeller blade, which resulted in a total of 20 optimisation parameters as both maximum thickness and chord length were optimised for each section. The objectives were to minimise cavitation and maximise efficiency. Optimal number of propeller blades were determined, and for this blade number the optimal RPM was found. The polynomial representation of K_T and K_Q in the Wa-

geningen B-series was used. (Mirjalili et al. 2015) reports that the MOPSO algorithm was efficient in exploring the search space, and sufficient convergence was achieved.

Comparing the analysis procedure of DEP to the work done by (Mirjalili et al. 2015), the DEP analysis makes the optimisation problem somewhat more complex as the thrust should be sufficiently close to the required thrust for the ship to reach its operational speed. In order to maintain the required thrust, a penalty method is required. The quadratic penalty method is convenient to implement and results in relatively quick convergence. Thus it was decided to use in this work. However, it is not directly applicable with swarm optimisers as they are not based on differentiating the objective function. In addition, the built-in particle swarm algorithm in MatLab only treats single-objective problems. For these reasons, the use of PSO to find the optimal propeller geometry in this work was discarded. A description of the quadratic penalty method is included in the following section.

3.4 Quadratic Penalty Method

Penalty methods are used for constrained optimisation problems (Nocedal & Wright 2006). Then the objective function is replaced by a penalty function that includes the original objective in addition to a penalty term. The penalty term should be zero within the feasible region of the constraint. If the constraint is violated, the objective should be penalised by a penalty. The use of a penalty function implies an iterative procedure, where the penalty should be increased for the minimiser to proceed towards the feasible region of the constraint.

In the quadratic penalty, each penalty is a multiple of the square of the constraint violation. If the original optimisation problem is to minimise a function $f(x)$, subject to the constraint $c_i(x) = 0$ for $i \in \varepsilon$, (Nocedal & Wright 2006) describes the quadratic penalty function as given in Equation 3.1. Where μ is the penalty that is increased for each iteration.

$$Q(x; \mu) \stackrel{\text{def}}{=} f(x) + \frac{1}{2\mu} \sum_{i \in \varepsilon} c_i^2(x) \quad (3.1)$$

Chapter 4

Background theory of propeller modelling

In this chapter is given some fundamental theory and background information required to understand the analysis procedure that has been used in this work. To begin with, a general description of propeller blade geometry is given. Emphasis is placed on the phenomena of induced velocities, as it is important to understand when using lifting line theory. The next section contains an introduction to Xfoil, which is a program used to determine properties of propeller blade sections. Thereafter, a section regarding propeller performance characteristics is provided. In this section some essential performance parameters are explained. The chapter is ended with a section about the Wageningen B-screw propeller series. The foil geometry of this series has been applied to the propellers in the DEP analysis and is therefore provided.

4.1 Propeller blade geometry

A propeller blade consists of foil sections that are stacked in the radial direction of the blade. The thrust and torque of the propeller are directly related to the lift and drag forces acting on the foil sections. Thus some fundamental principles from basic foil theory becomes important when designing and analysing propellers.

Generally, the force exerted from a foil section is normal to the inflow direction on the foil. From this it follows that the exerted force can be decomposed in one vertical lift component and one horizontal drag component. Due to three-dimensional effects there will be alterations of the inflow when foil sections are stacked together. Then the inflow is altered by an induced

velocity component called downwash, commonly symbolised as w_i . The angle between the two-dimensional inflow velocity and the altered inflow velocity is called the induced angle of attack, α_i . The consequence of the downwash is that the pressure distribution around the foil section is altered. Thus the exerted force on the foil section can be decomposed in a vertical lift force and an induced drag force. This is illustrated in Figure 4.1.

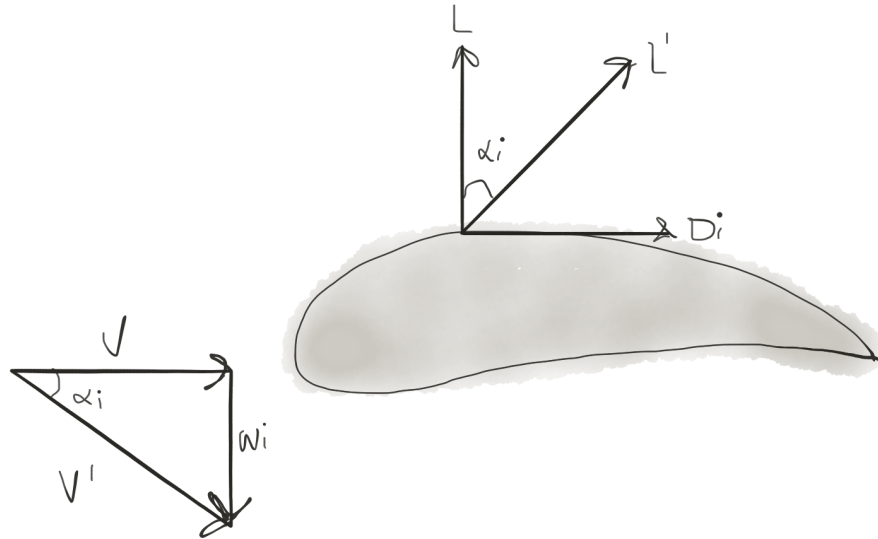


Figure 4.1: Induced drag on a foil section (Steen 2014)

For a propeller blade the concept of induced velocity are the same as described above. However, as the propeller also has a rotational motion, it is convenient to treat the downwash as two separate components; one axial, U_A , and one tangential, U_T . The sectional forces, velocities and angles that are crucial for propeller design and analysis using lifting line theory is illustrated in Figure 4.2. It is assumed that the induced velocities close to the propeller blade are half of their values far behind the propeller.

Xfoil is a useful program for design and analysis of propeller foil sections. It is used in this work to calculate the lift coefficient of the propeller blade sections at zero angle of attack, and to determine the minimum pressure coefficient to be used in cavitation considerations. The next section will make the reader more familiar with this tool.

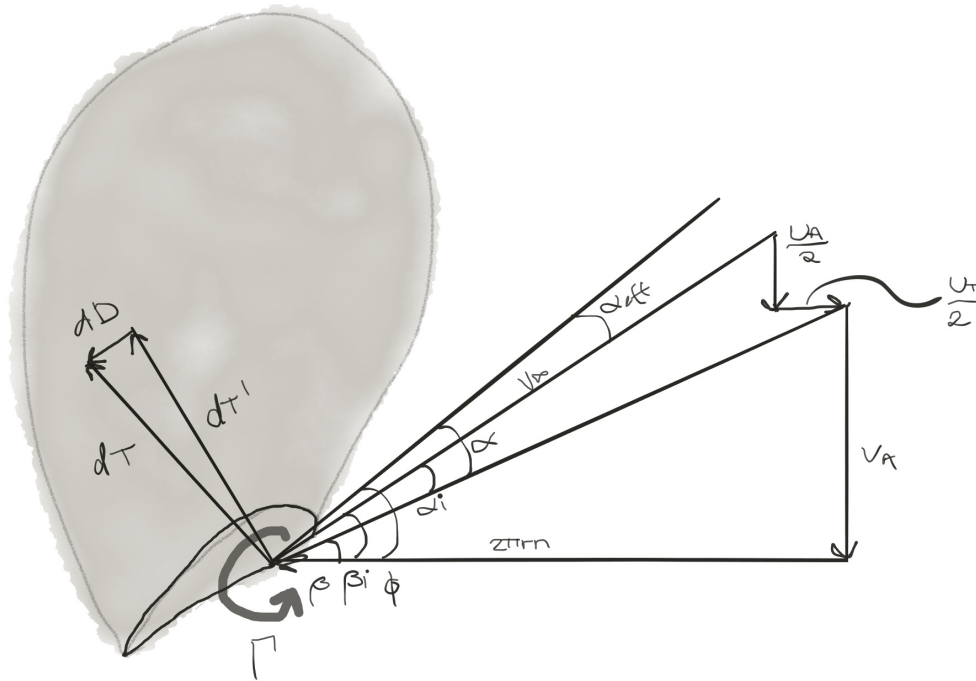
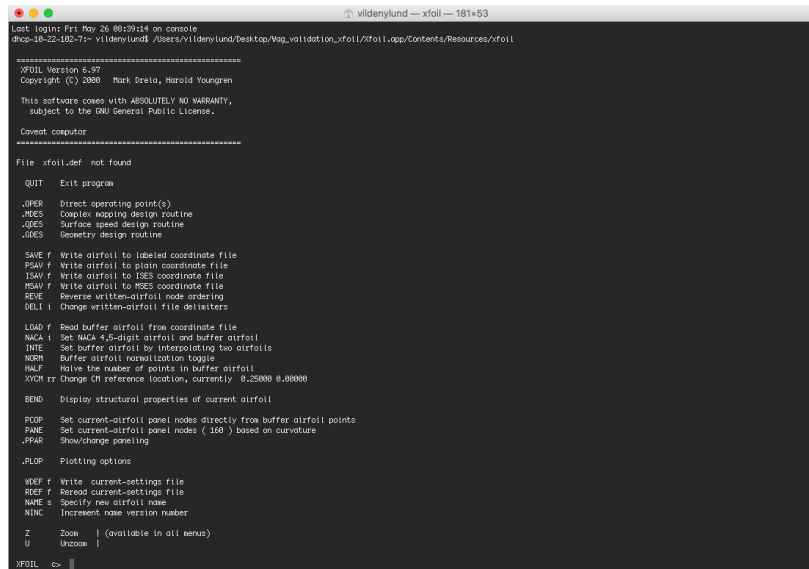


Figure 4.2: Force and velocity components of propeller blade section

4.2 Xfoil

Xfoil is an open source analysis and design tool for airfoils, written by Mark Drela. The main motivation for the development of Xfoil was to provide a more efficient tool to predict low Reynolds number airfoil flow fields (Drela 1989). It has shown to be very useful, and is also applicable to design and analysis of foil sections for marine propellers. One major benefit is that it is possible to run Xfoil via other codes, for example written in MatLab.

Xfoil provides complete polars and surface pressure distributions of foil sections for a given angle of attack, Reynolds number and Mach number. It is an inviscid linear-vorticity panel code, including a Karman-Tsien compressibility correction. Viscous analysis is made possible by superimposing source distributions on the foil and wake, such that the influence of viscous layers on the potential flow is included.



```

Last login: Fri May 26 08:59:14 on console
vildenylund -- xfoil -- 181x53
~/vildenylund/Desktop/Vag_validation_xfoil/xfoil.app/Contents/Resources/xfoil

=====
XFOIL Version 6.97
Copyright (C) 2000 Mark Drela, Harold Youngren

This software comes with ABSOLUTELY NO WARRANTY,
subject to the GNU General Public License.

-----
Convent computer

File xfoil.def not found

QUIT Exit program

.QDES Direct operating point(s)
.MSES Complex mapping design routine
.QDES Surface speed design routine
.QDES Geometry design routine

SAVE F Write airfoil to labeled coordinate file
PSAV F Write airfoil to plain coordinate file
ISAV F Write airfoil to ISES coordinate file
MSAV F Write airfoil to MSES coordinate file
REVI Reverse written-airfoil node ordering
DELI Change written-airfoil file delimiters

LOAD F Read buffer airfoil from coordinate file
NACA I Set NACA 4,5-digit airfoil and buffer airfoil
INTE Set buffer airfoil by interpolating two airfoils
WOPF Buffer airfoil normalization toggle
HALF Halve the number of points in buffer airfoil
XICR rr Change (r) reference location, currently 0.25000 0.00000

BEND Display structural properties of current airfoil

PCOP Set current-airfoil panel nodes directly from buffer airfoil points
PANE Set current-airfoil panel nodes ( 160 ) based on curvature
.PPAR Show/change paneling

.PLOP Plotting options

WDEF F Write current-settings file
RDEF F Reread current-settings file
NAME S Specify new airfoil name
NINC Increase name version number

Z Zoom | (available in all menus)
U Unzoom |

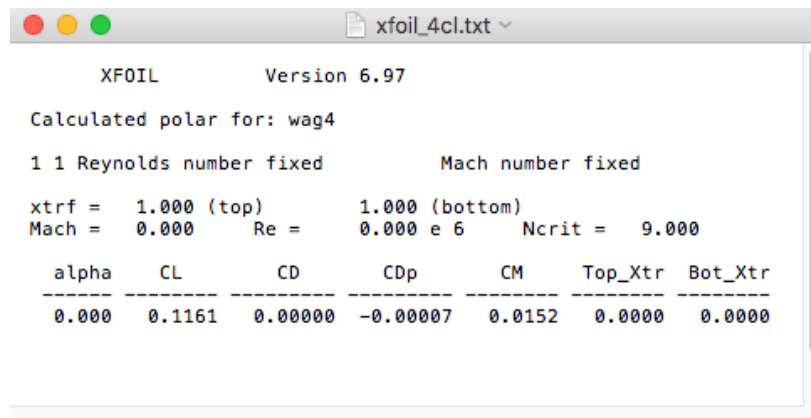
XFOIL >

```

Figure 4.3: Command window in Xfoil

The interface of Xfoil is presented in a terminal window. The analysis is conducted by menu driven routines, where also discretisation and geometry can be altered. The initial menu is illustrated in Figure 4.3 and the discretisation of a foil section is shown in Figure 4.5.

By defining the angle of attack, an inviscid analysis can be performed. Then the pressure around the foil is illustrated as shown in Figure 4.6, together with the data provided in the top right corner of the figure. If viscous analysis is desired for marine applications, the Reynolds number should be defined before the angle of attack. It is possible to export complete polars to text files. This is convenient when Xfoil is coupled to MatLab. An illustrative example of such a text file is given in Figure 4.4.



```

xfoil_4cl.txt
XFOIL      Version 6.97

Calculated polar for: wag4

1 1 Reynolds number fixed      Mach number fixed

xtrf = 1.000 (top)      1.000 (bottom)
Mach = 0.000      Re = 0.000 e 6      Ncrit = 9.000

-----
alpha  CL      CD      CDp      CM      Top_Xtr  Bot_Xtr
-----
0.000  0.1161  0.00000  -0.00007  0.0152  0.0000  0.0000

```

Figure 4.4: Polar exported from Xfoil

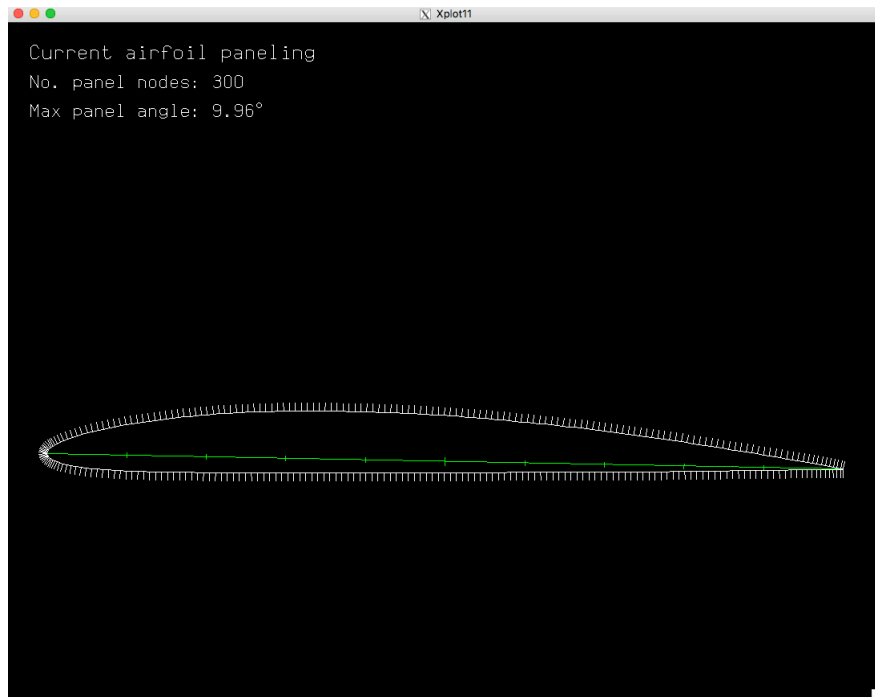
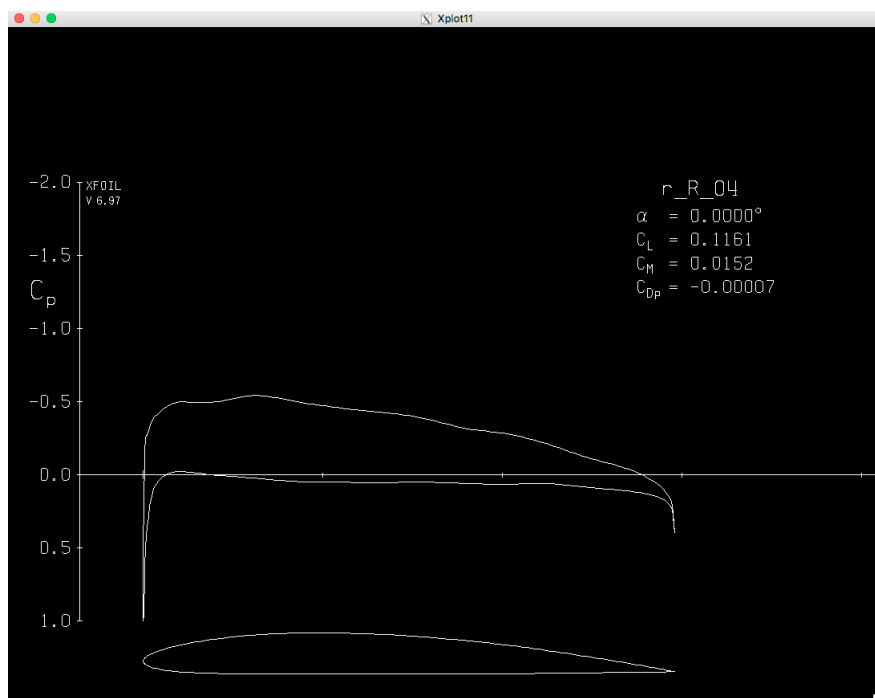


Figure 4.5: Foil section in Xfoil

Figure 4.6: Inviscid analysis in Xfoil for $\alpha = 0^\circ$

4.3 Propeller performance characteristics

For marine propellers it is commonly distinguished between open water performance characteristics and behind-hull characteristics. The open water characteristics are defined when the propeller is working in a uniform fluid stream which is parallel to the shaft centre line (Carlton 2011). From this it follows that the propeller will experience a steady loading. The behind-hull characteristics are based on the propeller working in the wake of a ship hull, where it experiences unsteady loading due to the non-uniform ship wake.

The open water performance are conveniently used to compare propellers as they are not affected by a certain hull shape, and can be determined in model scale. Based on an open water test, all operating conditions of a propeller of a certain geometry can be defined for a variation of pitch to diameter ratios. Results are usually presented in an open water diagram in terms of the non-dimensional characters shown in Equation 4.1 - 4.4, where J is advance number, K_T is thrust coefficient, K_Q is torque coefficient and σ is cavitation number. The propeller open water efficiency can then be calculated as a function of thrust and torque coefficients as shown in Equation 4.5.

$$J = \frac{V_A}{nD} \quad (4.1)$$

$$K_T = \frac{T}{\rho n^2 D^4} \quad (4.2)$$

$$K_Q = \frac{Q}{\rho n^2 D^5} \quad (4.3)$$

$$\sigma = \frac{p_0 - p_v + \rho gh}{0.5\rho V^2} \quad (4.4)$$

$$\eta = \frac{K_T V_A}{2\pi K_Q} \quad (4.5)$$

An open water diagram is given in Figure 4.7. It is desirable to operate the propeller at the combination of rate of revolution and advance velocity for which the efficiency is as high as

possible, as this is the most cost efficient. Open water diagrams are generally subject to scale effects due to boundary layer differences between model and full scale propellers.

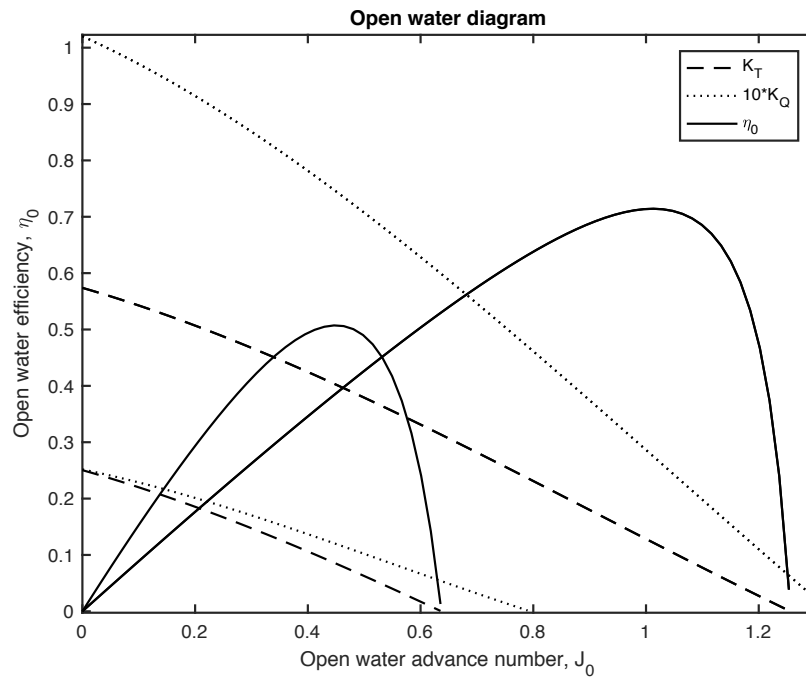


Figure 4.7: Open water diagram for pitch to diameter ratio of 0.6 and 1.2 for a Wageningen B4-80 propeller

Cavitation affects the propeller performance. Negative effects such as thrust loss, blade erosion and hull vibrations are all results of the pressure around the propeller blades dropping below the vapour pressure. According to (Carlton 2011), if cavitation are kept at a moderate level, the impact on the open water characteristics will be minor. However, generally it is strongly desired to completely prevent cavitation.

4.4 Wageningen B-screw series

The Wageningen B-screw series is a widely used propeller series for understanding of preliminary design and propeller performance. The propellers have fixed pitch and are non-ducted. The series is formed by varying the pitch to diameter ratio for a number of screw models (Oosterveld & van Oossanen 1975). Other characteristics such as the diameter, number of blades, blade area ratio and shape of blade sections are constant. The series consists of propellers ranging from 2 to 7 blades, with blade area ratios from 0.30 to 1.05 and pitch to diameter ratios from 0.5 to 1.4.

In (Oosterveld & van Oossanen 1975) is given the foil geometry of the Wageningen B-series as a function of pitch, blade area relationship and blade number. It is convenient within the time frame of this work to use this geometry as it limits the number of variables to be optimised. The blade geometry is presented in Table 4.1 and 4.2.

Table 4.1: Dimensions of Wageningen B-screw propellers with two or four to seven blades (Oosterveld & van Oossanen 1975)

	$\frac{r}{R}$	$\frac{C}{D} \cdot \frac{Z}{A_E/A_0}$	$\frac{a}{c}$	$\frac{b}{c}$	$t_m/D = A - BZ$	
					A	B
Z = 2, 4-7	0.2	1.662	0.617	0.350	0.0526	0.0040
	0.3	1.882	0.613	0.350	0.0464	0.0035
	0.4	2.050	0.601	0.351	0.0402	0.0030
	0.5	2.152	0.586	0.355	0.0340	0.0025
	0.6	2.187	0.561	0.389	0.0278	0.0020
	0.7	2.144	0.524	0.443	0.0216	0.0015
	0.8	1.970	0.463	0.479	0.0154	0.0010
	0.9	1.582	0.351	0.500	0.0092	0.0005
	1.0	0.000	0.000	0.000	0.0030	0.0000

Table 4.2: Dimensions of Wageningen B-screw propellers with three blades (Oosterveld & van Oossanen 1975)

	$\frac{r}{R}$	$\frac{C}{D} \cdot \frac{Z}{A_E/A_0}$	$\frac{a}{c}$	$\frac{b}{c}$	$t_m/D = A - BZ$	
					A	B
Z = 3	0.2	1.663	0.616	0.350	0.0526	0.0040
	0.3	1.832	0.611	0.350	0.0464	0.0035
	0.4	2.000	0.599	0.350	0.0402	0.0030
	0.5	2.120	0.583	0.355	0.0340	0.0025
	0.6	2.186	0.558	0.389	0.0278	0.0020
	0.7	2.168	0.526	0.442	0.0216	0.0015
	0.8	2.127	0.481	0.478	0.0154	0.0010
	0.9	1.657	0.400	0.500	0.0092	0.0005
	1.0	0.000	0.000	0.000	0.0030	0.0000

As shown in Table 4.1 and 4.2, the maximum blade thickness, t_m , can be calculated by means of the constants A_r and B_r when the blade number and diameter is known. The subscript r refers to the fact that the dimensions of the foil sections varies with their radial position on the blade. Other dimensions presented in the tables are a_r which is the distance between leading edge and generator line, b_r which is the distance between the leading edge and location of maximum thickness and c_r which is the chord length.

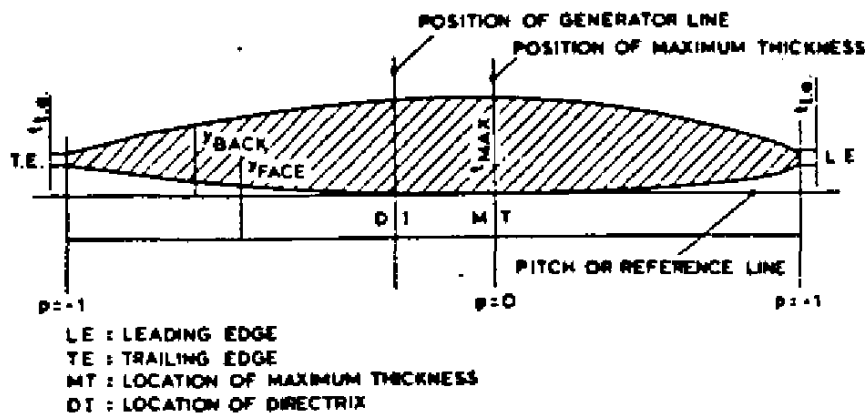


Figure 4.8: Geometric sectional parameters of the Wageningen B-screw series (Oosterveld & van Oossanen 1975)

The coordinates of the blade sections are defined by Equation 4.6 and 4.7, where the non-dimensional parameter, P , is given in Equation 4.8. The definitions of the geometric sectional parameters are illustrated in Figure 4.8. V_1 and V_2 are constants that are given in Figure 4.9 and 4.10, respectively. They are given as functions of radial position and the non-dimensional parameter, P .

$$\left. \begin{aligned} y_{face} &= V_1(t_{max} - t_{t.e.}) \\ y_{back} &= (V_1 + V_2)(t_{max} - t_{t.e.}) + t_{t.e.} \end{aligned} \right\} \text{for } P \leq 0 \quad (4.6)$$

$$\left. \begin{aligned} y_{face} &= V_1(t_{max} - t_{l.e.}) \\ y_{back} &= (V_1 + V_2)(t_{max} - t_{l.e.}) + t_{l.e.} \end{aligned} \right\} \text{for } P \leq 0 \quad (4.7)$$

According to (Oosterveld & van Oossanen 1975), the the trailing edge thickness, $t_{t.e.}$, and leading edge thickness, $t_{l.e.}$, are determined based on rules from classification societies and manufacturer requirements. However, in early stages of a design process such details are not always determined. Then $t_{t.e.}$ can be set to zero if no specific value is known, while $t_{l.e.}$ must be larger than zero for the nose of the foil sections to be a smooth curve. This is important in order to ensure the leading edge pressure to be of unity. In this work both $t_{l.e.}$ and $t_{t.e.}$ was set to zero. However, smoothening functions was applied in MatLab to ensure a smooth nose radius of the blade sections.

$$\begin{aligned} P &= -\frac{(x-b)}{b} && \text{for } 0 \leq x \leq b \\ P &= \frac{x-b}{c-b} && \text{for } b \leq x \leq c \end{aligned} \quad (4.8)$$

r/R \ P	-1.0	-.95	-.9	-.8	-.7	-.6	-.5	-.4	-.2	0
.7-1.0	0	0	0	0	0	0	0	0	0	0
.6	0	0	0	0	0	0	0	0	0	0
.5	.0522	.0420	.0330	.0190	.0100	.0040	.0012	0	0	0
.4	.1467	.1200	.0972	.0630	.0395	.0214	.0116	.0044	0	0
.3	.2306	.2040	.1790	.1333	.0943	.0623	.0376	.0202	.0033	0
.25	.2598	.2372	.2115	.1651	.1246	.0899	.0579	.0350	.0084	0
.2	.2826	.2630	.2400	.1967	.1570	.1207	.0880	.0592	.0172	0
.15	.3000	.2824	.2650	.2300	.1950	.1610	.1280	.0955	.0365	0

r/R \ P	+1.0	+.95	+.9	+.85	+.8	+.7	+.6	+.5	+.4	+.2	0
.7-1.0	0	0	0	0	0	0	0	0	0	0	0
.6	.0382	.0169	.0067	.0022	.0006	0	0	0	0	0	0
.5	.1278	.0778	.0500	.0328	.0211	.0085	.0034	.0008	0	0	0
.4	.2181	.1467	.1088	.0833	.0637	.0357	.0189	.0090	.0033	0	0
.3	.2923	.2186	.1760	.1445	.1191	.0790	.0503	.0300	.0148	.0027	0
.25	.3256	.2513	.2068	.1747	.1465	.1008	.0669	.0417	.0224	.0031	0
.2	.3560	.2821	.2353	.2000	.1685	.1180	.0804	.0520	.0304	.0049	0
.15	.3860	.3150	.2642	.2230	.1870	.1320	.0920	.0615	.0384	.0096	0

Figure 4.9: Values for the constant V_1 of the blade sections in the Wageningen B-screw series (Oosterveld & van Oossanen 1975)

r/R \ P	-1.0	-.95	-.9	-.8	-.7	-.6	-.5	-.4	-.2	0
.9-1.0	0	.0975	.19	.36	.51	.64	.75	.84	.96	1
.85	0	.0975	.19	.36	.51	.64	.75	.84	.96	1
.8	0	.0975	.19	.36	.51	.64	.75	.84	.96	1
.7	0	.0975	.19	.36	.51	.64	.75	.84	.96	1
.6	0	.0965	.1885	.3585	.5110	.6415	.7530	.8426	.9613	1
.5	0	.0950	.1865	.3569	.5140	.6439	.7580	.8456	.9639	1
.4	0	.0905	.1810	.3500	.5040	.6353	.7525	.8415	.9645	1
.3	0	.0800	.1670	.3360	.4885	.6195	.7335	.8265	.9583	1
.25	0	.0725	.1567	.3228	.4740	.6050	.7184	.8139	.9519	1
.2	0	.0640	.1455	.3060	.4535	.5842	.6995	.7984	.9446	1
.15	0	.0540	.1325	.2870	.4280	.5585	.6770	.7805	.9360	1

r/R \ P	+1.0	+.95	+.9	+.85	+.8	+.7	+.6	+.5	+.4	+.2	0
.9-1.0	0	.0975	.1900	.2775	.3600	.51	.6400	.75	.8400	.9600	1
.85	0	.1000	.1950	.2830	.3660	.5160	.6455	.7550	.8450	.9615	1
.8	0	.1050	.2028	.2925	.3765	.5265	.6545	.7635	.8520	.9635	1
.7	0	.1240	.2337	.3300	.4140	.5615	.6840	.7850	.8660	.9675	1
.6	0	.1485	.2720	.3775	.4620	.6060	.7200	.8090	.8790	.9690	1
.5	0	.1750	.3056	.4135	.5039	.6430	.7478	.8275	.8880	.9710	1
.4	0	.1935	.3235	.4335	.5220	.6590	.7593	.8345	.8933	.9725	1
.3	0	.1890	.3197	.4265	.5130	.6505	.7520	.8315	.8920	.9750	1
.25	0	.1758	.3042	.4108	.4982	.6359	.7415	.8259	.8899	.9751	1
.2	0	.1560	.2840	.3905	.4777	.6190	.7277	.8170	.8875	.9750	1
.15	0	.1300	.2600	.3665	.4520	.5995	.7105	.8055	.8825	.9760	1

Figure 4.10: Values for the constant V_2 of the blade sections in the Wageningen B-screw series (Oosterveld & van Oossanen 1975)

The pitch distribution of all propellers in this work was assumed as given in (Steen 2014) for the Wageningen B-screw series. This is illustrated in Figure 4.11.

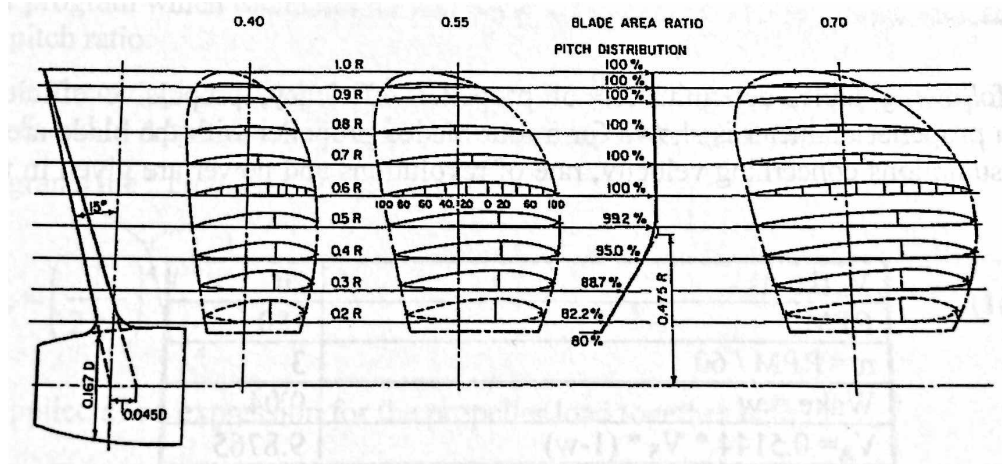


Figure 4.11: Pitch distribution of the Wageningen B-screw series, applied to all propellers in this work (Steen 2014)

(Oosterveld & van Oossanen 1975) has developed polynomials describing the open water characteristics of the Wageningen B-screw series. This was done by regression analysis of the 120 propeller models of the B-screw series. K_T and K_Q can be calculated by Equation 4.9 using the coefficients presented in Table 4.3 and 4.4 for thrust and torque, respectively.

$$K_T, K_Q = \sum_{s,t,u,v} C_{s,t,u,v} \cdot (J)^s \cdot \left(\frac{P}{D}\right)^t \cdot \left(\frac{A_E}{A_0}\right)^u \cdot (Z)^v \quad (4.9)$$

The polynomial coefficients provided in this work are valid for $Re = 2 \cdot 10^6$. Corrections for other Reynolds numbers can be found in (Oosterveld & van Oossanen 1975). However, they have not been used in this work. The polynomials have been useful for validation purposes of the lifting line code. They have also been used to find first values of geometrical properties for the interior-point algorithm. In Chapter 5 about analysis approach is provided more details regarding the validation process.

Table 4.3: Coefficients for K_T polynomial of the Wageningen B-screw series, valid for $R_e = 2 \cdot 10^6$ (Oosterveld & van Oossanen 1975)

Thrust coefficient, K_T									
$C_{s,t,u,v}$	s	t	u	v	$C_{s,t,u,v}$	s	t	u	v
0.00880496	0	0	0	0	0.010465	1	6	2	0
-0.204554	1	0	0	0	-0.00648272	2	6	2	0
0.166351	0	1	0	0	-0.008417228	0	3	0	1
0.158114	0	2	0	0	0.0168424	1	3	0	1
-0.147581	2	0	1	0	-0.00102296	3	3	0	1
-0.481497	1	1	1	0	-0.0317791	0	3	1	1
0.415437	0	2	1	0	0.018604	1	0	2	1
0.0144043	0	0	0	1	-0.00410798	0	2	2	1
-0.0530054	2	0	0	1	-0.000606848	0	0	0	2
0.0143481	0	1	0	1	-0.0049819	1	0	0	2
0.0606826	1	1	0	1	0.0025983	2	0	0	2
-0.0125894	0	0	1	1	-0.000560528	3	0	0	2
0.0109689	1	0	1	1	-0.00163652	1	2	0	2
-0.133698	0	3	0	0	-0.000328787	1	6	0	2
0.00638407	0	6	0	0	0.000116502	2	6	0	2
-0.00132718	2	6	0	0	0.000690904	0	0	1	2
0.168496	3	0	1	0	0.00421749	0	3	1	2
-0.0507214	0	0	2	0	0.0000565229	3	6	1	2
0.0854559	2	0	2	0	-0.00146564	0	3	2	2
-0.0504475	3	0	2	0					

Table 4.4: Coefficients for K_Q polynomial of the Wageningen B-screw series, valid for $R_e = 2 \cdot 10^6$ (Oosterveld & van Oossanen 1975)

Torque coefficient, K_Q									
$C_{s,t,u,v}$	s	t	u	v	$C_{s,t,u,v}$	s	t	u	v
0.00379368	0	0	0	0	-0.0397722	0	3	2	0
0.00886523	2	0	0	0	-0.00350024	0	6	2	0
-0.032241	1	1	0	0	-0.0106854	3	0	0	1
0.00344778	0	2	0	0	0.00110903	3	3	0	1
-0.0408811	0	1	1	0	-0.000313912	0	6	0	1
-0.108009	1	1	1	0	0.0035985	3	0	1	1
-0.0885381	2	1	1	0	-0.00142121	0	6	1	1
0.188561	0	2	1	0	-0.00383637	1	0	2	1
-0.00370871	1	0	0	1	0.0126803	0	2	2	1
0.00513696	0	1	0	1	-0.00318278	2	3	2	1
0.0209449	1	1	0	1	0.00334268	0	6	2	1
0.00474319	2	1	0	1	-0.00183491	1	1	0	2
-0.00723408	2	0	1	1	0.000112451	3	2	0	2
0.00438388	1	1	1	1	-0.0000297228	3	6	0	2
-0.0269403	0	2	1	1	0.000269551	1	0	1	2
0.0558082	3	0	1	0	0.00083265	2	0	1	2
0.0161886	0	3	1	0	0.00155334	0	2	1	2
0.00318086	1	3	1	0	0.000302683	0	6	1	2
0.015896	0	0	2	0	-0.0001843	0	0	2	2
0.0471729	1	0	2	0	-0.000425399	0	3	2	2
0.0196283	3	0	2	0	0.0000869243	3	3	2	2
-0.0502782	0	1	2	0	-0.0004659	0	6	2	2
-0.030055	3	1	2	0	0.0000554194	1	6	2	2
0.0417122	2	2	2	0					

Chapter 5

Analysis Procedure

In this chapter, the approach of the DEP analysis is described. Firstly, the assumptions applied in the calculations are stated. Secondly, the test vessel is presented. Then follows a description of the implementation of lifting line theory, together with some fundamental theoretical principles. Emphasis was placed on creating a lifting line code with sufficient accuracy. In the following section is presented the validation of the lifting line. Then follows descriptions of how the wake, cavitation considerations and optimisation procedure was treated. Uncertainties of the analysis procedure are listed in the next section. The chapter is ended with a section presenting the structure of the code work.

5.1 Assumptions

The assumptions that follows by using lifting line theory are listed in Section 2.1.3. In addition, the analysis in this work is based on the following assumptions

- The nominal model wake of the test vessel is assumed unscaled, and can be applied to full-scale analysis
- The propellers are sufficiently submerged not to disturb the free surface
- The relative rotative efficiency is 1
- Frictional resistance and residual resistance are the only hull resistance components
- The waterline coefficient is 0.84
- Linear foil theory is assumed valid

5.2 Vessel

The test vessel used in this work is the same as in the project thesis. It is called Duisburg Test Case. The hull design is of a typical 14 000 TEU container ship, powered by the use of a single screw propeller (el Moctar et al. 2012). Vessel data used in this work are provided in Table 5.1 together with the sea water density and kinematic viscosity used in this work. Data for the original propeller is given in Chapter 1 in Section 1.1.4 regarding the project thesis.

Table 5.1: Test vessel data

	Model	Full scale
$L_{PP}[m]$	5.976	355
$B_{WL}[m]$	0.859	51
$V[m/s]$	1.669	12.861
$C_B[-]$	0.661	0.661
$C_{WA}[-]$	0.84	0.84
$\rho[kg/m^3]$	-	1025
$\nu[m^2/s]$	-	$1.14 \cdot 10^3$

As stated in the assumptions, the waterline area coefficient, C_{WA} was set to 0.84. In this work it is used for calculating the thrust deduction fractions, t , based on the nominal wake fractions, w . The equation for t is empirical. Within the time frame of this work it was considered sufficient to assume a realistic value of C_{WA} , rather than spending time on finding its accurate value. The rest of the vessel data originates from (el Moctar et al. 2012).

5.3 Lifting line implementation

In the literature study in Chapter 2 was given an overview of the main principles concerning lifting line theory used in propeller design and analysis. In this section follows a more detailed explanation of the analysis approach used to determine the performance of DEP configurations. (John D. Anderson 2011) has outlined a numerical iterative solution for finite-wing properties using fundamental aspects of lifting line theory. There are differences between applying lifting

line theory to marine propellers and finite wings. The main difference is that the downwash is treated as two induced velocity components, which alters the incoming flow to the lifting line. (van Oossanen 1974) has approximated this effect by induction factors in a lifting line approach. Thus in this work, the procedure of (John D. Anderson 2011) has been applied together with the induction factors presented in (van Oossanen 1974).

As previously mentioned in the literature study in Chapter 2, the circulation around each foil section of a propeller blade is, in lifting line theory, lumped into a bound vortex located one quarter from the leading edge. The bound vortices of all foil sections of a propeller blade form a straight line in the radial direction of the blade. The strength of the bound vortices reduces gradually to zero at the blade tip (Steen 2014). This is illustrated in Figure 5.1.

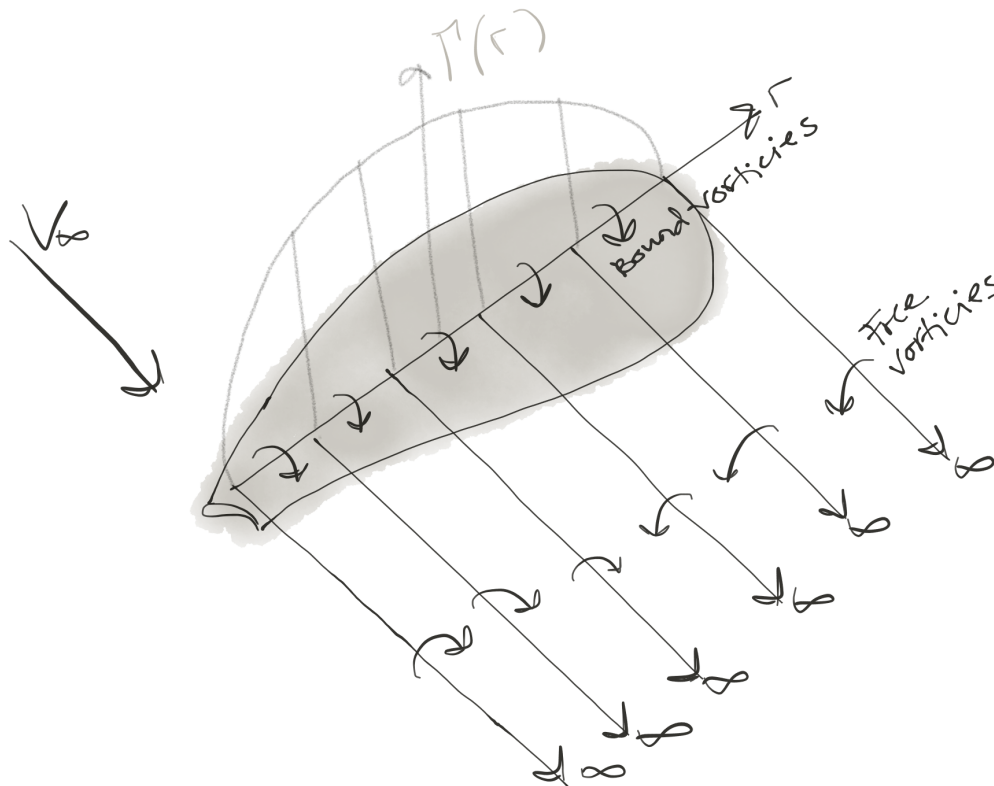


Figure 5.1: Lifting line of propeller blade

The section-wise variation of circulation results in shedding of free vortices with the same strength as the reduction in the bound vortices. This is expressed mathematically in Equation 5.1, where r is in the radial direction of the propeller blade. This behaviour is necessary in order to fulfil Kelvin's theorem.

$$\gamma_F = \frac{\partial \Gamma(r)}{\partial r} \quad (5.1)$$

The free trailing vortex sheets forms helical patterns behind the propeller. A consequence of this is that axial and tangential velocity components are induced. In other words; the section-wise variation of circulation are a three-dimensional effect that leads to induced velocity components, as mentioned in Section 4.1 about propeller geometry.

The propeller induced velocities on the position of a bound vortex can be expressed in terms of Biot Savart's law as Equation 5.2. As seen from the expression, the induced velocity at one section depends on contributions from the free vortices of all the other sections. The coordinate of a fixed position is symbolised r_0 , while r represents running points.

$$U_{A,T}(r_0) = \frac{1}{2\pi} \int_{r_h}^R I_{A,T}(\beta_i, Z, r_0) \frac{\gamma_F}{r_0 - r} dr \quad (5.2)$$

Induction factors, I_A and I_T , were included in Equation 5.2. They account for the fact that due to the propeller having a finite blade number, the induced velocities increase close to the blades compared with calculations for an actuator disk. Other alternatives to using induction factors are Prandtl's method, Goldstein factors and lifting surface methods. The former two alternatives are mainly for simple calculations, and their accuracy was considered too low for this work. Lifting surface methods was discarded for use as they are computationally demanding. (van Oossanen 1974) has defined the induction factors in his work. They can also be found in Appendix A.

In this work Equation 5.2 was solved numerically. Cubic spline interpolation was used to fit the circulation, Γ , to each section of the lifting line, represented by radial position, r_0 . Then the resulting values were used to define Γ as a function of r_0 , and differentiated once to find the strength of the free vortices, γ_F .

Contributions to the induction factors from all radial positions, r , were calculated at each radial position r_0 . When calculating the integrand of 5.2, a singularity occurs when r_0 is equal to r . This was treated by averaging the previous value of the integrand with the next value and extrapolate at the ends. The trapezoidal rule was used to solve the integral numerically. The integration was executed from the hub to the propeller blade tip.

When the induced velocities were calculated with Equation 5.2, the resulting inflow velocity to the propeller and the induced hydrodynamic pitch angle was found using Equation 5.3 and 5.4, respectively.

$$V_{\infty} = \sqrt{(V_A + U_A)^2 + (2\pi r n - U_T)^2} \quad (5.3)$$

$$\beta_i = \arctan\left(\frac{V_A + U_A}{2\pi r n - U_T}\right) \quad (5.4)$$

Knowing the induced hydrodynamic pitch angle, β_i , the effective angle of attack was calculated by subtracting β_i from the pitch angle, ϕ , as seen in Equation 5.5.

$$\alpha_e = \phi - \beta_i \quad (5.5)$$

Since linear foil theory was assumed valid, the contributions to lift from camber and angle of attack was superimposed as shown in Equation 5.6.

$$C_L = 2\pi\alpha_e + C_{Lc} \quad (5.6)$$

The lift coefficient due to camber was calculated in Xfoil via MatLab. The input foil geometry files and command files needed in Xfoil was generated in MatLab as text files. Xfoil exported polars to text files. They were processed in MatLab such that C_{Lc} was obtained for each foil section. In order to save computational time, it was found sufficient to analyse sections from 0.2R to 0.9R, with 0.1R between each section, in Xfoil. At R, the camber lift coefficient was set to zero. C_{Lc} were then interpolated to all N foil sections, using shape-preserving piecewise cubic interpolation.

When C_L was determined, the corresponding circulation was obtained using Kutta Joukowski's theorem and the definition of the lift coefficient. This yields

$$\Gamma = \frac{1}{2}V_{\infty}cC_L \quad (5.7)$$

Since the circulation distribution is input to Equation 5.2 and β_i was required to calculate the induction factors, an iterative procedure was imposed. The values of Γ and β_i used as input

for the next iterations were updated according to Equation 5.8 and 5.9, respectively.

$$\Gamma = \Gamma_{old} + \delta_{\Gamma}(\Gamma_{new} - \Gamma_{old}) \quad (5.8)$$

$$\beta_i = \beta_{i,new} \quad (5.9)$$

δ_{Γ} is a damping factor that was determined such that the iteration procedure was stable and efficient. It was found that $\delta_{\Gamma} = 0.005$ was sufficient.

When the circulation distribution and hydrodynamic pitch angle was found by iteration with an accuracy of four decimals, the thrust and torque could be calculated.

The viscous drag was included in terms of a drag coefficient, calculated by Equation 5.10. It will be shown that induced drag was accounted for by directly including the induced velocities in Kutta Joukowski's theorem. In Equation 5.10, the term $\frac{2t_m}{c}$ represents the form factor of the foil sections (Steen 2014). The lift coefficient was included in the equation to account for the fact that the foil sections of a propeller is asymmetric, i.e. they are producing lift due to camber and angle of attack. Due to the asymmetric shape of the foil sections, the velocity on the pressure side is higher than on the suction side. Since the drag force is proportional to the velocity squared, the increase in drag force due to increased velocity on the pressure side is larger than the reduction on the suction side. Thus, the contribution in the second brackets in Equation 5.10 are increasing the drag coefficient as the lift of the foil sections increases.

$$C_D = 2C_F \left(1 + \frac{2t_m}{c}\right) \left(1 + \frac{C_L^2}{8}\right) \quad (5.10)$$

The frictional resistance coefficient used in Equation 5.10 was calculated using the ITTC'57 friction line as shown in Equation 5.11.

$$C_F = \frac{0.075}{(\log(R_e) - 2)^2} \quad (5.11)$$

The drag force of each foil section was then calculated according to Equation 5.12.

$$dD = \frac{1}{2} \rho V_{\infty}^2 C_D c dr \quad (5.12)$$

Thrust and torque from each foil section were determined according to Equation 5.13 and 5.14, respectively. In Equation 5.13, the thrust of each foil section is reduced by $\rho\Gamma U_T dr$. This represents the induced drag. Similarly is $\rho\Gamma U_A dr$ the addition of torque due to the induced drag.

$$dT = \rho\Gamma(2\pi r n - U_T) dr - dD \sin(\beta_i) \quad (5.13)$$

$$dQ = \rho\Gamma(V_A + U_A) dr \cdot r - dD \cos(\beta_i) \cdot r \quad (5.14)$$

In circumferentially uniform flow, all blades have the same circulation distribution (Kerwin & Hadler 2010). Thus, the resulting thrust and torque from the propeller equals the sum over the lifting line and number of propeller blades.

$$T = \sum dT \quad (5.15)$$

$$Q = \sum dQ \quad (5.16)$$

The performance of each propeller were added together and the total efficiency was calculated. The calculation procedure for the efficiency will be further explained in Section 5.5 regarding the implementation of the wake.

In order to save computational time, a convergence test was conducted for the number of foil sections to be used in the lifting line. A propeller design was chosen randomly, and the lifting line analysis was conducted for various numbers of foil sections. The results are shown in Figure 5.2.

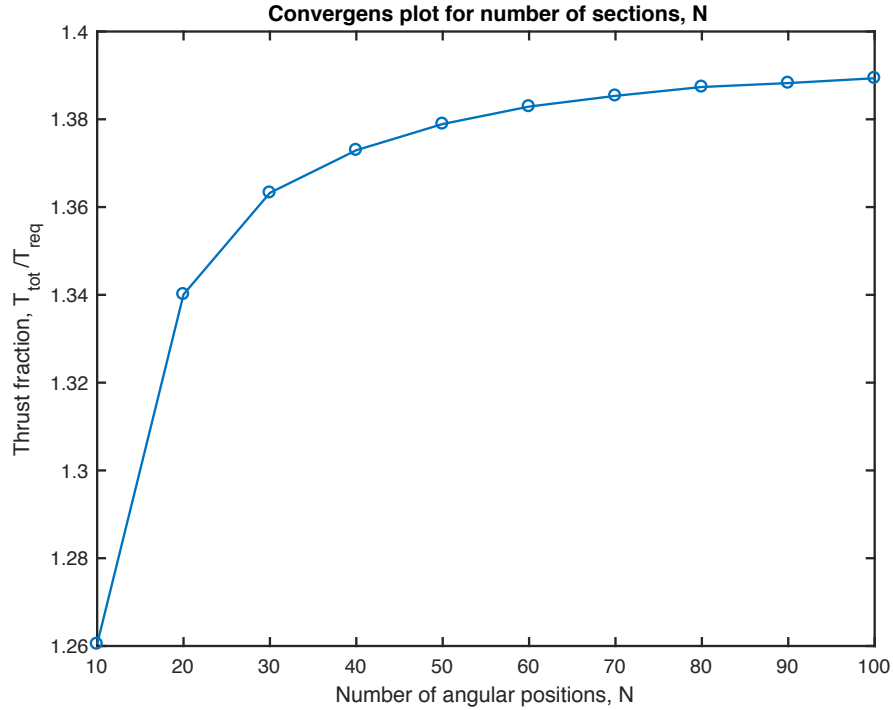


Figure 5.2: Convergence plot for number of foil sections required in lifting line. N is the number of foil sections

The number of foil sections used in the lifting line has not only great influence on the accuracy, but also the computational time. It is highly desired to find the number of foil sections that gives satisfying accuracy within a reasonable time frame. The maximum difference in the resulting thrust fraction of neighbouring points in Figure 5.2 is 1.9 % if calculated for 30 foil sections and above. If results from all numbers of foil sections are included, the difference is 10.2 %. It was therefore considered sufficient to divide the propeller blade into 30 foil sections in the analysis.

Prior to the wake implementation, the lifting line code was validated against the Wageningen B series. The resulting open water diagrams are provided in Appendix B.

5.4 Validation of lifting line

As mentioned in Section 4.4 about the Wageningen B-screw series, the lifting line code was validated against the open water characteristics of the propeller series. The polynomial properties given in (Oosterveld & van Oossanen 1975), was implemented in MatLab, allowing for complete open water diagrams to be plotted. Since the polynomials are valid for $Re = 2 \cdot 10^6$ at 0.7R, the same Reynolds number had to be assured in the lifting line code. To find the Reynolds numbers of the remaining sections, the rate of revolution was first calculated using the Reynolds number of the section at 0.7R.

As induced velocities shall not contribute to the Reynolds number, the inflow velocity to be used in the validation calculations was defined as

$$V = \sqrt{V_A^2 + (2\pi r n)^2} \quad (5.17)$$

where V_A is equal to V_S as effects of the hull are not included in open water characteristics. Rearranging Equation 5.17 yields

$$V = n \cdot \sqrt{(JD)^2 + (2\pi r)^2} \quad (5.18)$$

Solving Equation 5.18 for n and using that $V = (Re v) / c$ gives

$$n = \frac{(Re v) / c}{\sqrt{(JD)^2 + (2\pi r)^2}} \quad (5.19)$$

When the rate of revolution was known, the Reynolds number of the remaining sections was calculated as

$$Re = \frac{n \sqrt{(JD)^2 + (2\pi r)^2} \cdot c}{v} \quad (5.20)$$

From the lifting line code K_T , K_Q and η_0 was calculated for a range of rate of revolutions. The properties were plotted against the open water advance numbers, J_0 , together with the open water diagrams based on the Wageningen polynomials. J_0 was calculated with Equation 4.1 using the ship velocity, V_S , not the advance velocity, V_A . Validation plots comparing the two open water diagrams were made for the propellers given in Table 5.2 for pitch to diameter ratios

of 0.6 and 1.2.

Table 5.2: Propellers from the Wageningen B-screw series that has been used for validation of lifting line code (Carlton 2011)

Z	A_E / A_0													
2	0.30													
3		0.35			0.50			0.65			0.80			
4			0.40			0.55			0.70			0.85	1.00	
5				0.45			0.60			0.75				1.05

A complete set of the validation plots are provided in Appendix B. In Figure 5.3 and 5.4 is presented validation plots for a single screw B4-55 Wageningen propeller for pitch to diameter ratios of 0.6 and 1.2, respectively. The validated results from the lifting line code are subscripted with v .

From the validation plots it is evident that the thrust and torque are somewhat underestimated by the lifting line code. It is also seen that for low pitch, the open water efficiency curve is somewhat offset. This trend was continuous for most of the propellers that were validated. However, some inconsistency was expected and accepted as empirical equations and other simplifications has been used in the lifting line code.

It was expected that the results would deviate from the polynomials for low values of the advance number, J_0 . This is noticeable from Figure 5.4 and 5.3. The reason for this is that lifting line theory are more accurate for lightly to moderately loaded propellers. Thus it was anticipated that the propellers would be too heavily loaded at low advance numbers for lifting line theory to provide results with sufficient accuracy.

The deviations at low advance numbers were not considered to be a problem with respect to the DEP analysis as the propellers were expected to be lighter loaded than a single screw propeller. Since the efficiency were indirectly maximised by minimising the effect delivered to the propellers, the operational point of the propellers were likely to be close to the peak of the efficiency curve. For these advance numbers, the accuracy of the lifting line is considered to be sufficient.

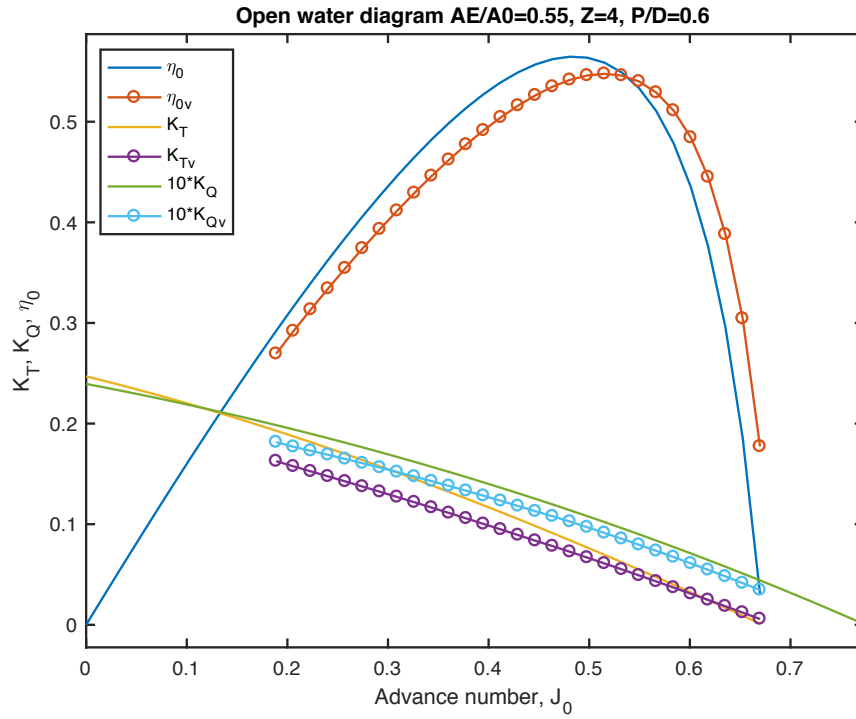


Figure 5.3: Validation plot for Wageningen B4-55 single screw propeller with $(P/D)_{0.7} = 0.6$

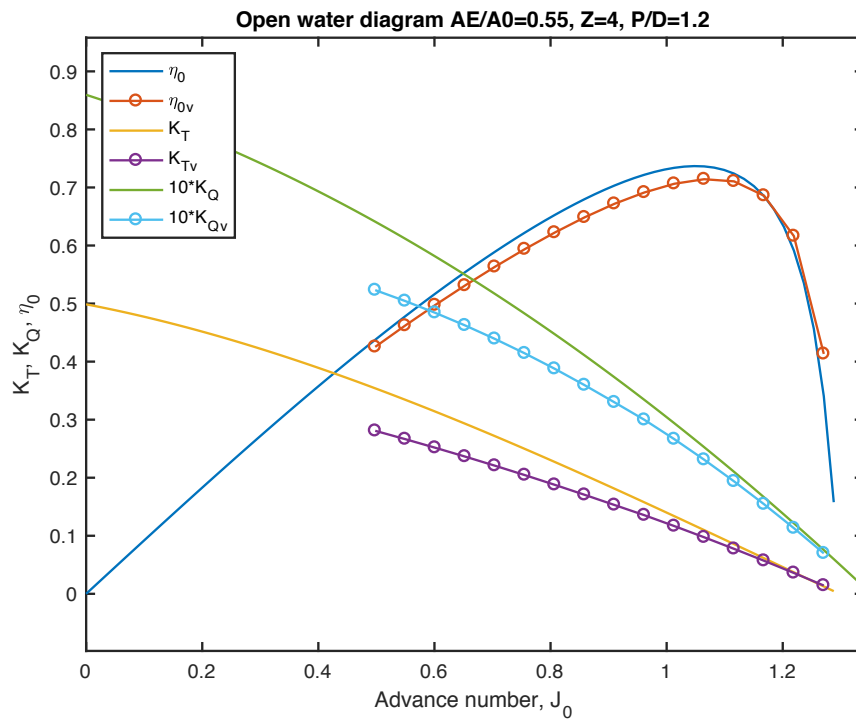


Figure 5.4: Validation plot for Wageningen B4-55 single screw propeller with $(P/D)_{0.7} = 1.2$

From the validation plots it is evident that the deviations in open water efficiencies calculated by the lifting line code and polynomials varies with the geometrical properties of the propellers. This is illustrated in Figure 5.5 and 5.6 for blade area ratios of 0.5 and 0.9, respectively. In the figures, the deviations are presented as functions of pitch to diameter ratios for propellers with blade numbers from two to five. In Equation 5.21 is given the deviation, $\Delta\eta_0$. Most likely, the operating point will be close to the peak of the efficiency curve. Therefore the deviations are calculated as the difference between the maximum open water efficiencies.

$$\Delta\eta_0 = \frac{\max(\eta_0) - \max(\eta_{0v})}{\max(\eta_{0v})} \quad (5.21)$$

In Figure 5.5 it is seen that the accuracy of the open water efficiency is varying from highly overestimated to underestimated as the number of blades increases. This is because the propellers becomes lighter loaded as the number of blades increases. Since lifting line theory is most accurate for moderately to lightly loaded propellers, the underestimation of open water efficiency for two- and three-bladed propellers are likely to be because they are heavily loaded. It is the four-bladed propellers that are most accurately analysed for this blade area ratio. The reason why the open water efficiency of five-bladed propellers are overestimated is likely to be a consequence of the simplifications and empirical relations applied in the lifting line code.

The deviations shows a different behaviour in Figure 5.6, compared to the previous figure. In Figure 5.6, the behaviour from Figure 5.5 is reversed; the open water efficiencies are overestimated for the two-bladed propellers while it is underestimating as the number of blades increases from three to five. The reason for this is that the blade area ratio has been increased, leading to heavier loaded propellers for a given pitch and number of blades.

The original propeller had a blade area relationship of 0.8. It was expected that propellers in DEP configurations would have lower blade area relationship as they would be less loaded. Therefore it was decided, based on the results of Figure 5.5, that emphasis should be placed on analysing four-bladed propellers. It was concluded that comparing results of the same configurations with different number of blades are inappropriate due to the variations in the accuracy between the blade numbers. It is expected to be relatively large variations in pitch for propellers in DEP configurations. Due to large variations in accuracy with pitch for two-bladed propellers, their results are discarded and will not be presented or further discussed in this work.

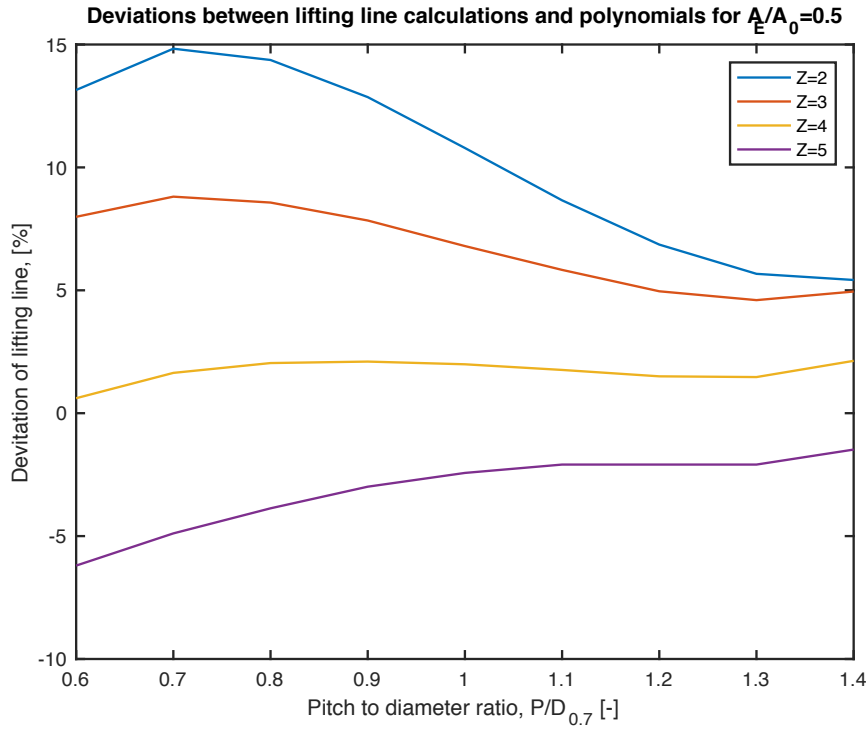


Figure 5.5: Difference between open water efficiencies for $A_E/A_0 = 0.5$

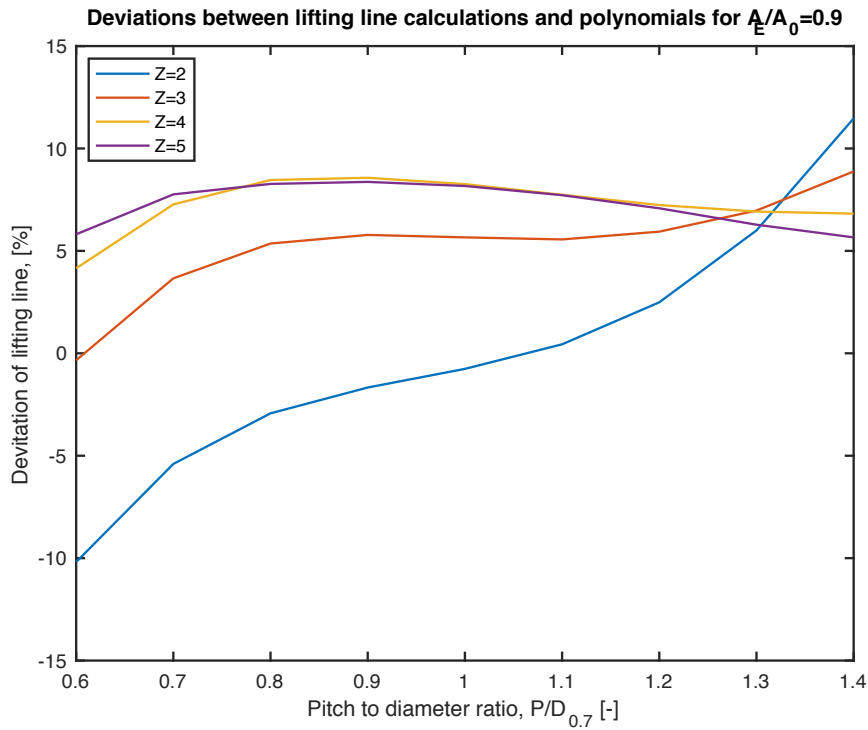


Figure 5.6: Difference between open water efficiencies for $A_E/A_0 = 0.9$

It should be emphasised that ideally both thrust and torque values should be analysed with respect to accuracy, since the open water efficiencies don't deviate if both the thrust and torque are inaccurately predicted by the same factor. However, it is seen from the validation plots that there are no unacceptable deviations between thrust and torque around the peak of the open water efficiency curve. Therefore the analysis presented in Figure 5.5 and 5.6 are considered to be sufficient.

After validating the lifting line procedure, the nominal wake was implemented in the analysis. This will be explained in the following section.

5.5 Wake implementation

The propeller(s) rotates in a non-uniform wake field behind the ship hull. The model scale nominal wake is illustrated in Figure 5.7. It has been used for full scale analysis in this work, in lack of suitable scaling methods for nominal wake. As the wake fractions alters the inflow to the propeller(s), the performance of the blades varies with their angular position in the wake. This implies that more than one lifting line should be applied to capture the effects of the non-uniform wake and gain sufficient accuracy of the analysis.

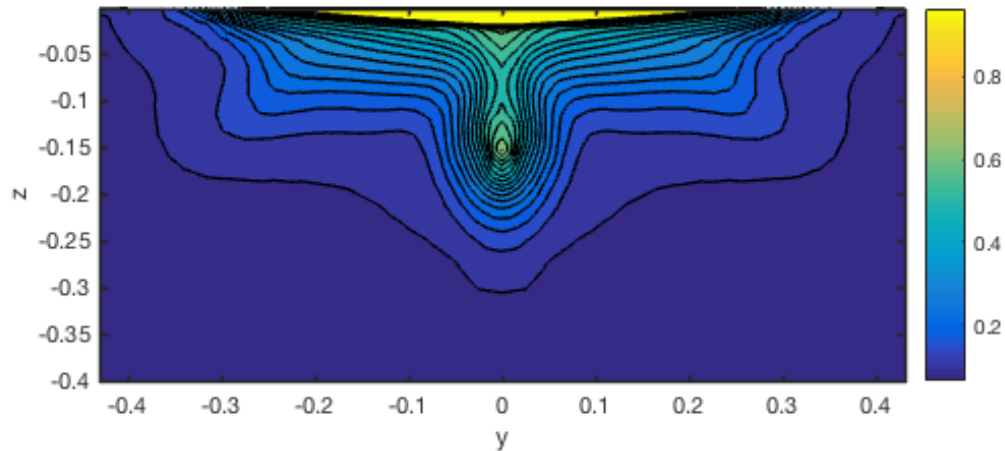


Figure 5.7: Unscaled wake

In order to estimate the wake fractions of the lifting lines of each propeller, the diameter and centre coordinates had to be known. A general equation to determine maximum diameter of each propeller in a grid configuration was derived in the project thesis, and has also been used

in this work.

The number of propellers vertically and horizontally was input to the equation. The grid dimensions was adjusted by visual inspection of the wake. The width was set to $y_{lim} = B_{WL}$ and the height was $z_{lim} = 8.91$ m in full scale, which corresponds to the diameter of the original propeller.

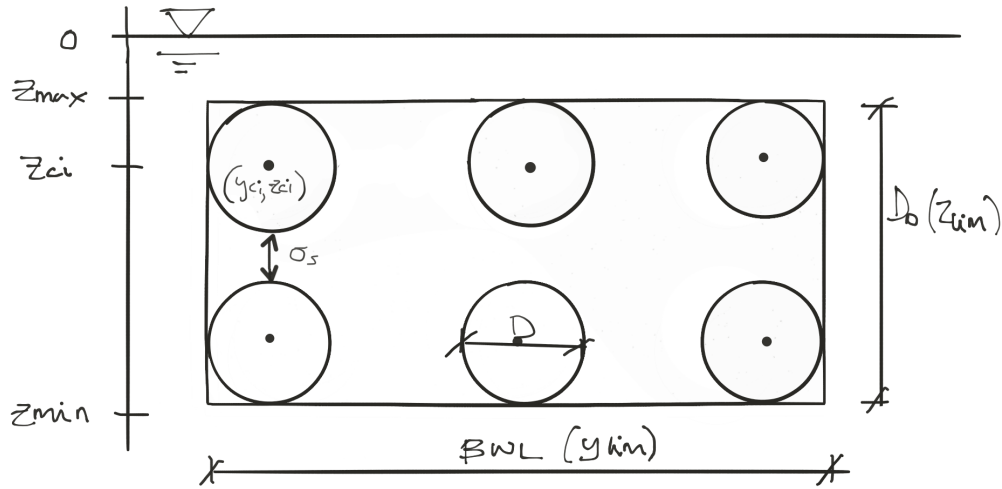


Figure 5.8: Diameter calculation of six propellers where col=3 and row=2

The maximum diameter was limited by either y_{lim} or z_{lim} , depending on how many propellers that were placed horizontally and vertically. Equation 5.23 and 5.24 was used to determine the propeller diameter. A safety factor of $\sigma_s = 0.1 \cdot D$ was applied between the propellers. The variable called row is the number of rows in the grid, while col is the number of columns. In other words row is the number of propellers vertically while col is the number of propellers horizontally. Figure 5.8 illustrates properties of the diameter calculation.

$$D_y = \frac{y_{lim}}{col + (col - 1) \cdot \sigma_s} \quad (5.22)$$

$$D_z = \frac{z_{lim}}{row + (row - 1) \cdot \sigma_s} \quad (5.23)$$

$$D = \min(D_y, D_z) \quad (5.24)$$

The centre coordinates, $(y, z) = (y_{centre}, z_{centre})$, was found by equation 5.25 and 5.26, where

z_{max} is the coordinate of the highest point of the grid.

$$y_{centre} = \frac{D_y}{2} + (col - 1) \cdot (D_y + \sigma_S D_y) - \frac{y_{lim}}{2} \quad (5.25)$$

$$z_{centre} = -\left(z_{max} + \frac{D_z}{2} + (row - 1) \cdot (D_z + \sigma_S D_z)\right) \quad (5.26)$$

When the centre and diameter of all propellers were known, the y- and z-coordinates of the lifting lines was found as

$$\left. \begin{aligned} y_n &= y_{centre} + r \cdot \cos(\theta) \\ z_n &= z_{centre} + r \cdot \sin(\theta) \end{aligned} \right\} \quad \text{For } 0 \leq \theta \leq 2\pi \quad (5.27)$$

Then the wake fractions corresponding to y_n and z_n for a given angular position could be identified from wake data provided by co-supervisor. When the wake fractions of the lifting line was known, the thrust deduction fractions was calculated by the empirical relation given in Equation 5.28 and (Steen 2014).

$$\frac{t}{w} = 1.57 - 2.3 \frac{C_B}{C_{WA}} + 1.5 C_B \quad (5.28)$$

It should be noted that Equation 5.28 is based on single screw propellers. A single screw propeller is generally located within an area of large wake fractions. Thus the application of this equation to the outermost propellers of the DEP configurations is conservative as large wake fractions leads to high thrust deduction, which reduces the propulsive efficiency.

Generally, the wake affects the propulsive efficiency in terms of a hull efficiency as shown in Equation 5.29 for propulsive efficiency. The hull efficiency can be calculated by Equation 5.30.

$$\eta_D = \eta_0 \cdot \eta_H \cdot \eta_R \quad (5.29)$$

$$\eta_H = \frac{1 - t}{1 - w} \quad (5.30)$$

In this work the wake was implemented in the lifting line calculations such that the contribution from the wake fractions to the propulsive efficiency was already included. Thus it was

not the open water efficiency that was calculated from the lifting line analysis. Therefore, only the contribution from the thrust deduction fractions was multiplied by the efficiency calculated in the lifting line calculations to yield the propulsive efficiency.

The thrust deduction fraction was assumed constant for each position of the lifting line, and the values at $0.7R$ was used. Their average value from the lifting lines and number of propellers were used in the expression for total propulsive efficiency. The relative rotative efficiency was assumed to be equal to 1. The equation for the propulsive efficiency, as used in this work, is given in Equation 5.31.

$$\eta_D = \frac{T_{tot} \cdot V_S}{P_{tot}} \cdot (1 - t) \quad (5.31)$$

The delivered effect to each propeller were calculated as $P = 2\pi r n Q$ for all angular positions in the lifting line code. They were averaged and summed over the number of propellers to find the total value of the propulsion system. This was also done for the thrust of each propeller. Total values are subscripted with tot in this work.

In order to evaluate the loading of each propeller and the propulsion system in total, a thrust loading coefficient was introduced. It is given in Equation 5.32 for evaluation of single propellers and Equation 5.33 for evaluation of the total thrust loading of the DEP configurations.

$$C_T = \frac{T}{0.5\rho A_p V_S^2} \quad (5.32)$$

$$C_{T,tot} = \frac{T_{tot}}{0.5\rho n_p A_p V_S^2} \quad (5.33)$$

A convergence test was performed to determine how many angular positions of lifting lines that were necessary to gain satisfying accuracy of the analysis. The results are presented in Figure 5.9.

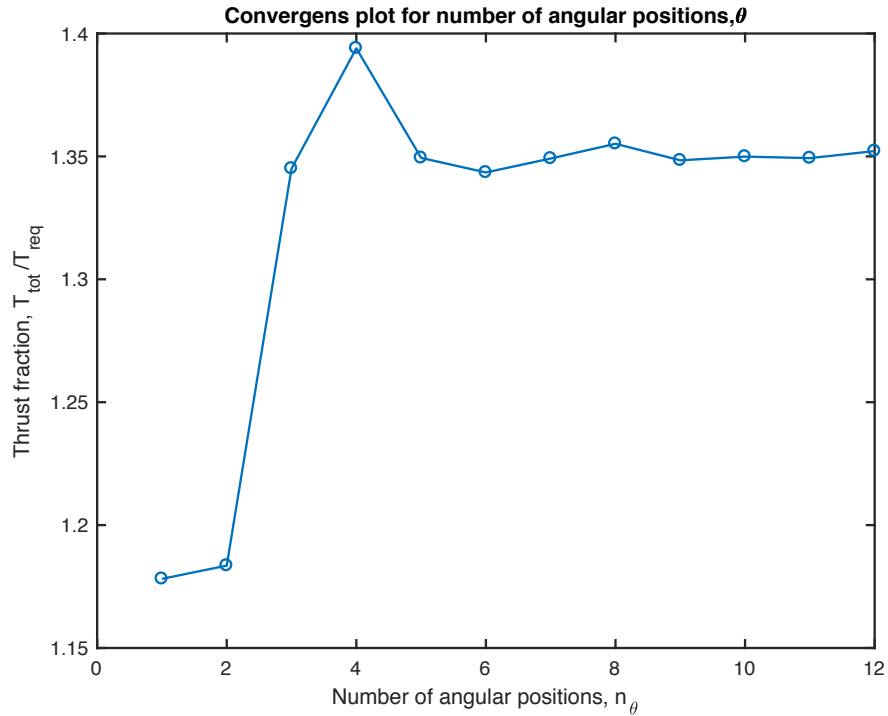


Figure 5.9: Convergence plot for number of angular positions required for lifting line calculations. n_θ is the number of angular positions

As seen from the convergence plot in Figure 5.9, the resulting fraction of thrust and required thrust is similar when the analysis is conducted with a number of angular positions of five and above. The maximum difference between neighbouring points in the plot is 0.9% if the number of angular positions are five and higher, while it is 18.3% if all angular positions are included. The number of angular positions used has great impact on the computational time. Thus it is desired to use as few angular positions as possible, and still gain sufficient accuracy of the analysis. It was concluded that five angular positions was sufficient.

5.6 Cavitation check

In the project thesis it was concluded that cavitation was likely to be a crucial and limiting factor for the propulsive efficiency of DEP configurations. Thus, in this work emphasis was placed on describing cavitation with higher accuracy than in the previous work.

A criteria for a non-cavitating foil section is presented in Equation 5.34. It states that in order to prevent cavitation, the minimum external pressure acting on a foil section must be larger than the water vapour pressure.

$$\sigma > -C_{p,min} \quad (5.34)$$

The cavitation number σ is given in Equation 4.4 in Section 4.3 about propeller performance characteristics. It was in this work calculated with a vapour pressure of 1500 Pa. The submergence of the foil sections was found by subtracting their radial position with respect to the hub from the absolute value of the submergence of the hub.

The minimum pressure coefficient, $C_{p,min}$, was determined in Xfoil. The procedure of the Xfoil analysis was the same as described for lift coefficient due to camber in Section 5.3. In general, the pressure coefficient increases with increasing effective angle of attack. Thus the effective angle of attack determined in the lifting line code had to be included. At the time when the camber lift coefficient was found, it had not yet been determined. Therefore the cavitation predictions involved that Xfoil had to be run two times during the analysis; one to find the lift coefficient due to camber and one to find the minimum pressure coefficient to be used in predictions of cavitation.

Running Xfoil two times increased the computational time significantly. In order to make the analysis more efficient it was found sufficient to check for cavitation when the blade was placed in top position (12 o'clock) only. This is conservative as the submergence of the foil sections are lowest for this angular position. Then the analysis became more efficient since Xfoil was not run for the remaining four angular positions included in the analysis.

The minimum pressure coefficient was determined for foil sections from 0.2R to 0.9R, with 0.1R between each section, and then interpolated to all N foil sections using shape-preserving piecewise cubic interpolation. Thus all N sections were checked for cavitation, and the total

measure of cavitation was the sum of all cavitating sections of all propellers.

An attempt of including cavitation in the quadratic penalty function in this work failed. The reason for the failure was that the effective angle of attack of the blade sections were relatively large, resulting in an unacceptable amount of cavitation on the blade tips. Thus it was concluded that in order to prevent cavitation, the pitch of each propeller had to be adjusted such that the effective angle of attack of the outermost foil section was close to zero when the blade was in top position. This was done in an iterative procedure.

The initial value of the pitch angle in the analysis was calculated by Equation 5.35. It was first attempted to force the effective angle of attack of the section at $0.7R$ to be close to zero. This improved with respect to cavitation. However, in order to prevent it, the effective angle of attack of the outermost section had to be forced close to zero instead of the section at $0.7R$. The pitch to diameter ratio of the outermost section is given by Equation 5.36.

$$\phi_{1.0} = \tan^{-1}\left(\frac{V_s}{2\pi R n}\right) \quad (5.35)$$

$$\left(\frac{P}{D}\right)_{1.0} = \frac{2\pi R \cdot \tan(\phi)}{D} \quad (5.36)$$

From Figure 4.2 in Chapter 3 about theory for analysis it is clearly depicted that for the effective angle of attack to be zero, the pitch angle, ϕ , must equal the hydrodynamic pitch angle, β_i . It was decided that if the pitch angle was within 1% of the induced hydrodynamic pitch angle calculated in the lifting line analysis, the iteration procedure was completed. If the requirement for the pitch angle was not met, the pitch angle for the next iteration was set equal to the induced hydrodynamic pitch angle calculated in the current iteration. This procedure was successful with respect to cavitation. The iterative procedure was relatively efficient, requiring around six iterations per propeller to converge.

The effect of requiring the effective angle of attack of the outermost foil section to be zero is illustrated in Figure 5.10. These figures are from the pitch iteration procedure of a four-bladed single screw propeller. They depict the minimum negative pressure coefficient and the cavitation number resulting from the first and last iteration, respectively.

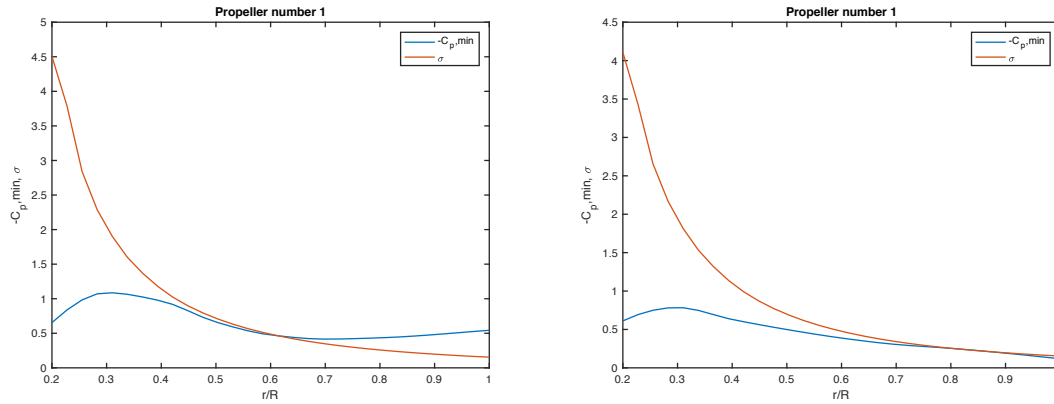


Figure 5.10: Cavitation plots before and after reducing α_e of the outermost blade section 12 o'clock, for a single screw four-bladed propeller

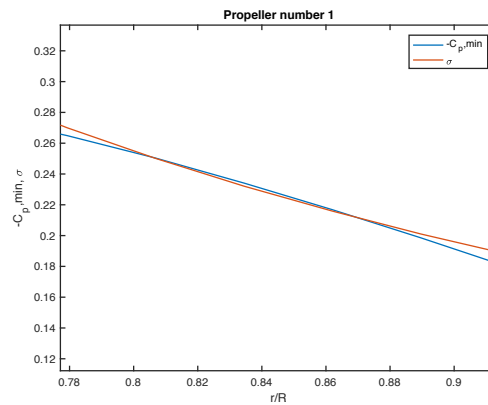


Figure 5.11: Cavitating part of cavitation plot for a single screw four-bladed propeller, when α_e has been reduced

Even though in this case cavitation could not be prevented, it is clearly seen that it is significantly reduced in the last iteration with respect to the first. The slightly higher minimum negative pressure coefficients for radial positions around $0.8R$ to $0.9R$ resulted in cavitation of three foil sections. This is illustrated on Figure 5.11

5.7 Optimisation procedure

As previously mentioned in Chapter 3 about optimisation theory, optimisation algorithms was used in order to determine the most efficient propeller designs for the DEP configurations. In MatLab, there are various built-in optimisation algorithms in the optimisation toolbox. In this work, it was decided to make use of these as it allowed for more time to be spent on other parts of the code work.

The objective of the optimisation was to minimise the effect delivered to the propellers, without any cavitation on the blades and with the propellers providing the required thrust to maintain the operational speed of the ship. In the project thesis, the required thrust was calculated by Froude scaling. It was assumed that frictional resistance and residual resistance was the only resistance components. The required thrust was then 1453.3 kN, which has been used in this work.

The thrust was decided to be sufficient within an interval of 3% of the required thrust. This constraint was imposed using the quadratic penalty method. It implied that the optimisation had to be part of an iterative procedure, which was completed when the thrust was within the feasible region of the constraint. Mathematically the objective function, including the penalty term, was formulated on dimensionless form as

$$obj = \min \left(\frac{P}{T_{req} \cdot V_S} + \mu_T \left(1 - \frac{T}{T_{req}} \right)^2 \right) \quad (5.37)$$

where μ_T is the penalty for not choosing the required thrust. For each iteration where the thrust constraint was violated, the penalty were increased by a factor of 15. The process of defining the penalty was cumbersome, as it was based on trial and failure, as well as experience. Firstly setting a low penalty and then increasing it to check if the number of iterations required could be lowered, was a time consuming process. It was found that starting with a penalty of 0.02 was satisfactory as it resulted in around four iterations for most DEP configurations.

The function `fmincon` in MatLab was used for optimisation of propeller geometry. This implied that initial values of the optimisation variables had to be determined. A particle swarm algorithm was used to find the initial values from the Wageningen B-screw open water polynomials given in (Oosterveld & van Oossanen 1975). The particle swarm algorithm was chosen as

it does not require any initial values and was convenient to implement. Since the initial values were based on open water data, it was found by trial and failure that more appropriate initial values was achieved by reducing the values from the particle swarm algorithm by 30%.

The `fmincon` function can be used on constrained, non-linear, multi-variable optimisation problems. As mentioned in Chapter 3 about the theoretical background for the optimisation procedure, it is especially useful for large scale problems. This was considered an advantage as the optimisation problem for DEP configurations with many propellers becomes relatively large. When the particle swarm algorithm was used, a built-in function named `particleswarm` was called in MatLab. It was decided to use a swarm of 100 particles as a larger swarm was not necessary to provide sufficient initial values.

The rate of revolution was optimised for each propeller, while all propellers were optimised to have the same blade area relationship in each configuration. For simplicity, the rate of revolution was made non-dimensional by the open water advance number as this was convenient with respect to the initial values. Bound constraints were imposed on the variables to ensure that they were determined within realistic values. Lower boundaries for blade area relationship and open water advance number was 0.3 and 0.4, respectively. The upper boundaries were 1.05 and 5 for blade area relationship and open water advance number, respectively. If values very close to the boundary were chosen for the optimal solution, it would most likely have been a more optimal solution outside the boundaries. Therefore, it was checked that no resulting geometry was at the ends of the boundaries. Thus they were considered sufficient.

The symmetry of the wake was exploited to make the optimisation process more efficient. This means that propellers placed within the same wake fractions were set to have the same geometry. An example of this is the configuration of three propellers, shown in Figure 5.12. Propeller number 1 and 3 are located within the same wake fractions. Thus in the analysis of this configuration only the propeller geometry for propeller number 1 and 2 was optimised, as the optimal geometry for propeller number 3 is the same as for propeller number 1.

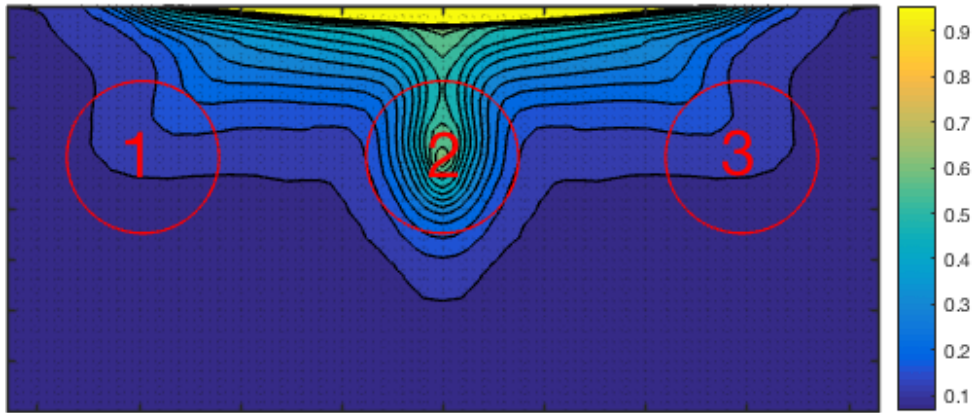


Figure 5.12: Outline of three propellers placed in the ship wake

Generally speaking, the number of iterations required for convergence of the IP algorithm was between 10 and 20. The optimisation process could be monitored graphically. Then the value of the objective function was plotted for each iteration as the optimisation was proceeding. In Figure 5.13 is given an example of such a plot. This is the last iteration of the quadratic penalty procedure for seven four-bladed propellers in one row. Thus the function value of iteration number 20 is the resulting objective value of the complete analysis of this DEP configuration.

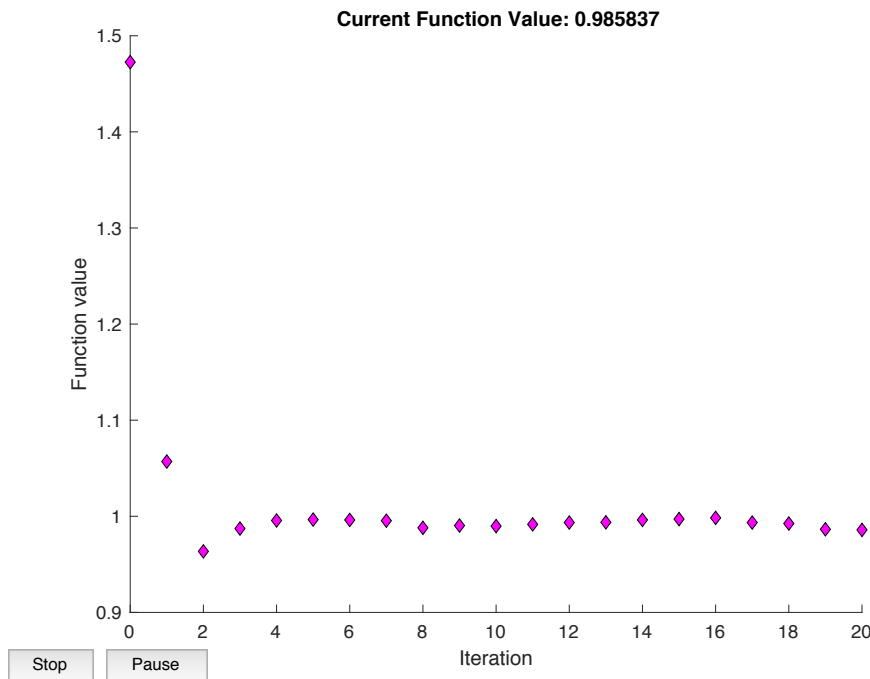


Figure 5.13: optimisation procedure for seven four-bladed propellers in one row

The optimisation worked well for most configurations. However, for some configurations of propellers with two and five blades the algorithm failed to converge. Then the step size was decreased from $1 \cdot 10^{-3}$ to $1 \cdot 10^{-4}$. This increased the computational time significantly, but the algorithm converged. It has been shown in Section 5.4 regarding validation of the lifting line that the results for two- and five-bladed propellers are somewhat uncertain. Thus, since these results alone were not decisive when evaluating the effects of DEP, the step size was not reduced for the configurations that converged with $1 \cdot 10^{-3}$.

An attempt to use an unconstrained line search algorithm to check if the results corresponded with those from the IP algorithm, failed after a couple of iterations. It was also noticed that the computational time of each iteration was long compared to the interior point algorithm. Thus it was concluded that the IP algorithm was preferable within the time frame of this work.

5.8 Uncertainties

Based on the analysis procedure that has been presented in this chapter, the following uncertainties are likely to affect the resulting efficiencies of the DEP configurations:

- There are discrepancies in the open water diagrams from the lifting line and Wageningen B-screw polynomials. Thus the use of the lifting line itself provides some uncertainty. An attempt of quantifying this is given in Section 5.4 for number of blades varying from two to five
- The thrust deduction fractions were calculated based on an empirical relation for single screw propellers. It depends on the water plane area coefficient, C_{WA} , which was assumed to be 0.84. The use of an equation aimed at single screw propellers are conservative for propellers in DEP configurations
- The variations of the thrust deduction across the lifting lines was neglected
- No convergence test regarding properties such as step length was conducted for the optimisation algorithm. Consequently, there may be solutions that are more optimal

5.9 Code structure

In this section follows a description of the code work. This is to provide a better understanding of how the parts mentioned in the above sections are coupled together. In Appendix C is provided the codes with the lifting line analysis that has been used in this work. A complete set of codes has been attached in a digital appendix. Figure 5.14 is an overview over how these are coupled together. Each code are saved as .m-files as they are programmed in MatLab.

From the `optimisation.m` script, the optimisation is initiated. This script contains the particle swarm algorithm that finds the initial values, as well as a while-loop where the functions `runnested.m` and `main_no_opt.m` are called, and the quadratic penalty is adjusted. The while-loop is completed when the thrust is within 3% of the required thrust. The `runnested.m` function is a so-called nested function, which means that a function is completely defined within another function. This was necessary in order to pass the quadratic penalty and the required thrust into the objective function from the `optimisation.m` script. In `runnested.m` the optimisation algorithm are called by the built-in function called "fmincon" and all the optimisation properties are defined. The `main_no_opt.m` function contains the same codes as the `runnested.m` function, except those who are optimisation related. Thus this is not a nested function. After the optimisation is completed, this function is called in order to get the output required for the while-loop in `optimisation.m` to continue.

In the functions `runnested.m` and `main_no_opt.m` are properties independent of which propeller that is analysed firstly defined. Such properties are input data of the test vessel and environment, diameter of the propellers, variables and nominal wake. Then a for-loop is introduced around all the functions with outputs that depends on which propeller in the configuration that is analysed. Firstly is the initial pitch angles introduced. Then a while-loop is initiated. It adjusts the pitch in order to achieve a sufficiently low effective angle of attack. Within this loop, the geometry of the propellers is obtained and used as input in the `xfoil.m` function to calculate the lift coefficient due to camber. In the `xfoil.m` function, the foil coordinates of each foil section is calculated and then Xfoil is ran from the script to calculate the camber lift coefficient based on the foil coordinates.

The `analysis_nested.m` is called in the `runnested.m` function while the `analysis.m` is called

in the `main_no_opt.m` function. When they are completed, the induced hydrodynamic angle of attack, β_i , are compared with the pitch angle, ϕ , to check if the effective angle of attack is small enough. If ϕ is outside the range of 1% of β_i , the effective angle of attack is considered too high and a new iteration is initiated. This is done by setting the variable called `search_pitch` to 0. ϕ is then updated to be equal to the β_i calculated in the previous iteration. If ϕ are within the acceptable range of β_i , the effective angle of attack is considered sufficiently low and the iteration procedure is completed by setting `search_pitch` to 1.

In the `analysis.m` and `analysis_nested.m` function, the performance of each propeller is analysed. The difference between them is that cavitation predictions are included in `analysis.m`. The reason why it is not in `analysis_nested.m` is that cavitation are implicitly included in the optimisation by adjusting the pitch to force the effective angle of attack close to zero. Thus non of the output variables from the cavitation check are required in the objective function, and significantly computational time is saved as the `cavitation_check.m` function involves running Xfoil.

The `analysis.m` and `analysis_nested.m` functions analyses the propeller performance at each angular position, θ . The analysis contains the function `LL_wake.m` which extracts the wake fractions of the lifting line located at the angular position that is evaluated. Then the wake fractions are input to the `LL_iter.m` which contains the lifting line code that analyses the propeller performance in terms of thrust and torque. In this function, the `induction_factors.m` function containing the induction factors are called. The factors are calculated for all radial positions when located at a specific position. Thus a double for-loop is required.

As previously mentioned, it is only in the `analysis.m` function that it is checked for cavitation using the `cavitation_check.m` function. The function is called for the first angular position, which is when the blade is in its top position (12 o'clock). In `cavitation_check.m`, Xfoil is ran for radial positions up to the blade tip and minimum pressure coefficient, C_p , is imported into MatLab. The number of foil sections that are cavitating are determined in this function.

The thrust and delivered power to each propeller are evaluated in the `runnested.m` and `main_no_opt.m` functions. When imported from the `analysis_nested.m` or `analysis.m` they are matrices with values for each angular position for each propeller. Their resulting values are taken as the average over angular positions for each propeller, and the sum over all propellers. Then the resulting propulsive efficiency can be calculated based on these values.

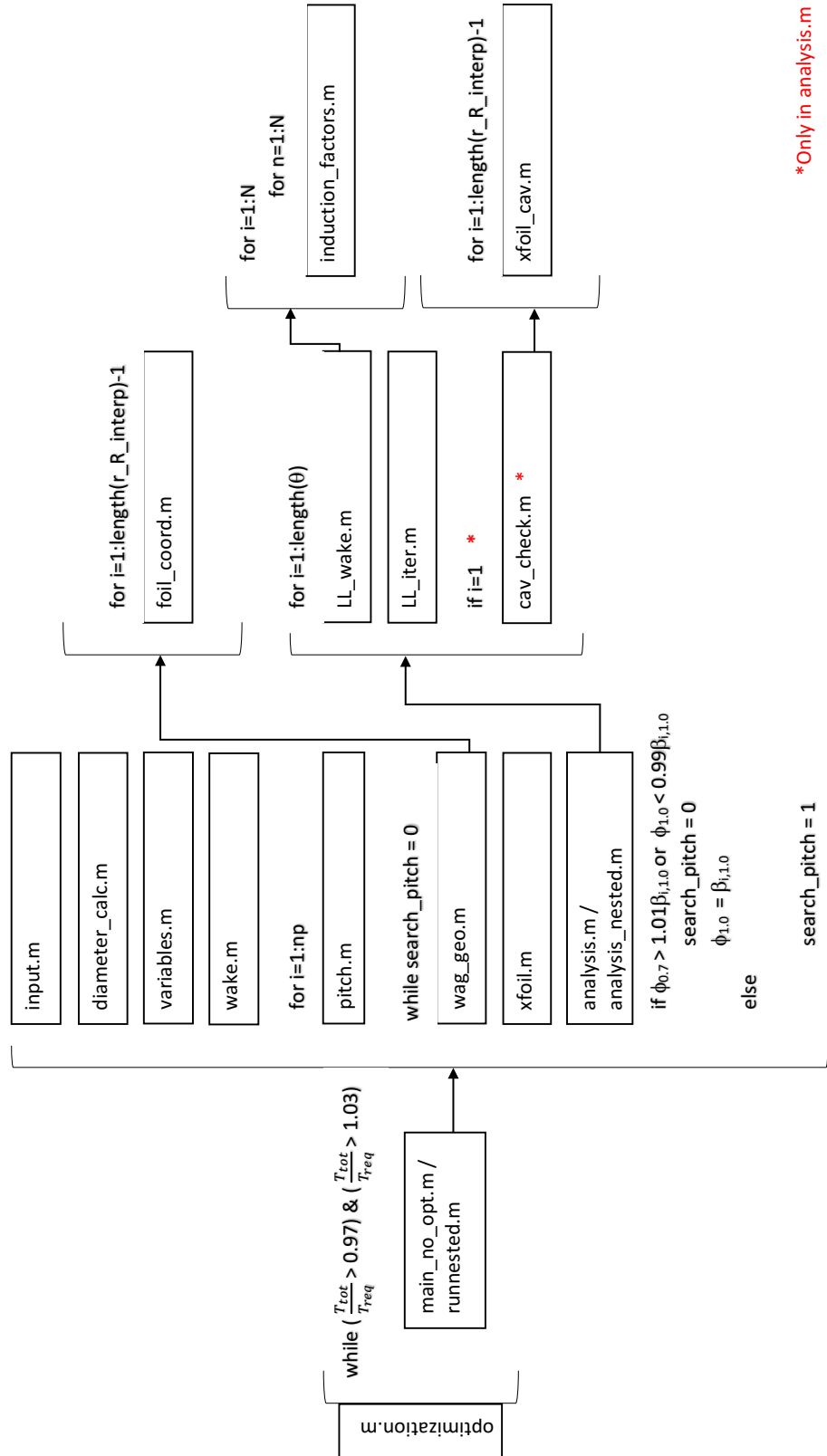


Figure 5.14: Code structure

Chapter 6

Results

In this chapter is presented the results of the analysis of DEP configurations. Emphasis was placed on analysing grid configurations distributed over one row. In Table 6.1 is presented an overview of the configurations that were analysed, as well as the resulting diameter and propeller disk area of the propellers. The propeller disk area, A_p , was calculated as $\frac{\pi}{4} \cdot D^2$. The configurations in Table 6.1 were analysed for propellers with number of blades varying from three to five.

Table 6.1: Grid configurations analysed for propellers with three to five blades

Row	1	1	1	1	1	1	1	1	1
Col	1	2	3	4	5	6	7	8	9
D [m]	8.91	8.91	8.91	8.91	8.91	7.85	6.71	5.87	5.21
$A_p[m^2]$	62.36	124.72	187.08	249.44	311.80	290.43	247.84	216.15	191.65

In addition, further analysis of four-bladed propellers was conducted for the following configurations:

- two rows, with two and three propellers horizontally in each row
- five propellers in one row, within a compressed horizontal domain
- T-configuration with seven propellers above one large

This chapter is organised as follows; firstly is presented results based on potential theory for the configurations presented in Table 6.1. Secondly, resulting propulsive efficiencies and

hull efficiencies are presented for three- to five-bladed propellers. Then is given the results of additional configurations of four-bladed propellers, mentioned in the above list. The chapter is ended with a detailed presentation of the most efficient configuration. This includes propeller geometry, performance details of each propeller and cavitation considerations.

6.1 Potential theory

Total thrust loading coefficient and ideal efficiency was calculated with Equation 5.33 and 2.1, respectively, for the configurations presented in Table 6.1. It should be noted that effects of propeller geometry are not included in potential theory. Thus these results are for comparison only. In Figure 6.1 and 6.2 is plotted the total thrust loading coefficient, $C_{T,tot}$, versus total propeller disk area and number of propellers, respectively. According to potential theory, the configuration with five propellers has the lightest loading, with a thrust loading coefficient of 0.0537. This is 26% lower than the configuration with four propellers, 10% lower than the configuration with six propellers and 28% lower than the configuration with seven propellers.

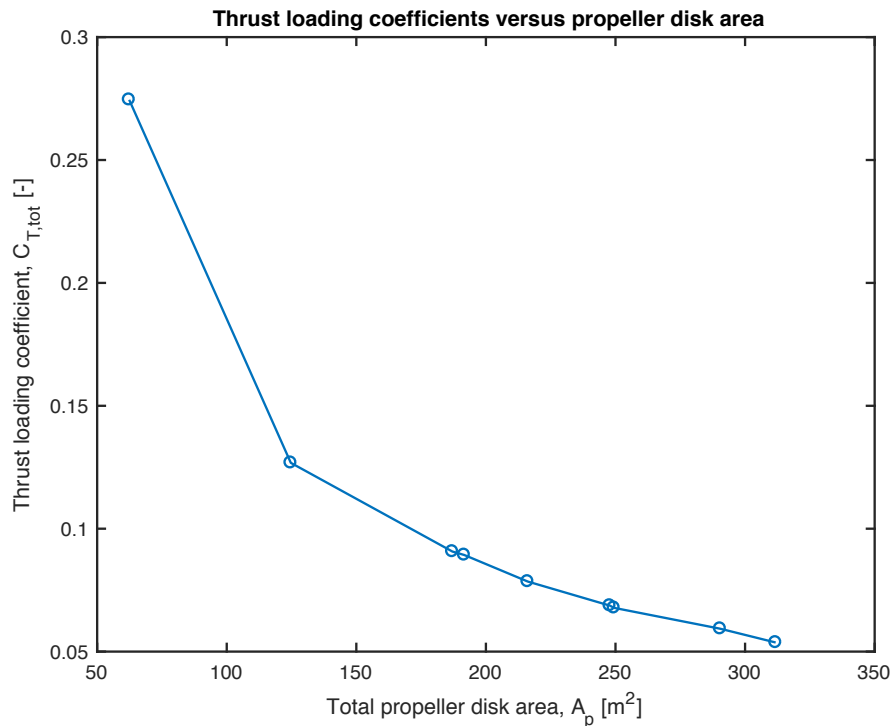


Figure 6.1: Thrust loading versus total propeller disk area

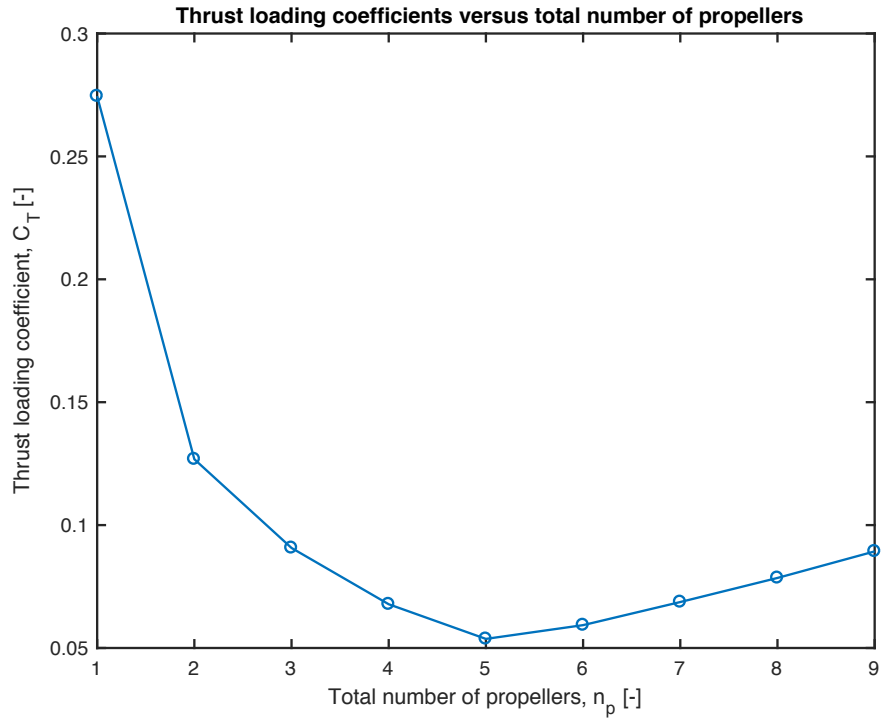


Figure 6.2: Thrust loading versus number of propellers

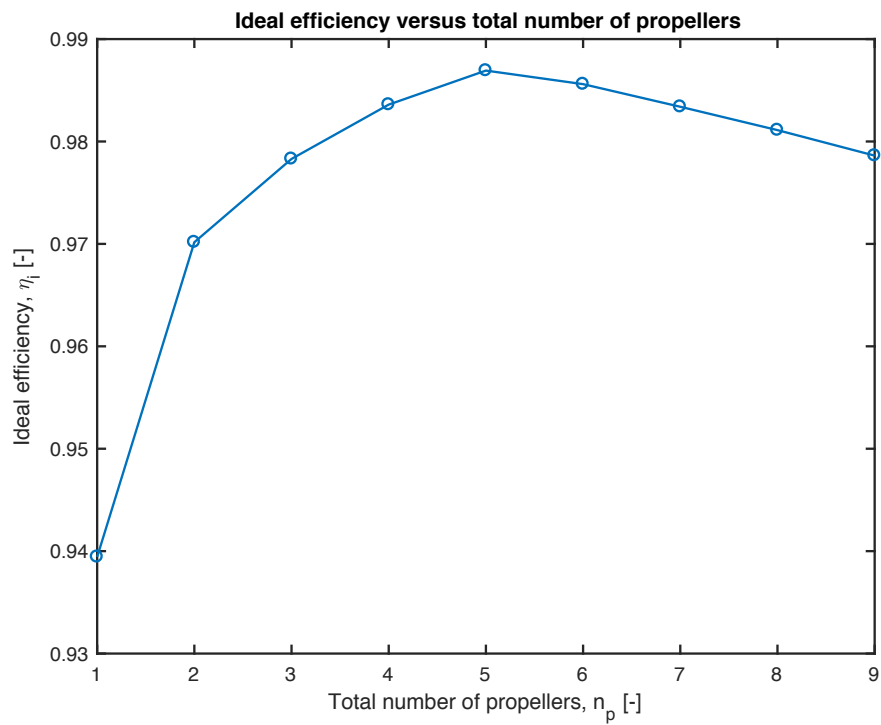


Figure 6.3: Ideal efficiency versus number of propellers

In Figure 6.3, the ideal efficiency is plotted against the number of propellers. It is increasing with reduced loading. Thus the configuration of five propellers has the highest ideal efficiency, which is slightly below 99%. It should be noted that there is a difference of 4.75% between the ideal efficiency of the single screw propeller and the maximum ideal efficiency.

6.2 Grid configurations with three- to five-bladed propellers

In this section is presented the resulting efficiencies of the grid configurations in Table 6.1, for three- to five-bladed propellers. Lifting line theory and an optimisation algorithm was used in the analysis to determine performance and optimal geometry, respectively. The procedure is explained in the previous chapter. Total propulsive efficiencies of the configurations are plotted against the number of propellers in Figure 6.4. The hull efficiencies are given in Figure 6.5. They were calculated according to the definition given in 5.30. As it is independent of the number of propeller blades, only one curve is displayed.

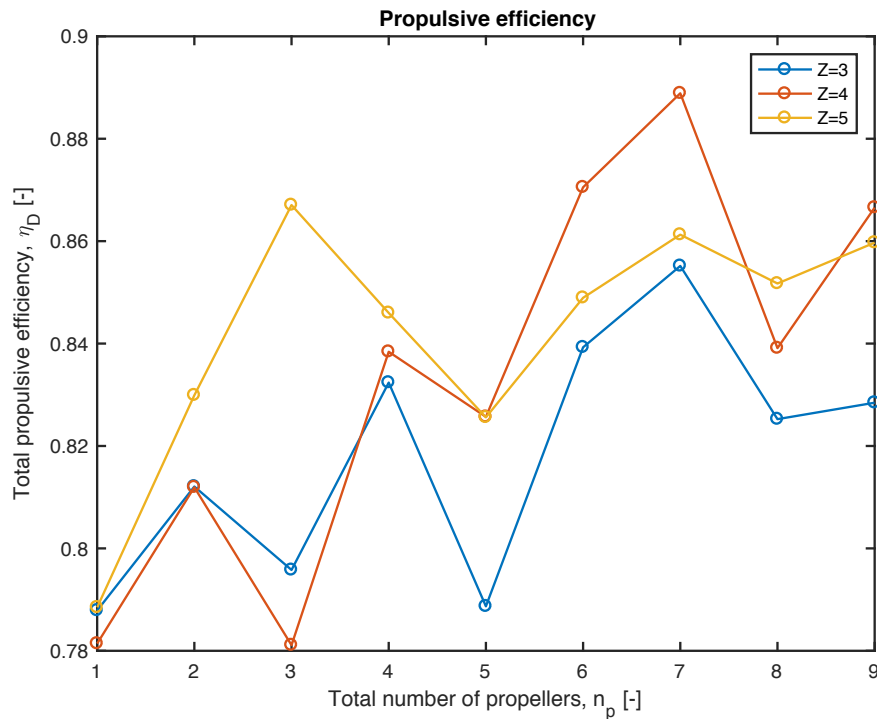


Figure 6.4: Propulsive efficiency versus number of propellers for Z=3-5

6.3 Further analysis of four-bladed propellers

In addition to the configurations that has been presented, those described in Table 6.3 was analysed for four-bladed propellers. The analysis procedure was the same as explained for the grid configuration in the above section. As cavitation was a problem, the percentage of the blades that were cavitating is also presented.

Table 6.3: Additional configurations analysed for four-bladed propellers

Type	Grid	Grid	Grid	T
Row	2	2	1	2
Col	2	3	5	7/1
D [m]	4.24	4.24	6.96	3.5643/5.94
$A_p[m^2]$	56.56	84.85	190.39	97.56
Cavitation [%]	52	24	0	7

Propulsive efficiencies including configurations of two rows

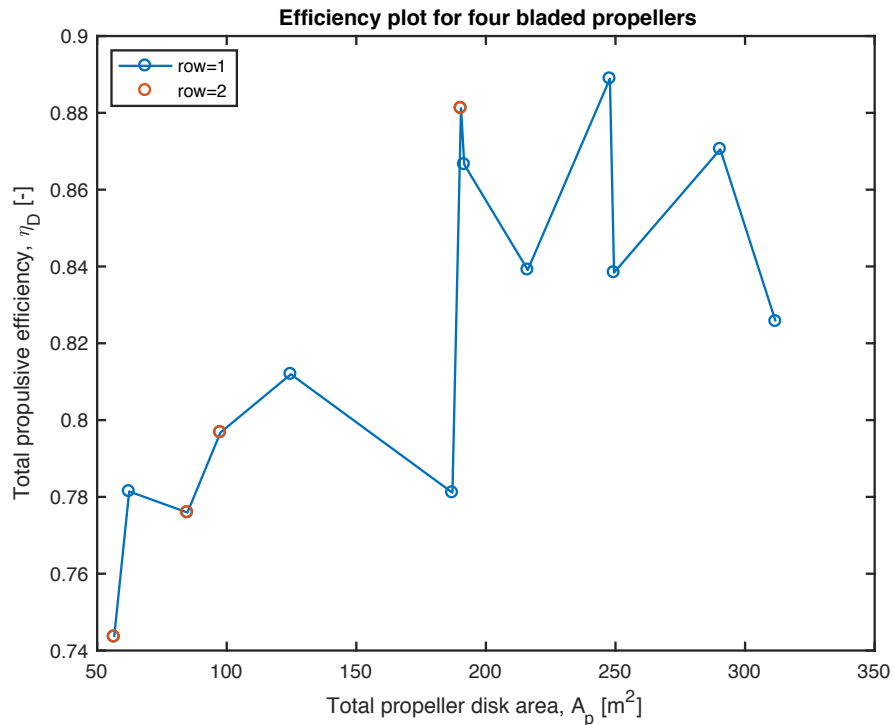


Figure 6.6: Propulsive efficiency versus total propeller disk area for four blades

In Figure 6.6 is presented the propulsive efficiencies of all the four-bladed configurations, plotted against the total propeller disk area. The additional configurations with two rows are highlighted. The following sections will further describe the additional four-bladed configurations.

Grid with two rows

Configurations with two rows of propellers were analysed for four and six propellers. Their resulting geometry is presented in Figure 6.7 and 6.8. Due to problems with cavitation and limited time frame of this work, no further analysis was conducted for such configurations. Their resulting propulsive efficiencies were 74% and 78% for four and six propellers, respectively.

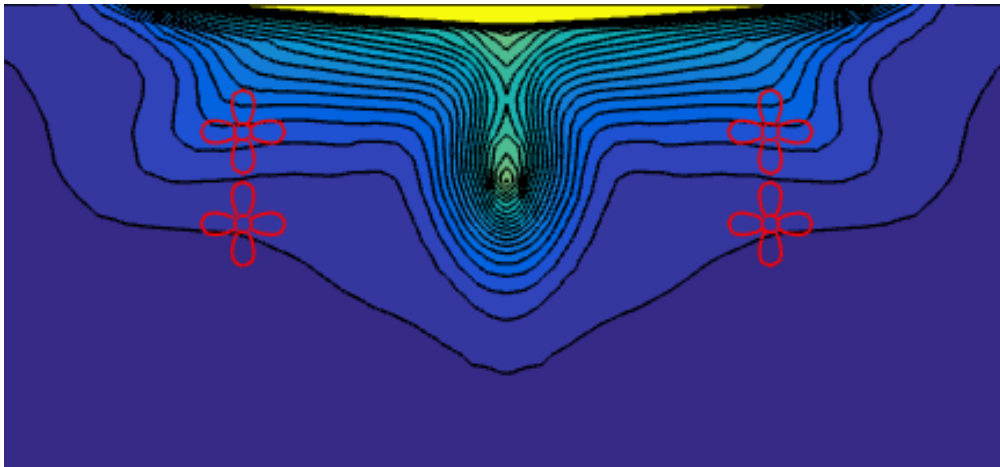


Figure 6.7: Grid configuration of four propellers over two rows

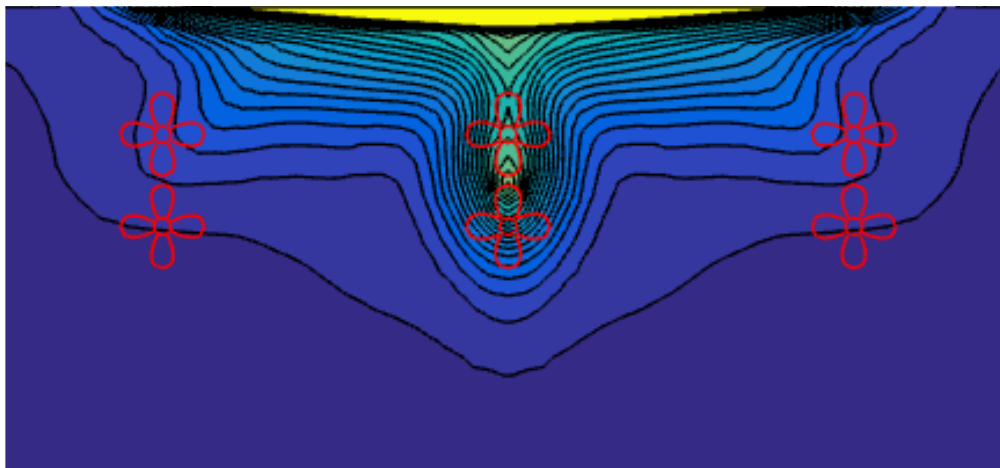


Figure 6.8: Grid configuration of six propellers over two rows

T-configuration

In the project thesis, it was found that placing seven propellers over one larger propeller could potentially increase the total propulsive efficiency. Therefore, an analysis of this configuration was conducted. Due to the large propeller having a different diameter than the above propellers, the computational time of the analysis was significantly increased. Thus, when this configuration was found to be cavitating, no further analysis of such configurations was prioritised within the time frame of this work.

In Figure 6.9 is plotted the propellers of this configuration. The resulting propulsive efficiency was 80%.

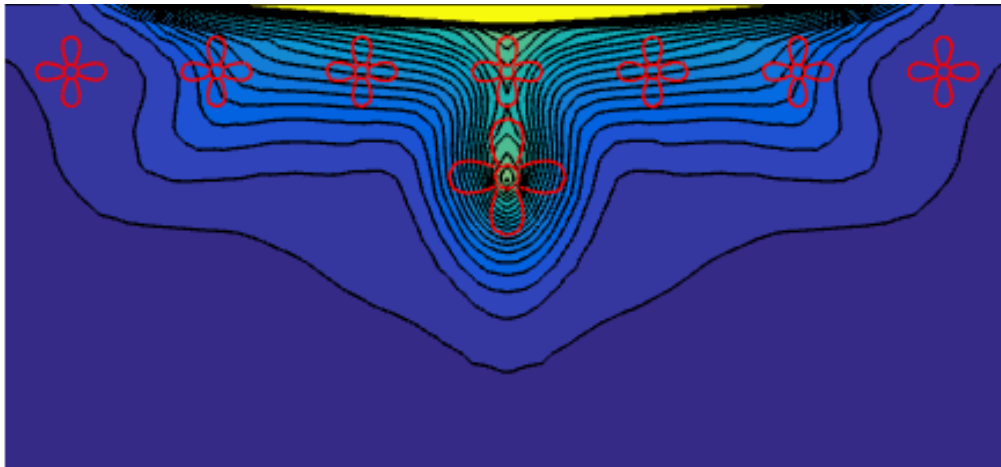


Figure 6.9: T-configuration including propeller geometry

Compressing the configuration of five propellers

The outermost propellers of the configuration with seven propellers are lightly loaded and located within relatively low wake fractions. It was anticipated that they did not contribute much to the propulsive efficiency. Therefore a configuration with five propellers was analysed, with the horizontal domain, Y_{lim} , reduced from B_{WL} to $B_{WL} - 2 \cdot 6.71$.

In Table 6.4 is given some propulsive properties for comparison. The resulting propeller geometry is given in Figure 6.10 for grid width equal to B_{WL} and in Figure 6.11 for reduced grid width. The hull efficiency and propulsive efficiency have increased by 0.9% and 6.7%, respectively, relative to the configuration of five propellers with B_{WL} as grid width.

Table 6.4: Properties of grid configuration with five propellers

Y_{lim}	B_{WL}	$B_{WL} - 2 \cdot 6.71$
A_E/A_0	0.59269	0.58367
η_H	1.0534	1.0632
η_D	0.8257	0.8812

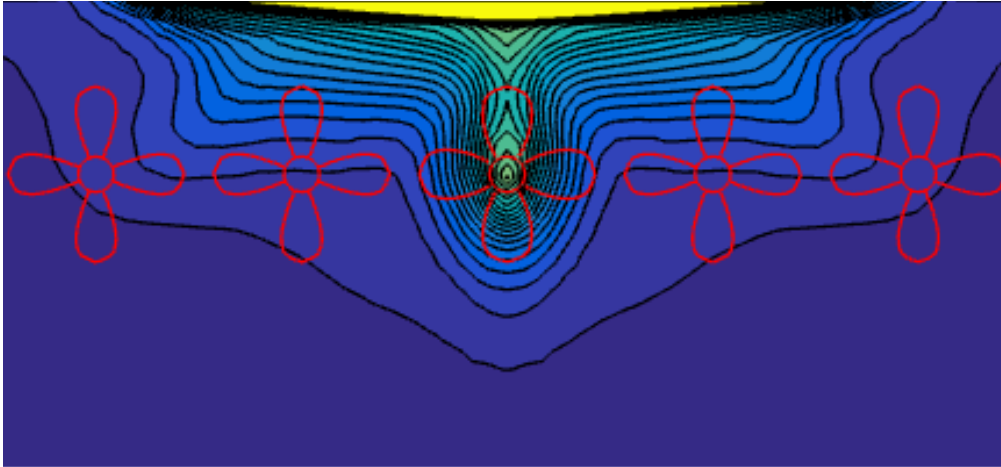


Figure 6.10: Configuration of five propellers including propeller geometry

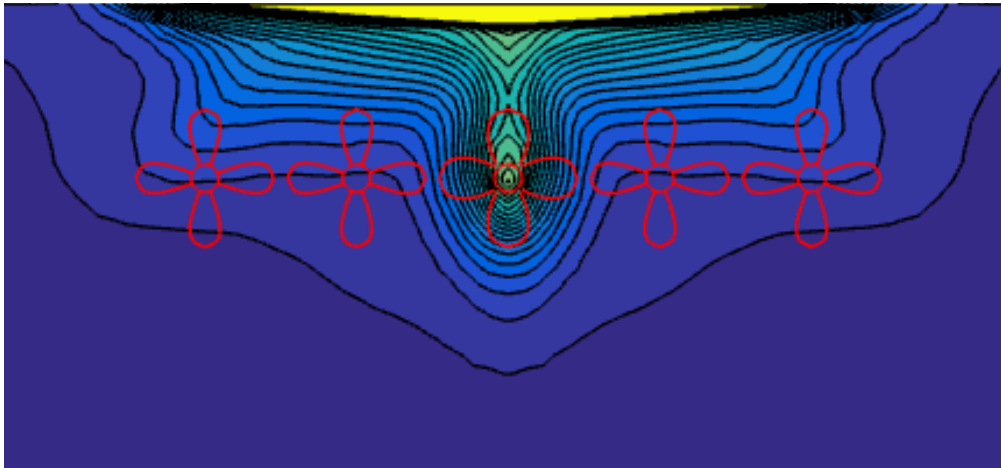


Figure 6.11: Configuration of five propellers with compressed domain including propeller geometry

6.4 Most efficient configuration

In this section is presented geometrical properties and performance, as well as details regarding cavitation, of the propellers in the most efficient configuration. Firstly, an overview of the geometry and performance are provided. Secondly, more detailed results of the cavitation check is given.

The geometry of the propellers are illustrated in Figure 6.12. The centre propeller has the lowest pitch angle, which is why the blades look fuller in the figure.

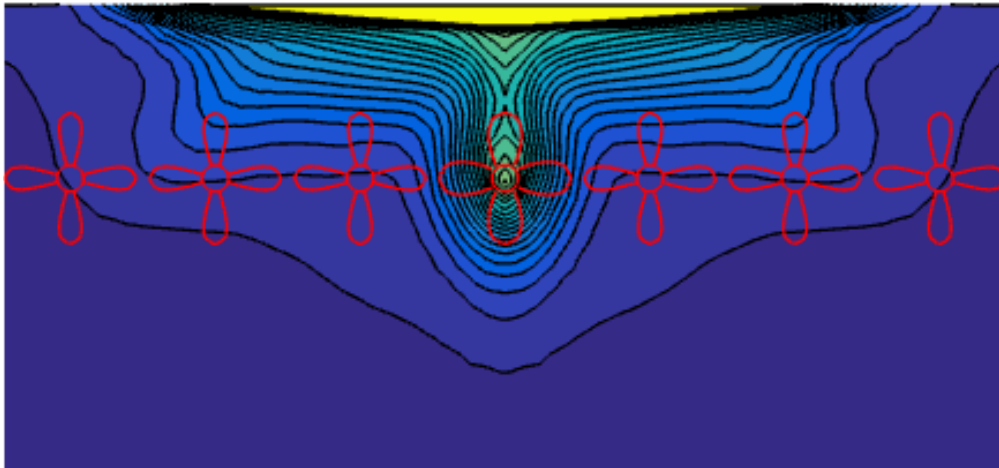


Figure 6.12: Configuration of seven propellers including propeller geometry

In Table 6.5 is presented the geometry and performance of each propeller. Number one refers to the outermost propeller and number four is the centre propeller. Due to symmetry it is only the four first propellers from left to right that are presented. Propeller number seven has the same geometry and performance as number one, and so on.

The centre propeller are far heavier loaded than the other propellers. Roughly speaking, it is around three times heavier loaded than the rest of the propellers. In order to study the loading of the propellers more detailed, the lift coefficients were plotted against radial positions on the propeller blades for all propellers. The plots are given in Figure 6.13 and 6.14.

Table 6.5: Geometry of propellers in grid configuration with seven propellers horizontally

Propeller number	RPM	$P/D_{0.7}$	$\phi_{0.7} [^\circ]$	A_E/A_0	Thrust [kN]	Cavitation [%]
1	42.36	2.7133	31.67	0.4960	188.4	0
2	41.28	2.5345	29.95	0.4960	128.5	0
3	41.26	2.5260	29.87	0.4960	127.4	0
4	97.80	0.8594	11.06	0.4960	553.9	0

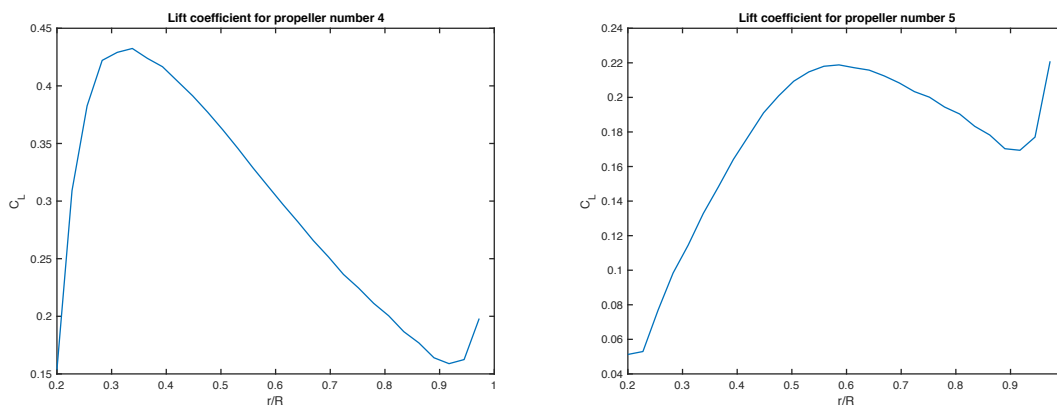


Figure 6.13: Lift coefficients for propeller number 4 and 5

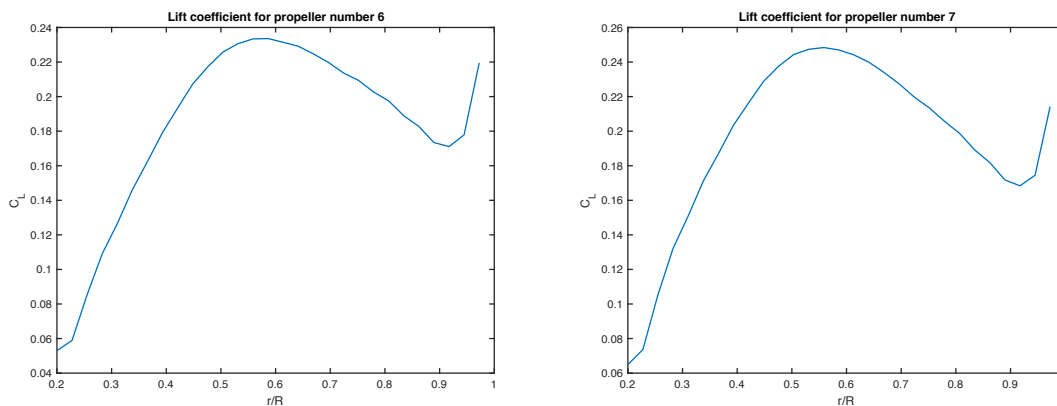


Figure 6.14: Lift coefficients for propeller number 6 and 7

The propellers were checked for cavitation by comparing the negative minimum pressure coefficient of the foil sections with the cavitation number, σ . In order to prevent cavitation, the effective angle of attack was forced close to zero in an iterative procedure. Figure 6.15 to 6.18

contains the cavitation curves for both the first and last iteration. Thus it can be seen the impact on cavitation from the effective angle of attack.

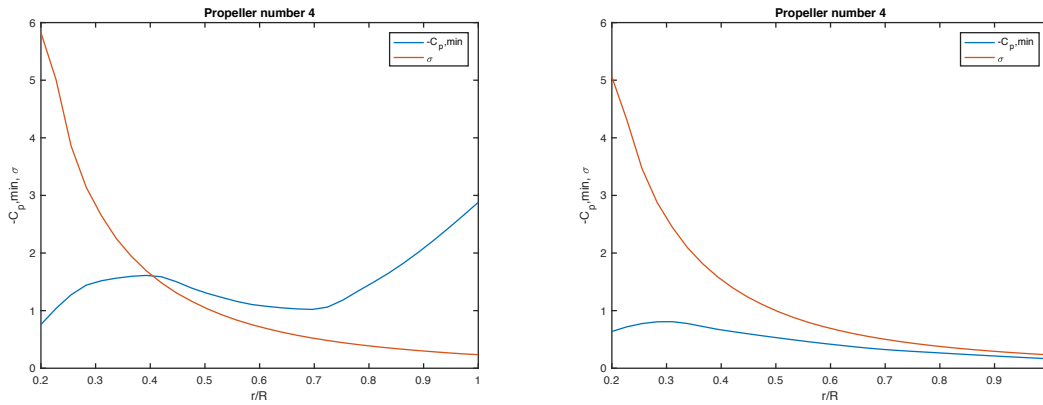


Figure 6.15: Cavitation plot from first and last iteration of α_e for propeller number 4

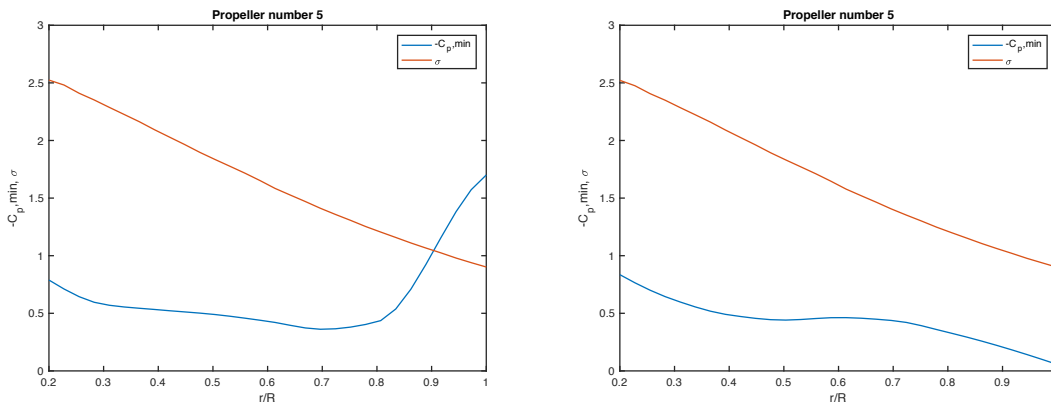


Figure 6.16: Cavitation plot from first and last iteration of α_e for propeller number 5

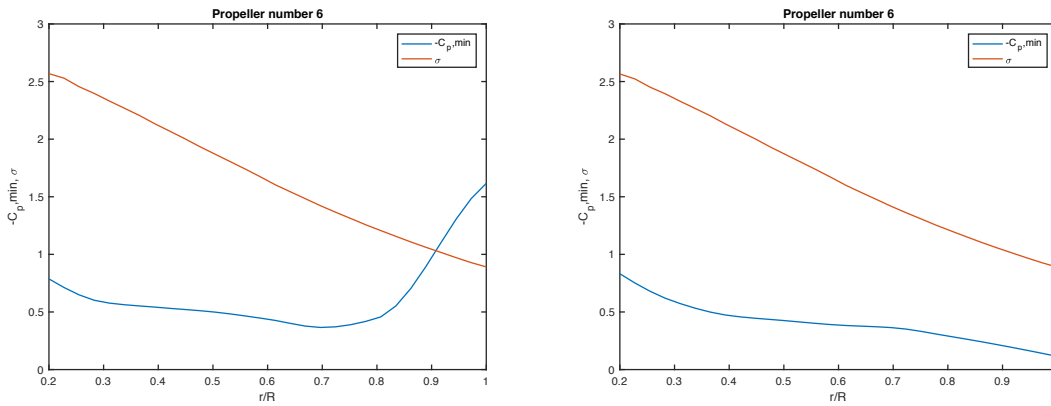


Figure 6.17: Cavitation plot from first and last iteration of α_e for propeller number 6

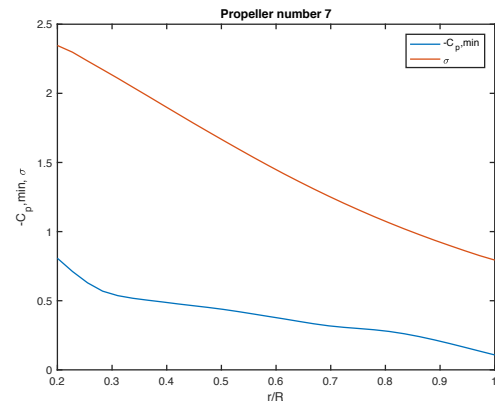


Figure 6.18: Cavitation plot for propeller number 7, no iteration was necessary for α_e

Chapter 7

Discussion of results

In this chapter, the results presented in the previous chapter are discussed. The discussion is organised such that the results that was first presented in the previous chapter is discussed first in this chapter.

7.1 Potential theory

Since the total thrust can be distributed over a larger area, the thrust coefficient was expected to decrease when the total propeller disk area increases. This is evident from Figure 6.1. It is the configuration with five propellers in one row that has the largest propeller disk area. Hence it has the lowest thrust loading. This is shown in Figure 6.2. It follows that this configuration has the highest ideal efficiency.

7.2 Grid configurations with three- to five-bladed propellers

In Figure 6.4 is presented the efficiencies for DEP configurations of propellers with three to five blades. Analysis of two-bladed propellers were discarded due to poor results in the validation process. According to polynomials representing the open water characteristics of the Wageningen B-screw series, the open water efficiency increases with decreasing number of propeller blades. From Figure 6.4 it is seen that the opposite behaviour is present. However, from the validation work it was concluded that results for propellers with different blade numbers are in-

comparable as their accuracy is varying. More information regarding the validation is found in Section 5.4 about validation of the lifting line code.

It was expected that the configurations with five propellers in one row would be most efficient, as they have highest ideal efficiency. However, from Figure 6.4 it is evident that the expectations was not met. Based on potential theory, the difference in loading between the configurations of five and seven propellers are relatively low. Thus the influence of the wake fractions are likely to be the reason why seven propellers are most efficient for three- and four-bladed propellers.

For five-bladed propellers it is the configuration with three propellers that has the greatest efficiency. Numerical difficulties of the lifting line analysis, for example with regards to treatment of singularities, are likely to be the reason of this sudden increase of efficiency. Furthermore, it should be noted that from the validation of the lifting line code it was found that the open water efficiency of five-bladed propellers was overestimated by around 5% for a blade area relationship of 0.50. As the blade area relationship of the five-bladed configuration with three propellers is 0.53, there is reason to believe that its efficiency is overestimated as a consequence of simplifications applied to the lifting line analysis.

For four-bladed propellers, the propulsive efficiency of the most efficient configuration is 10.75% higher than for a single screw propeller. This is over twice as high as the difference in ideal efficiency between a single screw and the lightest loaded propeller disk. Thus, the results suggests that optimising each propeller for the local wake it is operating in is increasing the propulsive efficiency. However, it should be emphasised that the simplifications made in this work must be taken into account when interpreting the results.

From Figure 6.4 it is seen that the configuration of three four-bladed propellers does not improve the propulsive efficiency with respect to the four-bladed single screw propeller. This can be a consequence of using a coarse step size in the optimisation algorithm.

In general, the hull efficiency increases with increasing wake fractions. Thus it was expected to be higher for the configurations containing odd numbers of propellers in each row. This is evident in Figure 6.5. However, the difference between odd and even numbers of propellers becomes less profound as the number of propellers increases. The hull efficiency is highest for the single screw configuration. The reason for this is that it is located in the area of the highest

wake fractions. From Figure 6.5 it is evident that as the number of propellers increases, the wake becomes less exploited as the hull efficiency is decreasing.

It is likely that it is the affection of the wake that leads to the choppy behaviour of the curves in Figure 6.4. However, the peaks are not consistent with the peaks of the hull efficiency curve. Thus it is anticipated that the affection of the wake fractions on the advance velocity has larger influence on the total propulsive efficiency than the hull efficiency itself.

From Figure 6.5 it is seen that it is the configurations with even numbers that have the best performance for low numbers of propellers. As the number of propellers increases, the effect becomes less profound. Since the nominal wake used in this work is a model wake, the effects of the wake fractions are anticipated to be less profound for the full scale wake. The reason for this is that models in general have higher frictional wake fractions due to boundary layer effects.

As it was evident from the results of the configurations with one row that the propulsive efficiency can be increased significantly if DEP is applied, it was not prioritised within the scope of this work to make alterations of the stern design. However, as results indicate that the propulsive efficiency are highly dependent on exploiting areas of large wake fractions, it is anticipated that it can be further increased if the stern is optimised for application of DEP. This remains to be investigated.

7.3 Further analysis of four-bladed propellers

Since it was found in the validation of the lifting line code that the four-bladed propellers could be analysed with relatively high accuracy, further analysis of other configuration types was conducted for this blade number. The grid configurations of two rows and the T-configuration was cavitating. This was anticipated as the propellers have relatively small diameter and low submergence.

Cavitation was expected to decrease with decreasing loading of the propellers. This is because when the propeller loading decreases, the pressure on the suction side of the blades is increased. As mentioned in Section 5.6 about the cavitation check, the single screw propeller of four blades was slightly cavitating at the blade tip when located in top position. Non of the other four-bladed configurations with one row of propellers were cavitating. However, for the

configurations with two rows, cavitation became a problem. There are two main reasons for this; firstly, since the propellers are distributed over two rows, the propellers on the top row will be located higher than if the configurations had only one row. Secondly, the diameter of the propellers becomes smaller as a safety factor between the vertical propellers are required. Thus the total propeller disk area is relatively low for the configurations that were analysed.

It was found that the propellers in both rows were cavitating for both the grid configurations. Thus the latter is most likely the reason for cavitation. To avoid it, the two row grid configurations should therefore be analysed with a larger number of propellers. For example ten propellers on each row in order to decrease the thrust loading of each propeller. However, as the computational time of the analysis is increasing significantly when the number of propellers in the configurations are increasing, this was not prioritised within the time frame of this work.

In the T-configuration it was only the propellers in the top row that were cavitating. Thus cavitation might be avoided if the submergence of the top propellers are increased. On the other hand, this limits the disk area of the lower propeller. As a consequence, its loading will increase and the risk of cavitation will be higher. It was therefore not conducted any further analysis of this type of configuration.

The increase in propulsive efficiency of the additional configurations with four-bladed propellers were low compared to the grid configurations with one row. This is because the total propeller disk area was relatively low for the additional configurations. This can be seen from Figure 6.6 where the total propulsive efficiency of all four-bladed configurations are plotted against the total propeller disk area. In addition, it is seen from Figure 6.7 and 6.8 that the wake is poorly exploited for grid configurations with two rows.

From the analysis it was noticed that the outermost propellers in the most efficient configuration, i.e. seven propellers with four blades, was relatively lightly loaded. Thus it was interesting to see how the propulsive efficiency changed when the outermost propellers were removed. If the efficiency are still maintained relatively high, it can be beneficial from a cost point-of-view to remove these propellers. In addition, it confirms that the propellers located within an area of low wake fractions has low affection on the total propulsive efficiency.

The results confirms that removing the outer propellers does not affect the propulsive efficiency significantly as it is reduced from 0.8889 to 0.8812. This is a very small reduction taken in

to consideration the uncertainties of the analysis. Comparing this modified configuration of five propellers with the original configuration of five propellers, there is a significant improvement in the propulsive efficiency when the width of the grid is reduced. It can be seen from Figure 6.10 and 6.11 that it is the pitch of the centre propellers that are the most noticeable difference between the propeller geometries. Therefore, the reason why one configuration has notably higher efficiency than the other is that the wake is better exploited, allowing the pitch of the centre propeller to be higher.

7.4 Most efficient configuration

In this section, details regarding performance and geometry are discussed for the configuration of seven four-bladed propellers.

From Table 6.5 it is evident that the centre propeller is relatively heavy loaded with respect to the other propellers. This is likely because it is located within an area of high wake fractions. As the analysis has been conducted with an unscaled nominal wake, it is anticipated that the importance of the centre propeller would have been less if the full-scale wake was used.

In Figure 6.13 and 6.14 the lift coefficients of the propellers are plotted against radial position. It is seen that the slopes of the lift curves are quite similar for all propellers, except the centre propeller. Most of the lift of the centre propeller is provided by the inner foil sections of the blades, around $0.3R$. For the other propellers, the lift distribution are somewhat more evenly distributed. The reason why the centre propeller has such a large drop in the lift coefficient at the blade tip is that the effective lift coefficient has been reduced at the tip in order to prevent cavitation. This was done by adjusting the pitch angle. The lift from the inner foil sections are provided by both camber and angle of attack, this was confirmed by plotting the effective angle of attack across the blades. For the other propellers, the lift is provided mainly by camber. However, the slight drop from $0.6R$ and outwards on the blades is due to reduction of effective angle of attack.

It is seen from the figures with the lift coefficients that there are some inconsistency of the lift slope next to the hub. This is due to a computational simplification. In order to ensure finite induced velocities close to the hub, the velocities induced by the inner foil section was extrap-

olated. However, due to computational problems with the extrapolation, the induced velocities of the inner foil sections was set equal to the induced velocities by the adjacent section. Hence the slope of the lift curve is deviating at these sections.

The cavitation curves for both the first and last iteration of the pitch is provided in Figure 6.15 to 6.18. From the figures it can be seen that the blades of all propellers, except the outermost, was initially cavitating when placed in top position. Then by reducing the effective angle of attack, cavitation was prevented. The large amount of initial cavitation on the centre propeller explains the steep reduction in the lift curve that can be seen in Figure 6.13.

On the other propellers, cavitation is not initially as profound as for the centre propeller. However, it can be seen that the blade tips were initially cavitating. When the effective angle of attack has been forced close to zero, the blades are relatively far from cavitating compared to the middle propeller. Reasons for these variations can be that the wake fraction within the centre propeller is large compared to the other propellers, and it spins much faster. The effective angle of attack of the outermost propellers are initially close to zero. Thus no cavitation was present and there was no need for iteration.

Chapter 8

Conclusions and recommendations for further work

In this chapter is presented conclusions and recommendations for further work. Firstly, a brief summary is given together with a list of conclusions. Then is presented recommendations for further work.

8.1 Summary and conclusions

Based on a literature study of the present state of propeller modelling methods, lifting line theory was chosen to analyse the potential benefits of using DEP on conventional ships. The arguments for using lifting line theory was the ability to include effects of propeller geometry and nominal wake within reasonable work load and computational time. In addition, it allowed for cavitation to be included with sufficient accuracy, which was considered important.

Thrust and torque of each propeller was calculated by lifting line theory. An optimisation algorithm was applied to find the optimal geometry of each propeller. Within the time frame of this work it was considered sufficient to use one of the algorithms in the optimisation toolbox in MatLab. The blade section geometry of the Wageningen B-screw series was used, as it limited the number of variables to be optimised.

The objective function was reduced from a multi-objective problem to a single-objective problem by the use of a quadratic penalty method. It forced the total thrust to be within 3% of

the required thrust, leaving the effect delivered to the propeller(s) as the remaining objective. An interior-point algorithm was used for the optimisation.

Emphasis was placed on programming a lifting line code that could determine propeller performance with sufficient accuracy. This involved extensive validation against the polynomials of the Wageningen B-screw open water characteristics. It was found that some inconsistency between the open water diagrams could not be avoided within the time frame of this work. However, the accuracy of the lifting line was considered sufficient to predict the potential benefits of using DEP with three- to five-bladed propellers.

Based on the discussion provided in the previous chapter, conclusions are listed below.

- Lifting line theory is to some extent providing results with sufficient accuracy for three- to five-bladed propellers
- Configurations with propellers of different number of blades are incomparable
- Due to affection of nominal wake, it is not the configuration with highest ideal efficiency that results in highest propulsive efficiency
- DEP with propellers located at one row can increase the propulsive efficiency of a conventional cargo ship
- Results suggests that a DEP configuration of seven four-bladed propellers in one row can increase the propulsive efficiency by 10.75%
- When the number of propellers increase, the wake becomes less exploited as the hull efficiency is decreasing
- The effects of wake fraction on advance velocity is highly influencing the propulsive efficiency
- Propellers located within an area of low wake fractions have low affection on the propulsive efficiency
- Cavitation is a decisive factor for the propeller design, even if the number of propellers are increased
- Due to cavitation, the wake close to the hull can not be exploited by the propellers in a DEP configurations
- Propeller blade sections with large angle of attack are most prone to cavitation

8.2 Recommendations for further work

The analysis conducted in this work has evaluated the benefits of using DEP on ships. However, more extensive analysis are highly recommended as the results in this work are based on simplifications and contains uncertainties. It is recommended that the lifting line approach of this work is improved such that the effects of blade number can be evaluated. There is also a potential of improving the general accuracy of the lifting line code.

For further work it is recommended that the following are included in the analysis:

- Lifting surface correction factors if lifting line theory is applied
- If lifting line theory is applied, the singularity of the integration should be treated more accurately
- Other blade section geometries than the Wageningen B-screw series. This is possible using the lifting line code from this work
- Convergence tests to determine parameters, such as step size, of the optimisation algorithm
- The interaction effect between propellers, and between propeller and hull should be accurately accounted for
- Locations of the propellers should be determined more strategically with respect to the ship wake
- Skew and rake should be included in the propeller geometry
- The added resistance due to propeller nacelles should be accounted for
- Practical challenges regarding design should be investigated and solved
- Benefits of optimising the stern design for DEP should be investigated
- Noise and vibrations from DEP should be analysed

References

- Amini, H. (2011), Azimut Propulsors in Off-design Conditions, PhD thesis, Norwegian University of Science and Technology.
- Breslin, J. P. & Andersen, P. (1993), *Hydrodynamics of Ship Propellers*, Cambridge Ocean Technology Series, Cambridge University Press.
- Carlton, J. (2011), *Marine Propellers and Propulsion*, 3 edn, Butterworth-Heinemann.
- CessnaAircraftCompany (2004), *172S Skyhawk Information Manual*, Cessna Aircraft Company.
- Dejhalla, R. & Prpic-Orsic, J. (2006), 'A review of the state-of-the-art in marine hydrodynamics', *Brodogradnja* **57**(1), 13–22.
- Drela, M. (1989), 'An analysis and design system for low reynolds number airfoils', *Conference on Low Reynolds Number Airfoil Aerodynamics*.
- el Moctar, O., Shigunov, V. & Zorn, T. (2012), 'Duisburg test case: Post-panamax container ship for benchmarking'.
- Epps, B. P., Stanway, M. J. & Kimball, R. W. (2009), 'Openprop: An open-source design tool for propellers and turbines'.
- Hess, J. L. & Valarezo, W. O. (1985), 'Calculation of steady flow about propellers using a surface panel method', *Journal of Propulsion and Power* **1**(6), 470–476.
- Hu, X. (2010), 'Particle swarm optimization'.
URL: <http://www.swarmintelligence.org/index.php>

- Huuva, T. & Törnros, S. (2016), 'Computational fluid dynamics simulation of cavitating open propeller and azimuth thruster with nozzle in open water', *Ocean Engineering* **120**, 160 – 164.
URL: <http://www.sciencedirect.com/science/article/pii/S002980181500606X>
- John D. Anderson, J. (2011), *Fundamentals of aerodynamics*, McGraw-Hill.
- Kennedy, J. & Eberhart, R. (1995), Particle swarm optimization, *in* 'Proceedings of ICNN'95 - International Conference on Neural Networks', Vol. 4, pp. 1942–1948.
- Kerwin, J. E. & Hadler, J. B. (2010), *Principles of Naval Architecture Series - Propulsion*, Society of Naval Architects and Marine Engineers (SNAME).
- Kerwin, J. E. & Lee, C.-S. (1978), Prediction of steady and unsteady marine propeller performance by numerical lifting-surface theory, number 8, The Society of Naval Architects and Marine Engineers.
- Kulunk, E. (2011), 'Aerodynamics of wind turbines', <http://cdn.intechweb.org/pdfs/16241.pdf>.
- Larsson, L., Stern, F. & Visonneau, M. (2014), *Numerical Ship Hydrodynamics*, Springer.
- MathWorks (2017), 'fmincon'.
URL: https://se.mathworks.com/help/optim/ug/fmincon.html#busoq0w-3_head
- Mirjalili, S., Lewis, A. & Mirjalili, S. A. M. (2015), 'Multi-objective optimisation of marine propellers', *Procedia Computer Science* **51**, 2247 – 2256.
URL: <http://www.sciencedirect.com/science/article/pii/S1877050915013125>
- Nocedal, J. & Wright, S. J. (2006), *Numerical Optimization*, Springer.
- Oosterveld, M. & van Oossanen, P. (1975), 'Further computer-analyzed data of the wageningen b-screw series', *International Shipbuilding Progress* **22**(251).
- Palt, K. (2017), 'Cessna 172 skyhawk'.
URL: http://www.flugzeuginfo.net/acdata_php/acdata_cessna172_en.php
- Pestana, H. (2014), *Future trends of electrical propulsion and implications to ship design*, CRC

Press, pp. 797–803.

URL: <http://dx.doi.org/10.1201/b17494-105>

Politis, G. K. (2004), ‘Simulation of unsteady motion of a propeller in a fluid including free wake modeling’, *Engineering Analysis with Boundary Elements* **28**(6), 633 – 653.

URL: <http://www.sciencedirect.com/science/article/pii/S0955799703001826>

Sánchez-Caja, A., Martio, J., Saisto, I. & Siikonen, T. (2014), ‘On the enhancement of coupling potential flow models to rans solvers for the prediction of propeller effective wakes’.

Spakovszky, Z. S. (2009), ‘Production of thrust with a propeller’.

URL: <http://web.mit.edu/16.unified/www/SPRING/propulsion/UnifiedPropulsion7/UnifiedPropulsion7.htm>

Steen, S. (2014), *Naval Hydrodynamics, Foil and Propeller Theory*, Akademika Forlag.

Stoll, A. M. (2015), Aviation technology, integration and operations conference, in ‘Comparison of CFD and Experimental Results of the LEAPTech Distributed Electric Propulsion Blown Wing’.

Stoll, A. M., Bevirt, J., Moore, M. D., Fredericks, W. J. & Borer, N. K. (2014), Aviation technology, integration and operations conference, in ‘Drag Reduction Through Distributed Electric Propulsion’.

Szantyr, J. (2008), ‘The crucial contemporary problems of the computational methods for ship propulsor hydrodynamics the crucial contemporary problems of the computational methods for ship propulsor hydrodynamics’, *Archives of Civil and Mechanical Engineering* **8**, 69–95.

van Oossanen, P. (1974), Calculation of performance and cavitation characteristics of propellers including effects of non-uniform flow and viscosity, PhD thesis, Netherlands ship model basin Wageningen.

Appendix A

Induction Factors

The induction factors are calculated according to (van Oossanen 1974).

$$\begin{aligned}
 & \left. \begin{aligned} I_A &= \left(\frac{y_0}{y} - 1\right) \frac{ZA^*}{\tan(\beta_i)} \\ I_T &= \left(1 - \frac{y}{y_0}\right) Z(1 + A^*) \end{aligned} \right\} \text{For } y_0/y > 1 \\
 & \left. \begin{aligned} I_A &= \cos(\beta_i) \\ I_T &= \sin(\beta_i) \end{aligned} \right\} \text{For } y_0/y = 1 \\
 & \left. \begin{aligned} I_A &= \left(1 - \frac{y_0}{y}\right) \frac{Z}{\tan(\beta_i)} (1 + B^*) \\ I_T &= \left(\frac{y}{y_0} - 1\right) ZB^* \end{aligned} \right\} \text{For } y_0/y < 1
 \end{aligned}$$

$$A^* = f \cdot \left[\frac{1}{u-1} - \frac{1}{24Z} g \cdot \ln\left(\frac{1}{u-1}\right) \right]$$

$$B^* = f \cdot \left[\frac{u}{1-u} + \frac{1}{24Z} g \cdot \ln\left(\frac{1}{1-u}\right) \right]$$

$$f = \sin^{-0.5} \beta_i \cdot p^{-0.25}$$

$$g = \sin^3(\beta_i) \left(2 + \frac{9}{\tan^2(\beta_i)} \right) + (3p - 5) \cdot p^{-1.5}$$

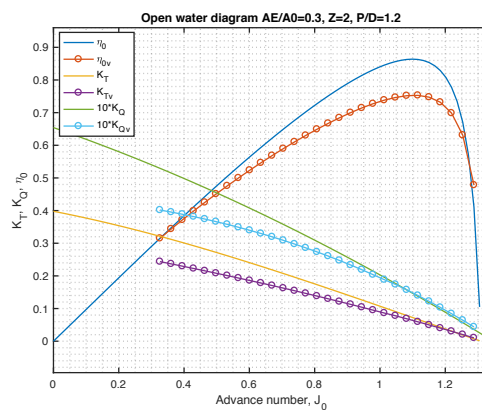
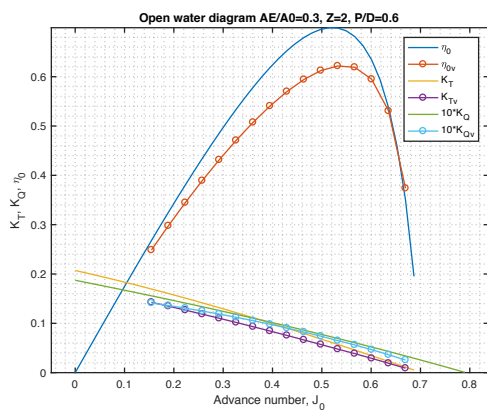
$$p = 1 + \frac{(y_0/y)^2}{\tan^2(\beta_i)}$$

$$u = \exp \left[Z \left(\ln \left[(p^{0.5} - 1) \left(\frac{1}{\sin(\beta_i)} - 1 \right)^{-1} \cdot \frac{y}{y_0} \right] + p^{0.5} - \frac{1}{\sin(\beta_i)} \right) \right]$$

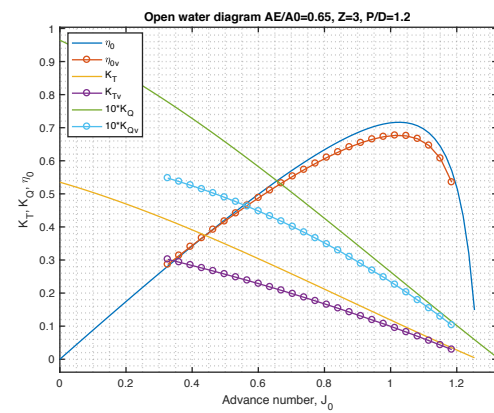
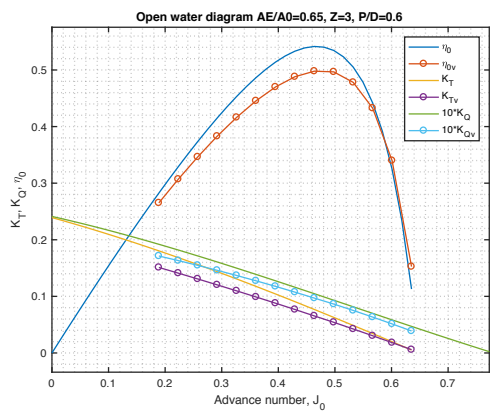
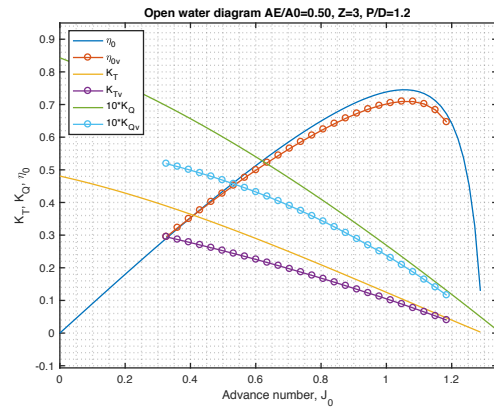
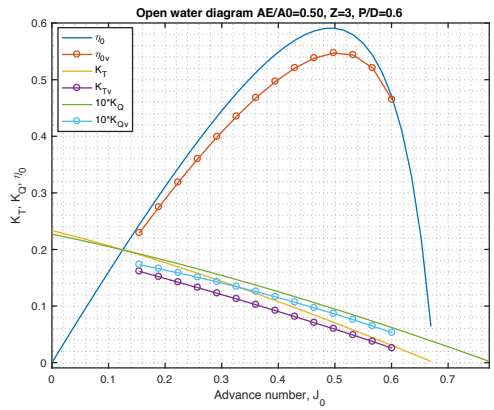
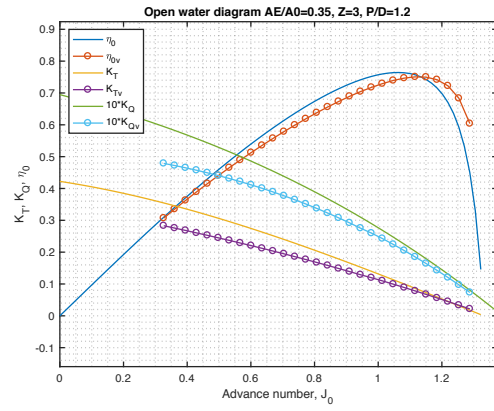
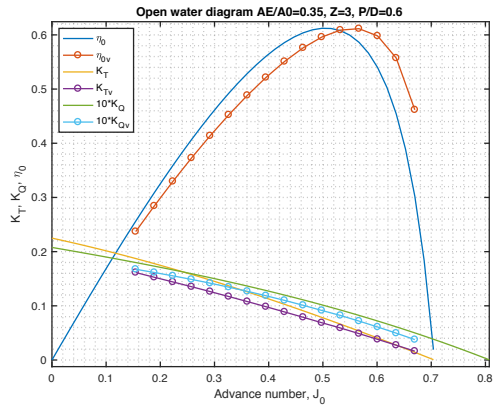
Appendix B

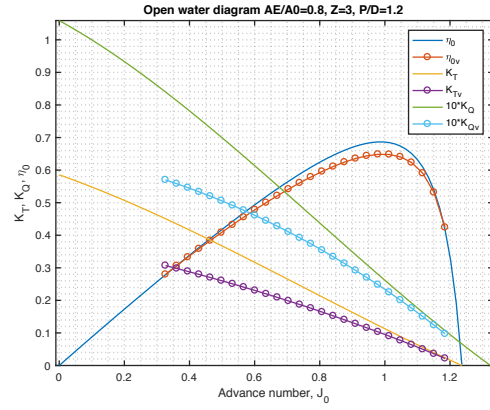
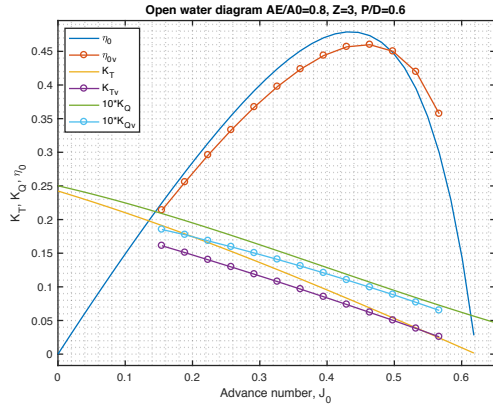
Validation Plots

B.1 Z=2

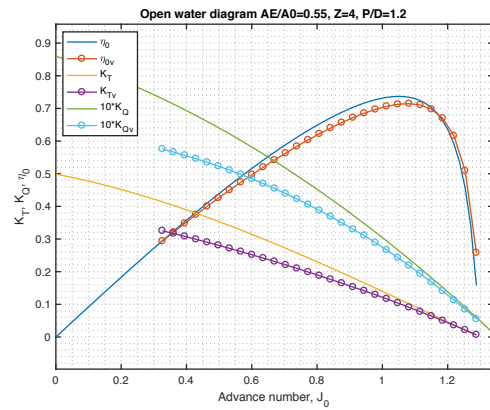
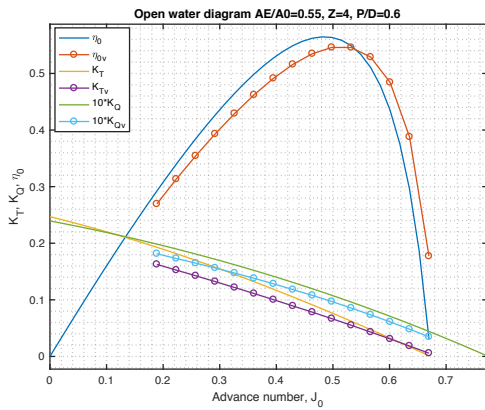
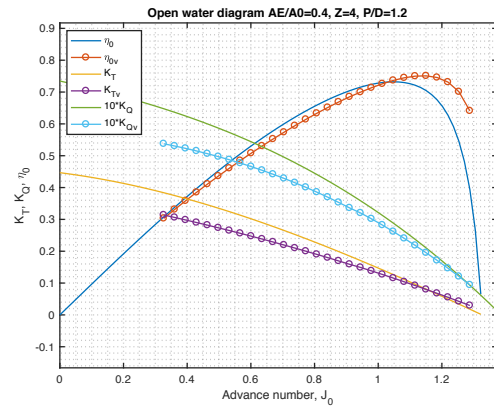
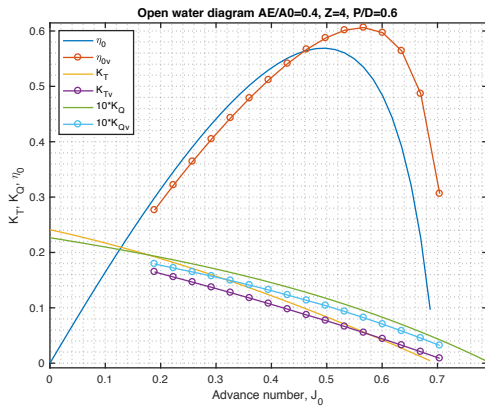


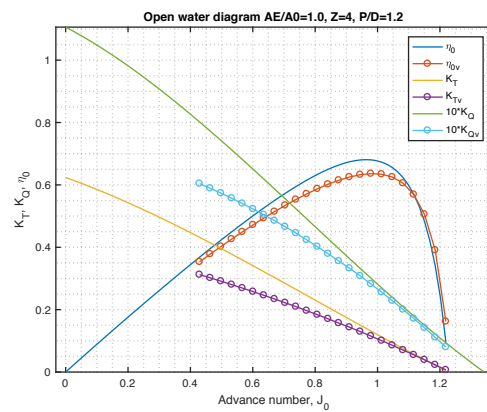
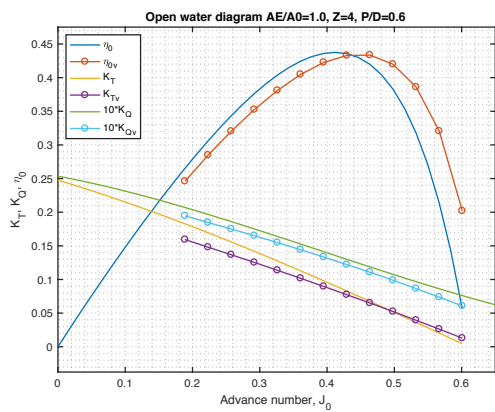
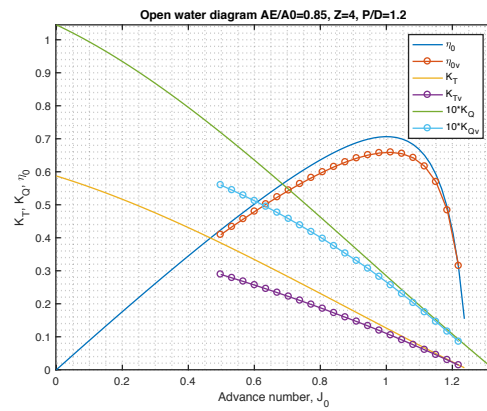
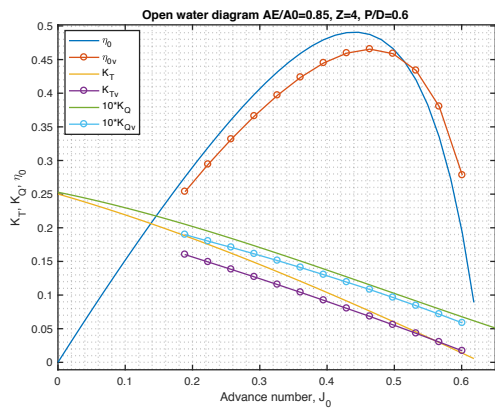
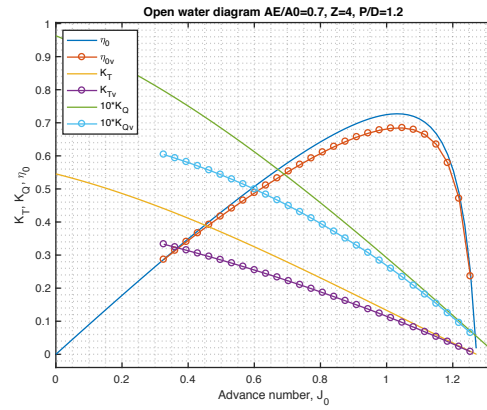
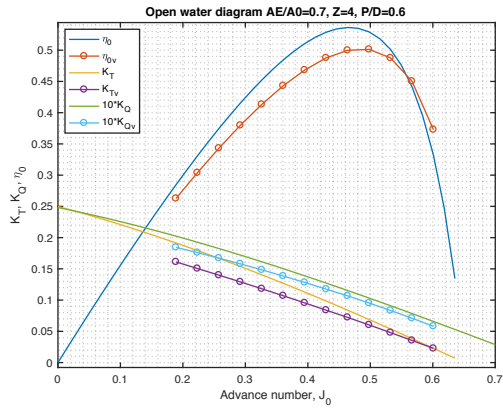
B.2 Z=3



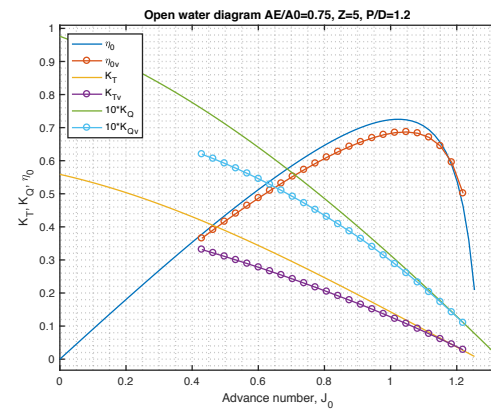
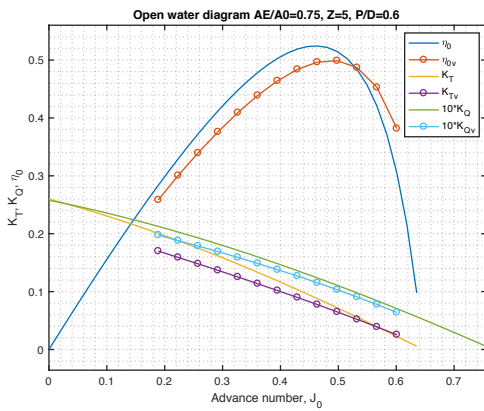
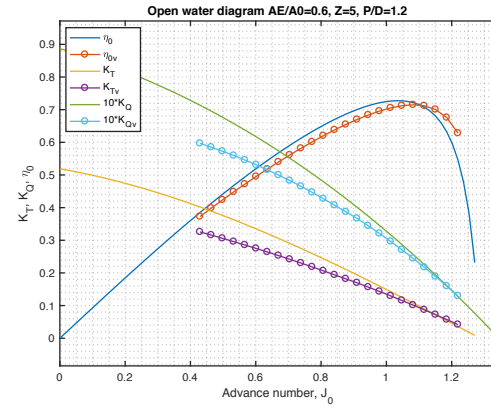
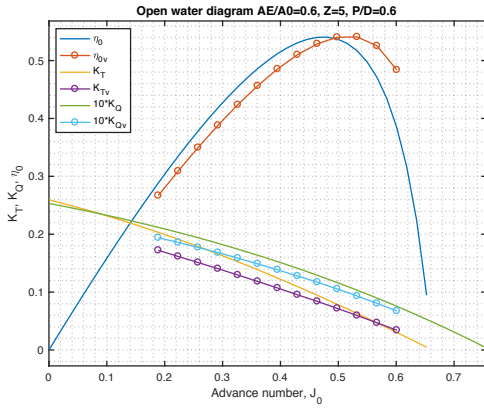
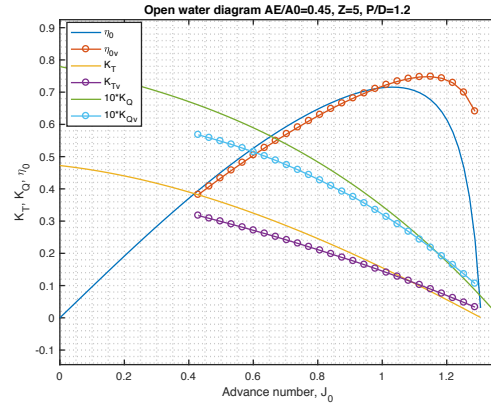
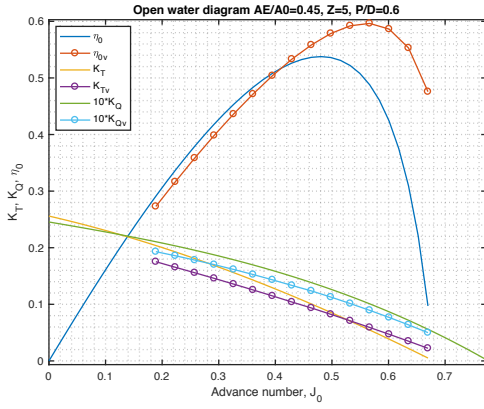


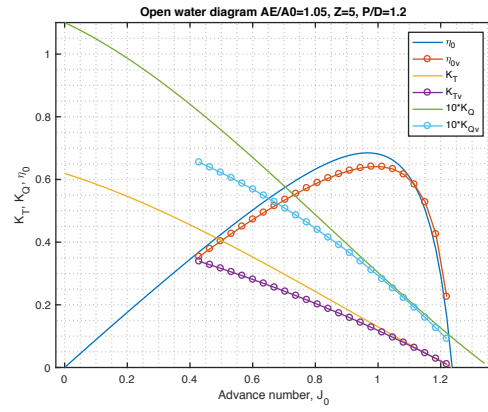
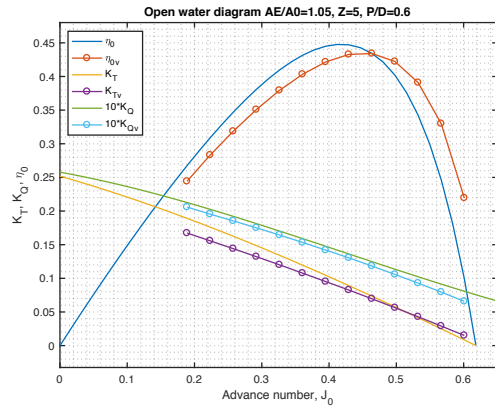
B.3 Z=4





B.4 Z=5





Appendix C

MatLab Codes

The codes for the lifting line analysis are provided in this section. A complete set of the codes used in this work is attached in a digital appendix.

main.m

```
1 % Preparation
2 clc
3 clear all
4 close all
5
6 % Importing input data
7 input;
8
9 % Defining number of spanwise stations
10 N = 30;
11
12 % Defining radial variables
13 R      = D/2;
14 R_boss = R/5;
15 dr     = (R-R_boss)/N;
16 r      = linspace(R_boss, R, N);
```

```
17 y      = r./R;
18 y_boss = R_boss/R;
19
20 % Importing the Wageningen open water diagram to be used for validation
21 [KT, KQ, J, eta_0] = wag_openwater(PD_07, AEA0, Z);
22
23 % Importing geometry
24 [tm, c, fi, tm_interp, c_interp, b_interp, r_R_interp] = wag_geo(D, Z, y, r,
    AEA0, PD_07);
25
26 % Running Xfoil to determine camber lift coefficient
27 [C_Lc_wag] = xfoil(b_interp, tm_interp, c_interp, r_R_interp);
28
29 % Defining rate of revolutions
30 J_val = J(12:1:40);
31 n_rev = V_s./(J_val.*D);
32
33 % Preallocation
34 eta_0_val = zeros(1, length(J_val));
35 KT_val = zeros(1, length(J_val));
36 KQ_val = zeros(1, length(J_val));
37 U_A = zeros(length(J_val), N);
38 U_T = zeros(length(J_val), N);
39
40 % Analyzing for all advance numbers
41 for i = 1:length(J_val)
42
43 % Lifting line calculations
44 [eta_0_val(i), KT_val(i), KQ_val(i)] = LL_iter(N, R, dr, r, y, tm, c, fi,
    n_rev(i), V_s, R_boss, Z, rho_s, D, C_Lc_wag, Re_wag, nu_s);
```

```
45
46 end
47
48 %% The difference in open water efficiency between the plynomials and lifting
    line results
49 %The difference in open water efficiency
50 diff_eta = max(eta_0)-max(eta_0_val);
51
52 % The fraction of the deviation with respect to lifting line results
53 diff_eta_ratio = diff_eta/max(eta_0_val);
54
55 %% Validation plot
56 % Open water diagram
57 ow=figure;
58 plot(J, eta_0);
59 hold on
60 plot(J_val, eta_0_val, '-o');
61 hold on
62 plot(J, KT);
63 hold on
64 plot(J_val, KT_val, '-o');
65 hold on
66 plot(J, 10.*KQ);
67 hold on
68 plot(J_val, 10.*KQ_val, '-o');
69 axis equal
70 grid minor
71 xlabel('Advance number, J_0')
72 ylabel('K_T, K_Q, \eta_0')
73 title('Open water diagram AE/A0=0.55, Z=4, P/D=0.6')
```

```
74 legend('\eta_0', '\eta_0_v', 'K_T', 'K_T_v', '10*K_Q', '10*K_Q_v')
75 set(ow, 'Units', 'Inches');
76 pos = get(ow, 'Position');
77 set(ow, 'PaperPositionMode', 'Auto', 'PaperUnits', 'Inches', 'PaperSize', [pos(3),
    pos(4)])
```

input.m

```
1 % Input data
2 % Environment
3 g      = 9.81;           % Acceleration of gravity [m/s^2]
4 rho_s  = 1025;          % Sea water density [kg/m^3]
5 nu_s   = 1.19E-6;      % Sea water kinematic viscosity [m^2/s]
6 pv     = 1500;          % Vapor pressure [Pa]
7 pa     = 101325;        % Atmospheric pressure [Pa]
8
9 % Ship speed
10 V_s   = 25*0.514444444; % Ship speed [m/s]
11
12 % Propeller blade
13 D     = 1;              % Blade diameter [m]
14 Z     = 4;              % Number of propeller blades [-]
15 AEA0  = 0.7;           % Expanded blade area relationship [-]
16 PD_07 = 1;             % Pitch to diameter ratio (0.5-1.4) [-]
17
18 % Wageningen Reynolds number
19 Re_wag = 2*10^6;
```

wag_openwater.m

```
1 function[KT, KQ, J, eta_0] = wag_openwater(PD_07, AEA0, Z)
2 % This function calculates open water performance based on polynomials.
3 % Polynomial coefficients are imported from .csv files
4
5 % KQ coefficients
6 filename = 'KQ.csv';
7 KQ_mat = csvread(filename,1,0);
8 B_abcd = transpose(KQ_mat(:,1));
9 a_kq = transpose(KQ_mat(:,2));
10 b_kq = transpose(KQ_mat(:,3));
11 c_kq = transpose(KQ_mat(:,4));
12 d_kq = transpose(KQ_mat(:,5));
13
14 % KT coefficients
15 filename = 'KT.csv';
16 KT_mat = csvread(filename,1,0);
17 A_abcd = transpose(KT_mat(:,1));
18 a_kt = transpose(KT_mat(:,2));
19 b_kt = transpose(KT_mat(:,3));
20 c_kt = transpose(KT_mat(:,4));
21 d_kt = transpose(KT_mat(:,5));
22
23 % Advance numbers, J, are defined in a vector
24 J = linspace(0, 1.7, 100);
25
26 % Preallocation
27 KT = zeros(length(PD_07), length(J));
28 KQ = zeros(length(PD_07), length(J));
29
```



```
30 %Calculating KT and KQ
31 for p = 1:length(PD_07)
32     for i = 1:length(J)
33         KT(p,i) = sum(A_abcd.*(J(i).^a_kt).*(PD_07(p).^b_kt).*(AEA0.^c_kt).*(
34             Z.^d_kt));
35
36         KQ(p,i) = sum(B_abcd.*(J(i).^a_kq).*(PD_07(p).^b_kq).*(AEA0.^c_kq).*(
37             Z.^d_kq));
38
39         % Negative KT are outside the range of the Wageningen B
40         % experimental results, correcting this by setting KT = NaN where KT
41         % is negative
42         if KT(p,i) < 0
43             KT(p,i) = NaN;
44         else
45             KT(p,i) = KT(p,i);
46         end
47
48         if KQ(p,i) < 0
49             KQ(p,i) = NaN;
50         else
51             KQ(p,i) = KQ(p,i);
52         end
53     end
54 end
55
56 %Open water efficiency
57 eta_0 = (KT.*J)./(2.*pi.*KQ);
58
59 end
```

wag_geo.m

```

1 function [tm, c, fi, tm_interp, c_interp, b_interp, r_R_interp] = wag_geo(D,
   Z, y, r, AEA0, PD_07)
2 % In this function, the geometrical properties of the Wageningen B series
3 % are calculated. Subscript interp indicates shorter vectors that are to be
4 % used in Xfoil. They corresponds to r_R_interp which is radial position on
5 % the blade from hub to tip, with length 9.
6
7 if Z==3
8     % Table 1 page 4 Oosterveld & Oossanen
9     r_R_interp = [0.2 0.3 0.4 0.5 0.6 0.7 0.8 0.9 1];
10    cr_D_Z_AEA0 = [1.663 1.832 2.000 2.120 2.186 2.186 2.127 1.657 0];
11    br_cr = [0.350 0.350 0.350 0.355 0.389 0.442 0.478 0.500 0.000];
12    Ar = [0.0526 0.0464 0.0402 0.0340 0.0278 0.0216 0.0154 0.0092 0.0030];
13    Br = [0.0040 0.0035 0.0030 0.0025 0.0020 0.0015 0.0010 0.0002 0.0000];
14
15 else
16     % Table 1 page 4 Oosterveld & Oossanen
17     r_R_interp = [0.2 0.3 0.4 0.5 0.6 0.7 0.8 0.9 1];
18     cr_D_Z_AEA0 = [1.662 1.882 2.050 2.152 2.187 2.144 1.970 1.582 0];
19     br_cr = [0.350 0.350 0.351 0.355 0.389 0.443 0.479 0.5 0];
20     Ar = [0.0526 0.0464 0.0402 0.0340 0.0278 0.0216 0.0154 0.0092 0.0030];
21     Br = [0.004 0.0035 0.0030 0.0025 0.002 0.0015 0.001 0.0005 0];
22 end
23
24 % Max section thickness
25 tm_interp = (Ar-(Br.*Z)).*D;
26 tm = interp1(r_R_interp, tm_interp, y, 'pchip');
27

```

```

28 % Radial chord length
29 c_interp = (AEA0/Z).*D.*cr_D_Z_AEA0;
30 c = interp1(r_R_interp, c_interp, y, 'pchip');
31
32 % Chordwise length from leading edge to position of maximum thickness
33 b_interp = br_cr.*c_interp;
34
35 % Pitch distribtion
36 P_table = [0.822 0.887 0.95 0.992 1 1 1 1 1].*PD_07.*D;
37 pitch = interp1(r_R_interp, P_table, y, 'pchip');
38 fi = atan(pitch./(2.*pi.*r));
39
40 end

```

xfoil.m

```

1 function [C_Lc_wag] = xfoil(b_interp, tm_interp, c_interp, r_R_interp)
2 % This function calculates the lift coefficient due to camber. Based in the
3 % geometrical properties subscripted with interp, the boordinates of the
4 % corresponding blade sections are calculated and imported into Xfoil.
5 % In Xfoil, their lift coefficients due to camber are calculated and
6 % interpolated to all N radial positions
7
8 % NOTE: This script contains one command where file paths have to be
9 % defined. These must be specified before running the optimization.
10
11 % NOTE2: The program Xfoil should be in the same folder as this
12 % script
13
14 % NOTE3: An empty text file called xfoilCMD.txt should be placed

```

```
15 % in the same folder as this function, prior to the analysis is initiated
16
17 % NOTE4: As this script enters the operating system of the computer,
18 % the codes depends on which operating system that is used. This script
19 % is for Mac. If Windows is used, use dos instead of system and
20 % \r\n for space when writing to text files
21
22 fclose('all');
23
24 % Deleting previous files
25 for i = 1:length(r_R_interp)-1
26     delete(['xfoil_' num2str(i) 'cl.txt'])
27 end
28
29 % Creating a text file and importing it to Xfoil for each foil section. The
30 % outermost section is not included, as it is assumed to be small enough
31 % for its camber lift coefficient to be zero
32 for i = 1:length(r_R_interp)-1
33
34     % Defining an index variable that is needed for the foil_coord function
35     index_r_R = i;
36
37     % Importing the coordinates of the foil section
38     [coord] = foil_coord(b_interp, tm_interp, c_interp, index_r_R, r_R_interp
39         );
40
41     % Defining the coordinates that are going to be put into the
42     % input text file for Xfoil
43     outputText = transpose(coord);
```

```
44 % Defining the name and format of file
45 fname = ['xFoil_' num2str(i) '.txt'];
46
47 % Opening the file in order to start writing
48 fileID = fopen(fname,'w');
49
50 % Writing the foil coordinates into the created text file
51 fprintf(fileID, '%8.4f %12.4f\r\n', outputText);
52
53 % Closing the file id
54 fclose(fileID);
55
56 %The input text file for Xfoil is now completed
57
58 % Opening the text file with commands that are going to be ran in Xfoil
59 fid = fopen('xfoilCMD.txt', 'w');
60
61 % Writing commands into the file. \n is indicating new line
62 % Loading the text file with the foil coordinates
63 fprintf(fid,'%s','load');
64 fprintf(fid,'\n');
65 fprintf(fid,'%s',['/Users/vildenyland/Desktop/FINAL/Validation_codes/
    xFoil_' num2str(i) '.txt']);
66 fprintf(fid,'\n');
67
68 % Defining a name of the foil
69 fprintf(fid,'%s',['wag' num2str(i)]);
70 fprintf(fid,'\n');
71
72 % Discretization of foil sections
```

```
73     fprintf(fid, '%s', 'gdes');
74     fprintf(fid, '\n');
75     fprintf(fid, '%s', 'cadd');
76     fprintf(fid, '\n');
77     fprintf(fid, '%s', '1');
78     fprintf(fid, '\n');
79     fprintf(fid, '%s', '1');
80     fprintf(fid, '\n');
81     fprintf(fid, '%s', '');
82     fprintf(fid, '\n');
83     fprintf(fid, '%s', '');
84     fprintf(fid, '\n');
85     fprintf(fid, '%s', 'ppar');
86     fprintf(fid, '\n');
87     fprintf(fid, '%s', 'N');
88     fprintf(fid, '\n');
89     fprintf(fid, '%s', '300');
90     fprintf(fid, '\n');
91     fprintf(fid, '%s', '');
92     fprintf(fid, '\n');
93
94     % Empty space (enter)
95     fprintf(fid, '%s', '');
96     fprintf(fid, '\n');
97
98     % Going into the oper menu
99     fprintf(fid, '%s', 'oper');
100    fprintf(fid, '\n');
101
102    % Claiming the polar data for the foil
```

```
103     fprintf(fid,'%s','pacc');
104     fprintf(fid,'\n');
105
106     % Creating a file for the polar data
107     fprintf(fid,['xfoil_' num2str(i) 'cl.txt']);
108     fprintf(fid,'\n');
109
110     % Creating a dump file for the polar data
111     fprintf(fid,'%s',['xfoil_' num2str(i) 'dump.txt']);
112     fprintf(fid,'\n');
113
114     % Defining angle of attack of the foil section
115     fprintf(fid,'%s','alfa');
116     fprintf(fid,'\n');
117     fprintf(fid,'%s','0');
118     fprintf(fid,'\n');
119
120     % Empty space
121     fprintf(fid,'%s','');
122     fprintf(fid,'\n');
123
124     % Quit
125     fprintf(fid,'%s','quit');
126
127     % Closing the file id
128     fclose(fid);
129
130     % Running Xfoil
131     system('Xfoil.app/Contents/Resources/xfoil < xfoilCMD.txt');
132
```

```
133 end
134
135 % Deleting unnecessary data
136 for i = 1:length(r_R_interp)-1
137     delete(['xfoil_' num2str(i) 'dump.txt']);
138 end
139
140 C_Lc_wag = zeros(1, length(r_R_interp));
141
142 % Processing the desired data
143 for i = 1:length(r_R_interp)-1
144     fname = ['xfoil_' num2str(i) 'cl.txt'];
145     fid = fopen(fname, 'r');
146     temp1 = textscan(fid, '%s');
147     temp2 = temp1{1};
148
149     size = length(temp2(:,1));
150
151     if size < 48
152         temp2{48,1} = '0';
153     end
154
155     C_Lc_wag(i) = str2num(temp2{48});
156     fclose(fid);
157 end
158
159 end
```



```
1 function [eta_0_val, KT_val, KQ_val] = LL_iter(N, R, dr, r, y, tm, c, fi,
      n_rev, V_s, R_boss, Z, rho_s, D, C_Lc_wag, Re_wag, nu_s)
2 % This function calculates the performance of the propeller using lifting
3 % line theory. The performance properties are subscripted val, as they are
4 % to be validated against the open water polynomials in the main.m script
5
6 % Importing wake data
7 w_s = 0;
8
9 % Calculating advance velocity
10 V_adv = V_s.*(1-w_s);
11
12 % Calculating beta
13 beta = atan(V_adv./(2*pi*r*n_rev));
14
15 % Assuming first value for beta_i to be equal to beta, i.e no induced
16 % velocities
17 beta_i = beta;
18
19 % Assuming first values of circulation to be elliptical
20 gamma_0 = 1;
21 gamma = gamma_0 * sqrt(1-((2.*((r-R_boss)./(R-R_boss))-1).^2));
22
23 % Defining the zero lift coefficient based on results from Xfoil
24 r_R_wag = [0.2 0.3 0.4 0.5 0.6 0.7 0.8 0.9 1.0];
25 C_Lc = interp1(r_R_wag, C_Lc_wag, y, 'pchip');
26
27 % Defining iteration variables
28 iter = 1;
29 iter_max = 1000;
```

```

30 difference_gamma = 1;
31 difference_beta_i = 1;
32 damping_gamma = 0.005;
33
34 while difference_gamma>0.00001 && difference_beta_i>0.00001 && iter<iter_max
35
36     %Numerical differentiation of the circulation using cubic spline fit
37     gamma_spline = csapi(r, gamma);
38     dgamma_dr = fnval(r, fnder(gamma_spline, 1));
39
40     % Inductions factors
41     [I_A, I_T] = induction_factors(y, Z, beta_i);
42
43     % Calculating the induced velocities by numerical integration
44     % Preallocation
45     integrand_A = zeros(N,N);
46     integrand_T = zeros(N,N);
47
48     for n = 1:N
49         for i = 1:N
50             if n ~= i
51                 integrand_A(n,i)=(I_A(n,i)*dgamma_dr(i))/(r(n)-r(i));
52                 integrand_T(n,i)=(I_T(n,i)*dgamma_dr(i))/(r(n)-r(i));
53             end
54         end
55     end
56
57     % Correcting for singularity when n=i
58     for n = 1:N
59         for i = 1:N

```

```

60     if i-1 == 0
61         integrand_A(1,1) = integrand_A(1,2);
62         integrand_T(1,1) = integrand_T(1,2);
63     elseif i+1 == N+1
64         integrand_A(N,N) = integrand_A(N,N-1);
65         integrand_T(N,N) = integrand_T(N,N-1);
66     elseif i == n
67         integrand_A(n,i) = 0.5*(integrand_A(n,i-1) + integrand_A(n,i
68             +1));
69         integrand_T(n,i) = 0.5*(integrand_T(n,i-1) + integrand_T(n,i
70             +1));
71     end
72 end
73 % Integrating with the trapezoidal rule to calculate induced velocities
74 U_A = (1/(4*pi)).*trapz(transpose(integrand_A)).*dr;
75 U_T = (1/(4*pi)).*trapz(transpose(integrand_T)).*dr;
76
77 % Removing singularities at the ends by extrapolating U_A(N) and U_T(N)
78 U_A = interp1(r(2:(N-1)), U_A(2:(N-1)), r, 'pchip', 'extrap');
79 U_T = interp1(r(2:(N-1)), U_T(2:(N-1)), r, 'pchip', 'extrap');
80
81 % Resulting inflow velocity at each foil section of propeller blade
82 V_inf = ((V_adv+U_A).^2 + (2.*pi.*r.*n_rev-U_T).^2).^0.5;
83
84 % New hydrodynamic pitch angle, including the effects of induced
85 % velocities
86 beta_i_new = atan((V_adv+U_A)./(2.*pi.*r.*n_rev-U_T));
87

```

```
88     % Resulting effective angle of attack
89     alpha_e = fi-beta_i_new;
90
91     % Section lift coefficients
92     C_L = 2.*pi.*alpha_e + C_Lc./c;
93
94     % Calculating circulation distribution from lift coefficients and
95     % Kutta-Joukowski theorem
96     gamma_new = 0.5.*V_inf.*C_L.*c;
97
98     %Forcing end values of new gamma to be 0
99     gamma_new(N) = 0;
100    gamma_new(1) = 0;
101
102    % Difference between the circulation distributions
103    difference_gamma = max(abs(gamma_new-gamma));
104    difference_beta_i = max(abs(beta_i_new-beta_i));
105
106    % Updating values for input to the next iteration
107    beta_i = beta_i_new;
108    gamma = gamma + damping_gamma.*(gamma_new - gamma);
109    gamma(N) = 0;
110    gamma(1) = 0;
111    iter = iter+1;
112
113 end
114
115 % Reynolds number
116 % Wageningen series is tested for Re = 2*10^6 at r=0.7R
117 % Finding the index for 0.7R
```

```

118 index_07 = find(round(y,1) == 0.7, 1, 'first');
119
120 % Finding the advance number
121 J = V_adv./(n_rev.*D);
122
123 % Calculation of rate of revolution based on rearranging definition of J
124 % and Re
125 n_rev_07 = ((Re_wag*nu_s)/c(index_07))/(sqrt((J*D)^2 + (2*pi*r(index_07))^2))
    ;
126
127 % The Reynolds number at all radial positions can then be found as
128 Re_s = (n_rev_07.*(sqrt((J.*D).^2 + (2.*pi.*r).^2)).*c)./nu_s;
129 Re_s(N) = 0;
130
131 % Frictional resistance coefficient according to ITTC'75
132 C_Fs = 0.075./((log10(Re_s)-2).^2);
133
134 % Viscous drag coefficient with ITTC'75 frictional coefficient
135 C_D = 2.*C_Fs.*(1+(2.*tm./c).*(1+(C_L.^2)./8));
136 C_D(N) = 0;
137
138 % Drag of each section
139 dD = 0.5.*rho_s.*(V_inf.^2).*C_D.*c.*dr;
140
141 % Thrust and torque of each section
142 dT = rho_s.*gamma.*(2.*pi.*r.*n_rev - U_T).*dr - dD.*sin(beta_i);
143 dQ = rho_s.*gamma.*(V_adv + U_A).*r.*dr + dD.*cos(beta_i).*r;
144
145 % Summing up over all blades to find total thrust and torque of propeller
146 T = sum(dT)*Z;

```

```

147 Q = sum(dQ)*Z;
148
149 % Resulting performance
150 KT_val = T./(rho_s.*n_rev.^2.*D.^4);
151 KQ_val = Q./(rho_s.*n_rev.^2.*D.^5);
152 eta_0_val = (KT_val.*J)./(2.*pi.*KQ_val);
153
154 % Displaying the resulting thrust and torque
155 disp('Thrust [kN]')
156 disp(T/10^3)
157 disp('Torque [kNm]')
158 disp(Q/10^3)
159
160 end

```

foil_coord.m

```

1 function [coord] = foil_coord(b_interp, tm_interp, c_interp, index_r_R,
   r_R_interp)
2
3 % Table 2 page 5 Oosterveld & Oossanen
4 r_R_V1 = transpose([0.20 0.30 0.4 0.5 0.6 0.7 0.8 0.9 1]);
5 x_V1 = [1 0.90 0.80 0.70 0.60 0.50 0.40 0.20 0 -0.20 -0.40 -0.50 -0.60 -0.70
   -0.80 -0.90 -1];
6
7 V_1 = [...
8     0.3560 0.2353 0.1685 0.1180 0.0804 0.0520 0.0304 0.0049 0 0.0172 0.0572
   0.0880 0.1207 0.1570 0.1967 0.2400 0.2826;...
9     0.2923 0.1760 0.1191 0.0790 0.0503 0.0300 0.1048 0.0027 0 0.0033 0.0202
   0.0376 0.0623 0.0943 0.1333 0.1790 0.2306;...

```

```

10     0.2181 0.1088 0.0637 0.0357 0.0189 0.0090 0.0033 0.0000 0 0.0000 0.0044
        0.0116 0.0214 0.0395 0.0630 0.0972 0.1467;...
11     0.1278 0.0500 0.0211 0.0085 0.0034 0.0008 0.0000 0.0000 0 0.0000 0.0000
        0.0012 0.0040 0.0100 0.0190 0.0330 0.0522;...
12     0.0382 0.0067 0.0006 0.0000 0.0000 0.0000 0.0000 0.0000 0 0.0000 0.0000
        0.0000 0.0000 0.0000 0.0000 0.0000 0.0000;...
13     0.0000 0.0000 0.0000 0.0000 0.0000 0.0000 0.0000 0.0000 0 0.0000 0.0000
        0.0000 0.0000 0.0000 0.0000 0.0000 0.0000;...
14     0.0000 0.0000 0.0000 0.0000 0.0000 0.0000 0.0000 0.0000 0 0.0000 0.0000
        0.0000 0.0000 0.0000 0.0000 0.0000 0.0000;...
15     0.0000 0.0000 0.0000 0.0000 0.0000 0.0000 0.0000 0.0000 0 0.0000 0.0000
        0.0000 0.0000 0.0000 0.0000 0.0000 0.0000;...
16     0.0000 0.0000 0.0000 0.0000 0.0000 0.0000 0.0000 0.0000 0 0.0000 0.0000
        0.0000 0.0000 0.0000 0.0000 0.0000 0.0000];
17
18 r_R_V2 = transpose([0.20 0.30 0.40 0.50 0.60 0.70 0.80 0.90 1]);
19 x_V2 = [1 0.90 0.80 0.70 0.60 0.50 0.40 0.20 0 -0.20 -0.40 -0.50 -0.60 -0.70
        -0.80 -0.90 -1];
20
21 V_2 = [...
22     0.0000 0.2840 0.4777 0.6190 0.7277 0.8170 0.8875 0.9750 1 0.9446 0.7984
        0.6995 0.5842 0.4535 0.3060 0.1455 0.0000;...
23     0.0000 0.3197 0.5130 0.6505 0.7520 0.8315 0.8920 0.9750 1 0.9583 0.8265
        0.7335 0.6195 0.4885 0.3360 0.1670 0.0000;...
24     0.0000 0.3235 0.5220 0.6590 0.7593 0.8345 0.8933 0.9725 1 0.9645 0.8415
        0.7525 0.6353 0.5040 0.3500 0.1810 0.0000;...
25     0.0000 0.3056 0.5039 0.6430 0.7478 0.8275 0.8880 0.9710 1 0.9639 0.8456
        0.7580 0.6439 0.5140 0.3569 0.1865 0.0000;...
26     0.0000 0.2720 0.4602 0.6060 0.7200 0.8090 0.8790 0.9690 1 0.9613 0.8426
        0.7530 0.6415 0.5110 0.3585 0.1885 0.0000;...

```

```

27     0.0000 0.2337 0.4140 0.5615 0.6840 0.7850 0.8660 0.9675 1 0.9600 0.8400
        0.7500 0.6400 0.5100 0.3600 0.1900 0.0000;...
28     0.0000 0.2028 0.3765 0.5265 0.6545 0.7635 0.8520 0.9635 1 0.9600 0.8400
        0.7500 0.6400 0.5100 0.3600 0.1900 0.0000;...
29     0.0000 0.1900 0.3600 0.5100 0.6400 0.7500 0.8400 0.9600 1 0.9600 0.8400
        0.7500 0.6400 0.5100 0.3600 0.1900 0.0000;...
30     0.0000 0.1900 0.3600 0.5100 0.6400 0.7500 0.8400 0.9600 1 0.9600 0.8400
        0.7500 0.6400 0.5100 0.3600 0.1900 0.0000;];
31
32 % Coordinates of foil section
33 % Dividing the foil into sections along the chord length
34 xxx = linspace(0, c_interp(index_r_R), 15);
35
36 % Defining non-dimensional coordinate along pitch line
37 P = zeros(1, length(xxx));
38
39 for i = 1:length(xxx)
40
41     if xxx(i) <= b_interp(index_r_R) % For 0<x<b
42         P(i) = -(xxx(i)-b_interp(index_r_R))./b_interp(index_r_R);
43     else % For b<x<c
44         P(i) = -(xxx(i)-b_interp(index_r_R))./(c_interp(index_r_R)-b_interp(
            index_r_R));
45     end
46
47 end
48
49 % Interpolating V_1 and V_2 according to P
50 V_1_interp = interp2(x_V1, r_R_V1, V_1, P, transpose(r_R_interp));
51 V_2_interp = interp2(x_V2, r_R_V2, V_2, P, transpose(r_R_interp));

```



```
52
53 % Calculating the y-coordinates of foilprofile
54 y_face = zeros(1, length(P));
55 y_back = zeros(1, length(P));
56
57 te = 0;
58 tl = 0;
59
60 for i = 1:length(P)
61
62     if P(i) <= 0
63         y_face(i) = V_1_interp(index_r_R,i)*(tm_interp(index_r_R)-te);
64         y_back(i) = (V_1_interp(index_r_R,i)+V_2_interp(index_r_R,i)).*(
65             tm_interp(index_r_R)-te)+te;
66     else
67         y_face(i) = V_1_interp(index_r_R,i).*(tm_interp(index_r_R)-tl);
68         y_back(i) = (V_1_interp(index_r_R,i)+V_2_interp(index_r_R,i)).*(
69             tm_interp(index_r_R)-tl)+tl;
70     end
71
72 end
73
74 coord_y = [fliplr(y_back), y_face(2:length(P))];
75 coord_x = [fliplr(xxx), xxx(2:length(P))];
76
77 coord_x = transpose(smooth(coord_x));
78 coord_y = transpose(smooth(coord_y));
79 coord_x = transpose(smooth(coord_x, 'lowess'));
80 coord_y = transpose(smooth(coord_y, 'lowess'));
81 coord_x = transpose(smooth(coord_x, 'sgolay'));
82 coord_y = transpose(smooth(coord_y, 'sgolay'));
```

```
80 coord_y = transpose(smooth(coord_y, 'sgolay'));
81
82 % Scaling after smoothening such that the chord lengths is matching
83 gap_xxx = max(xxx)-min(xxx);
84 gap_coord_x = max(coord_x) - min(coord_x);
85 gap = gap_xxx/gap_coord_x;
86
87 coord_x = coord_x*gap;
88
89 % Forcing leading edge to be at P = 0
90 coord_x = coord_x - min(coord_x);
91
92 % Transpose
93 coord_x = transpose(coord_x);
94 coord_y = transpose(coord_y);
95
96 % Final coordinate matrix
97 coord = [coord_x, coord_y];
98
99 end
```

induction_factors.m

```
1 function [I_A, I_T] = induction_factors(y, Z, beta_i)
2 % This function calculates the induction factors according to van Oossanen
3 % page 22
4
5 % Preallocation
6 p = zeros(length(y), length(y));
7 term = zeros(length(y), length(y));
```

```

8 u = zeros(length(y), length(y));
9 g = zeros(length(y), length(y));
10 f = zeros(length(y), length(y));
11 A = zeros(length(y), length(y));
12 B = zeros(length(y), length(y));
13 I_A = zeros(length(y), length(y));
14 I_T = zeros(length(y), length(y));
15
16 for n = 1:length(y)
17     for i = 1:length(y)
18         p(n,i) = 1 + ((y(n)/y(i))^2)/(tan(beta_i(i))^2));
19
20         term(n,i) = (sqrt(p(n,i))-1)*(((1/(sin(beta_i(i))))-1)^(-1))*(y(i)/y(
21             n));
22         u(n,i) = exp(Z*log(term(n,i)) + sqrt(p(n,i)) - (1/(sin(beta_i(i)))));
23
24         g(n,i) = (sin(beta_i(i))^3)*(2+ (9/(tan(beta_i(i))^2))) + (3*p(n,i)
25             -5)*p(n,i)^(-3/2);
26
27         f(n,i) = (p(n,i)^(-0.25))*sin(beta_i(i))^(-0.5);
28
29         if y(n)/y(i) > 1
30             A(n,i) = f(n,i)*((1/(u(n,i)-1)) - (1/(24*Z))*g(n,i)*log(abs(u(n,i)
31                 )/(u(n,i)-1))));
32             I_A(n,i) = ((y(n)/y(i))-1)*((Z*A(n,i))/(tan(beta_i(i))));
33             I_T(n,i) = (1-(y(i)/y(n)))*Z*(1+A(n,i));
34         elseif y(n)/y(i) == 1
35             I_A(n,i) = cos(beta_i(i));
36             I_T(n,i) = sin(beta_i(i));
37         else

```

```
35      B(n,i) = f(n,i)*((u(n,i)/(1-u(n,i))) + (1/(24*Z))*g(n,i)*log(abs
      (1/(1-u(n,i)))));
36      I_A(n,i) = (1-(y(n)/y(i)))*(Z/(tan(beta_i(i))))*(1+B(n,i));
37      I_T(n,i) = ((y(i)/y(n))-1)*Z*B(n,i);
38      end
39
40  end
41 end
42
43 end
```